Structural Engineering, Mechanics and Materials Division

Report No. UCB/SEMM-90/02

A UNIFIED APPROACH TO MIXED FINITE ELEMENT METHODS

By

Shmuel L. Weissman

Department of Civil Engineering
University of California
Berkelley, California 94720

April 1990

A UNIFIED APPROACH TO MIXED FINITE ELEMENT METHODS

By

Shmuel L. Weissman

ABSTRACT

A general formulation to generate assumed stress and strain fields in the context of mixed finite element methods is introduced. Both the Hellinger-Reissner and Hu-Washizu variational principles are considered. Finite elements based upon classical isoparametric displacement formulations exhibit locking behavior when applied to thin plates (plate bending) and to the nearly incompressible limit (plane strain). Therefore, the plate bending problem, based on the Reissner-Mindlin plate theory, and the in-plane problems (plane stress/strain) are used to illustrate the proposed formulation. While the objectives set to overcome locking at the nearly incompressible limit and shear locking seem to be unrelated, the same methodology is applied to both problems.

In formulating the plate bending problem an explicit coupling between the assumed moment and shear resultant fields is introduced in both variational principles. Also, in the case of the Hu-Washizu variational principle, an explicit coupling between the assumed curvature and assumed shear strain fields is introduced. It is demonstrated that as a result of these couplings the proposed formulations lead to elements that, as the thickness is reduced to zero, converge to the thin plate solution and do not lock in shear. Furthermore, shear locking is avoided at the element level.

For the case of plain strain, it is shown that the strain field generated by the proposed method can model a nearly incompressible state.

A method to generate fields possessing the desired properties is presented. The strain field is assumed as the sum of two independent fields, labeled "compatible" and

"incompatible." The assumed incompatible strain is constructed such that the resulting elements pass the patch test, provided the assumed displacement field can model the associated state of deformations. The desired stress field to be used in the variational principles is obtained by constraining the complementary energy associated with the incompatible modes to vanish in a weak sense over each element. The desired strain field is obtained by constraining the "strain energy" resulting from the coupling of the assumed compatible and incompatible strains to vanish in a weak sense over each element. As a result, if the material properties are constant over each element domain, the incompatible strains are identically zero pointwise.

The elements formulated by this method are shown to yield excellent results when applied to a wide range of problems. Furthermore, the variationally consistant stress resultants recovered at the element level produce excellent results.

ACKNOWLEDGEMENTS

I would like to express my sincere gratitude to my advisor Professor Robert L. Taylor for his guidance and continuous support during the course of this research. I would also like to thank Professors Jacob Lubliner and George C. Johnson for serving on the dissertation committee.

I would also like to thank all my friends in Berkeley for their support and encouragement during my studies at the University of California at Berkeley. A special word of gratitude to Kristin J. Berdan for her support and editorial advice.

My special thanks to my parents, Jeanisse and Michael Weissman, whose continuous love, support and encouragement made this dream come true. This dissertation is dedicated to them.

Table of Contents

CHAPTER 1: INTRODUCTION

1.1 Objective and Motivation

The objective of this dissertation is to present a general formulation that can be used to generate plate bending elements suitable for both thin and thick plate applications, as well as to generate membrane elements suitable for both plane stress and plane strain applications. These elements are to exhibit the following properties:

- Shear locking is avoided at the element level (plate bending).
- Locking at the nearly incompressible limit is avoided at the element level (plane strain).
- Recovery of stress resultants (i.e., membrane, transverse shear and moment resultants) is variationally consistent with the formulation used to obtain the displacement field.
- Good stress resultants are recovered at the element level.
- Convergence to the thin plate, or Kirchhoff, solution as the thickness is reduced to zero (plate bending).
- Correct rank (no spurious zero-energy modes).
- Applicable for both thin and thick plate problems (plate bending).
- Performance independent of coordinate system or user input data.

To avoid shear locking, much current plate element technology (see Section 1.2.2) resorts to the sharing of shear constraints across element boundaries. Consequently, shear locking is avoided only at the global level. In order to maintain full generality of the finite element method, different types of elements must be able to interact. This objective may not be obtained if the elements need to share constraints with their neighboring elements. As an example, consider the case of stress intensity analysis near cracks. In this class of problems special elements are used to model the vicinity near the crack tip. Current

element technology requires modifying these elements so that the constraint-sharing scheme will be applicable. For this reason it is essential that the element formulation does not impose constraints on its neighbors; i.e., shear locking should be avoided at the element level as well as at the global level.

Current finite element technology involves a different treatment for each field. Unfortunately, if special techniques are used for each field, no gain is obtained in solving other problems of similar type (i.e., same type of governing differential equations). For example, the B-bar method used to overcome locking at the nearly incompressible limit is not beneficial in solving the shear locking problem in thin plates and shells which account for shear deformations. Also, many recent developments of shell elements use different types of formulations and/or interpolations for the membrane, bending, and transverse shear parts of the theory (e.g., Simo, Fox & Rifai [1989]). From a conceptual perspective it is desirable to have a uniform treatment of all fields so that a better understanding of the finite element method will be obtained. Ideally, the same methodology would be used to solve all problems. For example, the same methodology would be used to avoid shear locking in thin plates and shells as would be used to overcome locking at the nearly incompressible limit in plane strain.

The complete solution of a mechanical problem involves the determination of the state of displacements and the state of stresses at any given point of the body at any given time. Recent finite element technology has made considerable progress in determining the state of displacements in plates and shells; currently, however, shear stress resultants are not recovered from a variationally consistent method (e.g., Hinton & Huang [1986]). It follows that the shear stress resultants recovered are only a weak approximation; therefore, shear stress resultants must be approximated as constant throughout the element. Furthermore, the stresses are usually the limiting factor on the design and not the displacement state. Accordingly, it is essential to develop a fully consistent and unified treatment of the field variables together with the use of appropriate variational methods.

1.2 Background

1.2.1 Plane Stress/Strain

Solution of problems by the finite element method necessitates that certain requirements be fulfilled by the formulation employed. Lax & Richtmyer [1956] proved that consistency and stability are necessary, and, for linear problems, they are sufficient requirements for convergence. Isoparametric formulations are known to satisfy consistency and stability conditions provided sufficient order quadrature is used (Bicanic & Hinton [1979]). However, equally well known is the "locking" behavior of these types of formulations for plane strain linear isotropic elasticity models with high Poisson's ratio (e.g., $\nu > 0.499$).

The simplest way to overcome locking at the nearly incompressible limit is to use an under-integrated stiffness matrix. In this case, the stiffness matrix satisfies necessary accuracy (consistency) requirements; however, it does not meet stability requirements. To overcome this difficulty, Hughes [1977] applied the selective reduced integration (SRI) technique to develop element stiffness matrices through the assumed displacement method. The SRI scheme used under-integration on the volumetric strain terms and full-integration on the deviatoric strain terms. Malkus & Hughes [1978] showed that the SRI method falls within the concept of a mixed finite element method for plane strain and three-dimensional analysis.

Hughes [1980] refined the SRI scheme into a general method, known as the B-bar method, for three-dimensional and axisymmetric elements. More recently, Simo, Taylor & Pister [1985] showed that it is possible to derive the B-bar method from the Hu-Washizu variational principle.

Belytschko and co-workers (e.g., Belytschko, Ong, Liu & Kennedy [1984] and Liu & Belytschko [1984]) took a different approach to overcome locking at the nearly incompressible limit. Using a projection operator, Flanagan & Belytschko [1981] showed that the usual finite element approximation can be rewritten in a form that leads to

decoupling of the stiffness matrix. The stiffness matrix is written as the sum of the decoupled under-integrated stiffness matrix and a "stabilization" stiffness matrix. This decoupling leads to an efficient implementation as well as to a better understanding of the element behavior in limit situations (such as the nearly incompressible limit). Following this approach Belytschko & Bachrach [1986] presented formulations based upon the Hu-Washizu functional. The best of the elements presented is known as the Quintessential Bending Incompressible (QBI). This element, however, is not frame invariant (i.e., it is dependent upon the coordinate system) unless a unique local coordinate system is defined and the element stiffness matrix and load vector, defined in the local coordinate system, are transformed to the global coordinate system.

Wilson, Taylor, Doherty & Ghaboussi [1973] took yet another approach. They observed that when the four-node element, based upon isoparametric displacement formulation, is subjected to a pure bending load it deforms in shear rather than in bending. To improve the behavior in bending they introduced a set of incompatible displacements. It was soon realized, however, that the distorted element did not pass the constant strain patch test. Taylor, Beresford & Wilson [1976] modified the incompatible modes element so that the resulting element passed the patch test. This result was obtained by replacing the derivatives associated with the incompatible modes with their values at the center of the element. Only recently it was observed that these element do not exhibit locking behavior when applied to model plane strain problems at the nearly incompressible limit.

Pian & Sumihara [1984] presented a four-node plane stress element based upon the Hellinger-Reissner variational principle. This element has excellent characteristics in bending applications. Also, when modified to account for the plane strain constitutive relations, it has excellent characteristics at the nearly incompressible limit. In addition, the element sensitivity to mesh distortion from a parallelogram shape appears to be the smallest of any four-node element evaluated to date. The assumed independent stress field is subjected to a set of constraint equations. These equations are interpreted as satisfying the

equilibrium equations in a weak sense relative to a set of incompatible displacement modes. Initially, the formulation required a quadratic perturbation of the element shape in order to obtain the required number of independent constraint equations. Recently, Pian & Wu [1988] presented a new formulation that avoids element perturbation. The constraint equations are obtained by constraining the stress field to perform no work along the element boundary when subjected to a set of assumed incompatible displacement modes. A general formulation to generate incompatible element functions was presented by Wu, Huang & Pian [1987].

Simo & Rifai [1989] presented four-node elements based upon the Hu-Washizu functional which introduced "enhanced strains." Results reported for these elements are almost identical to the results obtained by the element presented by Pian & Sumihara [1984].

1.2.2 Plate Bending

Solutions to plate bending problems pose a difficult task for the classical finite element method (displacement formulation). This problem was one of the first to be tackled by the finite element method in the early 1960s, yet today it is still the subject of intensive research. Obtaining a satisfactory solution of plate bending problems is a necessary prerequisite for the analysis of shells.

The original approach utilized thin plate theory. This approach introduced the difficulty of imposing C^1 continuity of the shape functions used by the finite element method. Also, the resulting elements were restricted to thin plate applications. Babuska & Scopolla [1989] showed how in an apparently very thin plate (thickness to span ratio equal to 0.01) differences of approximately 5% in the displacements are observed between the true behavior and that predicted by the thin plate theory. For these reasons, most elements presented recently in the literature are based on thick plate theories (i.e., theories that account for shear deformations; e.g., Reissner-Mindlin plate theory). These theories require only C^0 continuity of the shape functions. Furthermore, applicability for both thin

and thick plate problems is obtained.

Unfortunately, many of the proposed elements fail at the thin plate limit because of a phenomenon known as shear locking. Development of a general class of elements free of shear locking in all applications has been the focus of extensive research during the past two decades. The first successful developments were based on reduced integration and selective reduced integration (full integration on the curvature terms and reduced integration on the shear terms), concepts which were proposed simultaneously by Zienkiewicz, Taylor & Too [1971] and Pawsey & Clough [1971]. Later, Malkus & Hughes [1978] presented an equivalence theorem, which demonstrated that both reduced integration and selective reduced integration fall within the scope of a mixed finite element method.

Unfortunately, both reduced integration and selective reduced integration often result in unstable elements due to the presence of spurious zero-energy modes. In the case of selective reduced integration elements, the spurious modes can be controlled by a careful choice of the boundary conditions (e.g., Hughes [1987], pp. 334).

MacNeal [1978] presented a four-node shell element, known as QUAD4, in which the transverse shear strains are computed at special points. These points are located at $\pm \frac{1}{\sqrt{3}}$ on the element's natural axes. Later it was recognized that spurious zero-energy modes are present in some applications (MacNeal [1982]). A further difficulty was the presence of a tuning parameter.

Hughes & Tezduyar [1981] presented a four-node element, known as T1, that is free of spurious zero-energy modes and does not utilize tuning parameters. Furthermore, it does not exhibit shear locking on reasonable meshes. The underlying idea is that shear locking occurs when too many constraints are imposed on the shear field; thus, by sharing constraints across element boundaries it is possible for the global system not to be overconstrained, even when the individual elements are. As a result, shear locking is avoided. The sharing scheme is obtained by constraining the tangential component of the shear strain, for both elements sharing an edge, to be equal at the edge midpoint. Dvorkin &

Bathe [1984] justified this approach via the Hu-Washizu variational principle. A mathematical analysis of this scheme was presented by Bathe & Brezzi [1985, 1987]. A rigorous proof of uniform convergence for any thickness, however, is still lacking. Huang & Hinton [1984] extended the formulation to a nine-node element.

The scheme presented by Dvorkin & Bathe [1984] solved the problem of shear locking, but introduced the problem of shear resultants recovery. In obtaining the displacement field it was assumed that the shear resultant field is a set of concentrated forces at the midpoints of the element edges. Thus, the only possible way to recover the shear resultants at any given point is by using the shear strains together with the constitutive equations. This procedure, however, is not variationally consistent with the formulation used to obtain the displacement field. Furthermore, the shear resultants recovered pose potential difficulties in the interpretation of results obtained from the finite element analysis. As a result, it is necessary to introduce special sampling techniques in order to obtain "good" shear resultants (Hinton & Huang [1986]).

Simo, Fox & Rifai [1989] presented a four-node shell element in which the membrane and the moment stress resultant fields were modeled after Pian & Sumihara [1984]. The shear resultant field for the element is modeled after Dvorkin & Bathe [1984]. The displacements reported are excellent. However, no stress resultants are reported. Furthermore, shear stress resultants cannot be obtained in a variationally consistent form.

Simo & Rifai [1989] presented an assumed strain method which can be used to generate plate bending elements. Results reported for their proposed element are identical to the results obtained by the T1 element for square elements.

Belytschko and co-workers (e.g., Belytschko, Liu, Ong & Lam [1985] and Liu, Belytschko, Law & Lam [1987]) extended the stabilization approach introduced in the in-plane problem to shell applications. The Hu-Washizu variational principle was used to justify their approach. These formulations, however, use a tuning parameter. A "good" value for this parameter may be obtained if the true solution is known; this, however, is

usually not the case. Furthermore, an optimal parameter for one problem may not be appropriate for a different problem.

1.3 Dissertation Overview

The formulations proposed in this dissertation are developed within the framework of mixed finite element methods, and are based upon the Reissner-Mindlin plate theory. The plane strain problem is also tackled. While the objectives set in order to overcome locking at the nearly incompressible limit (plane strain problem) and shear locking (plate bending problem) seem to bear no connection, the same methodology is applied to both problems. Consequently, a unified methodology suitable for both plate bending and plane stress/strain problems is presented.

As noted in Section 1.2, the classical finite element method (i.e., displacement formulation) yields poor results at the nearly incompressible limit (plane strain) and at the thin plate limit (plate bending - using theories that account for shear deformations). This result was established in a limitation principle put forth by Fraeijs de Veubeke [1965]. In order to overcome this drawback, mixed formulations (i.e., formulations that use more than one type of variable) will be used in this dissertation. Two types of mixed variational principles are commonly used: the Hellinger-Reissner and Hu-Washizu principles. The former principle may be viewed as a special case of the latter. The Hu-Washizu principle is a three-field formulation (i.e., the stress, strain and displacement fields are assumed as independent fields) that can be easily used in conjunction with existing methods when non-linear material properties are encountered. This property is not shared by the Hellinger-Reissner formulation. In this dissertation, however, both principles will be used, in parallel and independently. This is done because the main ideas presented in this dissertation are more clearly conveyed via the Hellinger-Reissner variational principle.

A plate theory that accounts for shear deformations is presented in Chapter 2. As is evident from the strong form of the boundary value problem, plate bending and in-plane

problems are decoupled for homogeneous isotropic material properties. This dissertation will focus on this type of material. Also presented is the matrix notation used in formulating the finite element arrays.

The weak form, counterpart to the strong form presented in Chapter 2, and the finite element formulations are presented in Chapter 3. The formulations are presented independently for the plate bending and plane stress/strain elements. For each type of element the formulation is carried out via the Hellinger-Reissner variational principle and in parallel via the Hu-Washizu variational principle.

An explicit coupling between the assumed moment and shear resultant fields is introduced in both variational principles. In the case of the Hu-Washizu variational principle, an explicit coupling between the assumed curvature and shear strain fields is also introduced. It must be noted that the coupling between the moment and shear resultant fields is consistent with the structure of the equilibrium equations. Thus, the assumed coupling is viewed as a natural assumption.

In Chapter 4 it is formally proved that as a result of the couplings introduced in Chapter 3 the proposed formulation leads to elements which, as the thickness is reduced to zero, converge to the thin plate solution and do not lock in shear. Furthermore, shear locking is avoided at the element level.

Additionally, in Chapter 4 it is argued that locking at the incompressible limit (plane strain) can be avoided if the assumed strain field can *a priori* model a state of strains such that the trace of the strain goes to zero pointwise as Poisson's ratio goes to 0.5^{-}.

A method to generate the assumed stress resultant and strain fields used as independent fields in the variational formulations is presented in Chapter 5. First, the method is presented for a general three-dimensional body. The reduction to the in-plane problem is straightforward, and will also be presented. Next, the method is reformulated in resultant form for the plate bending problem. Finally, in order to show the generality of the method, the formulation for the axisymmetric problem is presented. Also presented is a set

of requirements which the assumed incompatible displacements, used in this method, must satisfy.

The method is presented as a three-field formulation. It can, however, be applied to the two-field formulation. The assumed strain field is assumed as the sum of two independent fields, which are termed compatible and incompatible. The assumed incompatible strain is constructed from a set of displacements not contained in the finite element approximation of the displacement solution space. The desired stress field to be used in the variational principles is obtained by constraining the complementary energy associated with the incompatible modes to vanish in a weak sense over each element. The desired strain field is obtained by constraining the "strain energy" resulting from the coupling of the assumed compatible and incompatible strains to vanish in a weak sense over the element. As a result, if the material properties are assumed to be constant over the element domain, the incompatible strains are identically zero pointwise.

It must be pointed out that the methodology outlined is a precursor for the finite element method, and at no point do the incompatible strains play any role in the finite element formulation. Consequently, the methodology presented yields fully compatible elements.

The assumed stress and strain fields as well as the assumed incompatible shape functions used to generate the proposed elements are presented in Chapter 6. These elements, however, are only an illustration of the method. The elements are shown to satisfy the requirements introduced in Chapter 4 in order to avoid locking.

An extensive numerical evaluation of the proposed elements is presented in Chapter 7. The elements are shown to perform well even in cases when other elements such as the S1 or T1 fail. Furthermore, the stress resultants recovered are shown to be good at the element level.

Closing remarks and suggestions for future work are presented in Chapter 8.

CHAPTER 2: PLATE THEORY WITH SHEAR DEFORMATIONS

2.1 Introduction

A theory of plates that accounts for shear deformation is presented in this chapter. This theory was first presented by Reissner [1945], based upon energy considerations and assumed stress distributions. Mindlin [1951] presented the kinematic assumptions used in this dissertation. The stress distributions used by Reissner, however, account for the warping of transverse planes. In this dissertation the warping effect is neglected. However, a shear correction factor is introduced to compensate for the lack of warping.

The in-plane and bending problems are shown to be decoupled in the case of homogeneous isotropic materials. In this dissertation only this class of material properties is considered. Consequently, the strong form for each problem is given separately in this chapter. The counterpart to the strong form, the weak form, will be presented in Chapter 3.

The in-plane problem is the usual plane stress problem. Since the kinematics for both plane stress and plane strain cases are the same, the constitutive equations for plane strain are also introduced.

Throughout this dissertation Greek subscripts take the values 1 and 2, while Latin subscripts take the values 1, 2 and 3. Repeated indices imply the usual summation convention. All quantities are referred to a fixed system of rectangular, Cartesian coordinates. A general point in this system is denoted by (x_1, x_2, x_3).

2.2 Plate Kinematics

2.2.1 Basic assumptions

A plate is a three-dimensional body embedded in an Euclidian three-space $\mathbf{R}^3$. In the undeformed configuration the plate domain Ω is of the following form:

$$\Omega := \left\{ \left(x_1, x_2, x_3\right) \in \mathbf{R}^3 \mid x_3 \in \left[\frac{-h(x_1, x_2)}{2}, \frac{h(x_1, x_2)}{2} \right], \left(x_1, x_2\right) \in A \subset \mathbf{R}^2 \right\}$$

where $h(x_1, x_2)$ is the plate thickness and A is a closed region in the x_1x_2 plane, bounded by a simple closed curve C. Let C_U and C_t be subregions of C such that $\overline{C_U \bigcup C_t} = C$ and $C_U \bigcap C_t = \phi$, where C_U is the part of C on which displacements are specified and C_t is the part of C on which tractions are specified. h is assumed to be small in comparison to a characteristic length of A. The plane $x_3 = 0$ is denoted the mid-surface of the plate. The outward normal unit vector to C in the x_1x_2 plane has the components ν_α, and the counterclockwise tangential unit vector has the components t_α.

The stress resultants are defined as:

$$Q_\alpha := \int_{\frac{-h}{2}}^{\frac{h}{2}} \sigma_{3\alpha}\, dx_3 \qquad \text{Shear resultants.}$$

$$M_{\alpha\beta} := \int_{\frac{-h}{2}}^{\frac{h}{2}} \sigma_{\alpha\beta}\, x_3 dx_3 \qquad \text{Moment resultants.}$$

$$N_{\alpha\beta} := \int_{\frac{-h}{2}}^{\frac{h}{2}} \sigma_{\alpha\beta} dx_3 \qquad \text{Membrane forces.}$$

The distributed loads are defined as:

$$\bar{Q} := \sigma_{33} \Big|_{\frac{-h}{2}}^{\frac{h}{2}} + \int_{\frac{-h}{2}}^{\frac{h}{2}} X_3\, dx_3 \qquad \text{Transverse load.}$$

$$\bar{M}_\alpha := \sigma_{\alpha 3} x_3 \Big|_{\frac{-h}{2}}^{\frac{h}{2}} + \int_{\frac{-h}{2}}^{\frac{h}{2}} X_\alpha x_3\, dx_3 \qquad \text{Couple loads.}$$

$$\bar{N}_\alpha := \sigma_{\alpha 3}\Big|_{\frac{-h}{2}}^{\frac{h}{2}} + \int_{\frac{-h}{2}}^{\frac{h}{2}} X_\alpha \, dx_3 \qquad \text{In-plane loads.}$$

where **X** is the body force vector.

The equilibrium equations for a three-dimensional body are given by:

$$\sigma_{\alpha i,i} + X_\alpha = 0 \tag{2.1a}$$

and

$$\sigma_{3i,i} + X_3 = 0 \tag{2.1b}$$

where the equilibrium equation in the x_3 direction, equation (2.1b), was separated from the other two equilibrium equations (2.1a). Integrating equations (2.1) through the thickness and substituting the definitions for stress resultants yields:

$$N_{\alpha\beta,\beta} + \bar{N}_\alpha = 0 \tag{2.2a}$$

and

$$Q_{\alpha,\alpha} + \bar{Q} = 0 \tag{2.2b}$$

Multiplying equation (2.1a) by x_3 and integrating through the thickness yields:

$$M_{\alpha\beta,\beta} - Q_\alpha + \bar{M}_\alpha = 0 \tag{2.2c}$$

Equations (2.2) are the equilibrium equations for the plate problem, written in resultant form.

The assumed displacement field is taken as:

$$u_\alpha(x_1, x_2, x_3) := U_\alpha(x_1, x_2) + x_3 e_{\alpha\beta}\theta_\beta(x_1, x_2) \tag{2.3a}$$

and

$$u_3(x_1, x_2, x_3) := w(x_1, x_2) \tag{2.3b}$$

where $e_{\alpha\beta}$ is the alternator tensor, defined as:

$$\left[e_{\alpha\beta}\right] := \begin{bmatrix} 0 & 1 \\ -1 & 0 \end{bmatrix}$$

It follows from equations (2.2) and (2.3) that the bending problem is decoupled from the membrane problem. In addition, by equations (2.3), a plane section in the reference configuration remains plane in the deformed configuration. θ_α may be interpreted as the rotation of a fiber initially normal to the plate mid-surface. θ_α is independent of $w_{,\alpha}$ and so a straight fiber initially normal to the mid-surface remains straight, but not necessarily normal to the mid-surface in the deformed configuration. Furthermore, it also follows from the assumed displacement field that the transverse displacement, w, does not vary through the thickness. Consequently, the assumed displacement field implies plane strain behavior.

Sign conventions for the rotations are shown in Figure 2.1, and sign conventions for stress resultants are shown in Figure 2.2.

2.2.2 Strain-displacement relations

It follows from the assumed displacement field, equations (2.3), that the strain-displacement relations are of the following form:

$$\gamma_\alpha = 2\epsilon_{\alpha 3} = 2\epsilon_{3\alpha} = e_{\alpha\beta}\theta_\beta + w_{,\alpha} \tag{2.4a}$$

and

$$\epsilon_{\alpha\beta} = \bar{\epsilon}_{\alpha\beta} - x_3\kappa_{\alpha\beta} \tag{2.4b}$$

where κ is the curvature tensor, defined as:

$$\kappa_{\alpha\beta} := -\frac{1}{2}(e_{\alpha\gamma}\theta_{\gamma,\beta} + e_{\beta\gamma}\theta_{\gamma,\alpha}) \tag{2.5}$$

and $\bar{\epsilon}_{\alpha\beta}$ is the membrane strain tensor, defined as:

$$\bar{\epsilon}_{\alpha\beta} := \frac{1}{2}(U_{\alpha,\beta} + U_{\beta,\alpha}) \tag{2.6}$$

Plate kinematics are summarized in Figure 2.3.

2.3 Boundary Conditions

The method of virtual work is used to derive the boundary conditions for the plate theory presented in Section 2.1. First, the following definitions are introduced:

$M_n := \nu_\alpha \nu_\beta M_{\alpha\beta}$ Normal bending moment.

$M_{nt} := \nu_\alpha t_\beta M_{\alpha\beta}$ Twist moment.

and

$Q_n := \nu_\alpha Q_\alpha$ Normal shear.

Let $\delta\epsilon$ denote a virtual strain field. The internal virtual work is defined as:

$$\begin{aligned}
\delta W_i &= \int_A \int_{\frac{-h}{2}}^{\frac{h}{2}} \sigma_{ij}\, \delta\epsilon_{ij}\, dx_3\, dA \\
&= \int_A \left\{ N_{\alpha\beta}\, \delta\bar{\epsilon}_{\alpha\beta} + e_{\beta\gamma} M_{\alpha\beta}\, \delta\theta_{\gamma,\alpha} + Q_\alpha (e_{\alpha\gamma}\, \delta\theta_\gamma + \delta w_{,\alpha}) \right\} dA \\
&= \int_A \left\{ (N_{\alpha\beta}\, \delta U_\beta + e_{\beta\gamma} M_{\alpha\beta}\, \delta\theta_\gamma + Q_\alpha\, \delta w)_{,\alpha} \right\} dA \qquad (2.7) \\
&\quad - \int_A \left\{ N_{\alpha\beta,\beta} \delta U_\alpha - e_{\alpha\gamma} (Q_\alpha - M_{\alpha\beta,\beta})\, \delta\theta_\gamma + Q_{\alpha,\alpha}\, \delta w \right\} dA
\end{aligned}$$

The virtual-work principle, $\delta W_i = \delta W_e$, may be rewritten as:

$$\delta W_i - \delta W_e^1 = \delta W_e^2 \qquad (2.8)$$

where δW_e^1 denotes the external virtual-work due to body forces and surface tractions on the planes $x_3 = \pm \frac{h}{2}$, and δW_e^2 denotes the external virtual-work due to applied forces and moments along the edge. Accordingly, δW_e^1 is given by:

$$\delta W_e^1 = \int_A \left[\bar{N}_\alpha \delta U_\alpha + e_{\alpha\gamma} \bar{M}_\alpha\, \delta\theta_\gamma + \bar{Q}\, \delta w \right] dA \qquad (2.9)$$

so that, upon using the two-dimensional divergence theorem and the equilibrium equations, equations (2.2), equations (2.7) and (2.9) may be combined to obtain:

$$\delta W_i - \delta W_e^1 = \int_C \nu_\alpha (N_{\alpha\beta} \delta U_\beta + e_{\beta\gamma} M_{\alpha\beta}\, \delta\theta_\gamma + Q_\alpha\, \delta w)\, ds \qquad (2.10)$$

Let $-e_{\alpha\beta}\theta_\beta = \nu_\alpha\theta_n + t_\alpha\theta_t$, where θ_n is the rotation about the tangent to the edge, and θ_t is the rotation about the normal to the edge; thus:

$$\nu_\alpha e_{\beta\gamma} M_{\alpha\beta}\delta\theta_\gamma = M_n\,\delta\theta_n + M_{nt}\,\delta\theta_t \tag{2.11}$$

Substituting equation(2.11) into equation (2.10) and taking notice of the normal shear definition, yields the following expression:

$$\delta W_i - \delta W_e{}^1 = \int_C \left[\nu_\alpha N_{\alpha\beta}\delta U_\beta + M_n\,\delta\theta_n + M_{nt}\,\delta\theta_t + Q_n\,\delta w \right] ds \tag{2.12}$$

Let the applied transverse shear be denoted as Q_n^a, the applied in-plane force along the edge be be denoted as N_α^a, the applied normal bending moment be denoted as M_n^a, and the applied twist moment be denoted as M_{nt}^a. Noting that M_n^a and M_{nt}^a may be specified independently, $\delta W_e{}^2$ is given by:

$$\delta W_e{}^2 = \int_C \left[N_\alpha^a\,\delta U_\alpha + M_n^a\,\delta\theta_n + M_{nt}^a\,\delta\theta_t + Q_n^a\,\delta w \right] ds \tag{2.13}$$

It follows from equations (2.8), (2.12) and (2.13) that the boundary conditions for the plate problem are as follows:

either $\nu_\beta N_{\alpha\beta} = N_\alpha^a$ or U_α is prescribed.

either $M_n = M_n^a$ or θ_n is prescribed;

either $M_{nt} = M_{nt}^a$ or θ_t is prescribed;

and either $Q_n = Q_n^a$ or w is prescribed.

In the above, s is the arc length along the boundary, and the superscript a stands for applied boundary conditions.

The bending boundary-value problem involves three types of homogeneous boundary conditions:

Simply supported: $w = M_n = 0$ and either $M_{nt} = 0$ or $\theta_t = 0$.

Clamped: $w = \theta_n = \theta_t = 0$.

Free: $M_n = M_{nt} = Q_n = 0$.

The in-plane boundary-value problem involves two types of homogeneous boundary conditions:

Fixed: $U_\alpha = 0$.

Free: $N_\alpha^a = 0$.

2.4 Constitutive Equations

The assumed displacement field implies plane strain behavior. This assumption, however, is not a valid representation of plate behavior. Rather, the stresses σ_{i3} are negligible in comparison to $\sigma_{\alpha\beta}$. Therefore, a plane stress assumption is a much better approximation of the plate behavior. σ_{33} is assumed to be zero pointwise. $\sigma_{\alpha 3}$, on the other hand, are needed for the equilibrium equations. In practice, the contradiction with the plane strain assumption causes no problem.

Substituting $\sigma_{33} = 0$ into the three-dimensional constitutive equations, eliminating ϵ_{33} and integrating through the thickness yields the constitutive equations for the plate. For the case of homogeneous isotropic linearly elastic materials the three-dimensional constitutive equations are as follows:

$$\sigma_{ij} := \lambda \delta_{ij} \epsilon_{kk} + 2\mu \epsilon_{ij}$$

where λ and μ are the Lamé coefficients and δ_{ij} is the Kronecker delta. $\sigma_{33} = 0$ implies:

$$\epsilon_{33} = \frac{-\lambda}{\lambda + 2\mu} \epsilon_{\alpha\alpha}$$

The constitutive equations for the plate are as follows:

$$\sigma_{\alpha\beta} = \bar{\lambda} \delta_{\alpha\beta} \epsilon_{\gamma\gamma} + 2\mu \epsilon_{\alpha\beta}$$

and

$$\sigma_{\alpha 3} = 2\mu \epsilon_{\alpha 3}$$

where

$$\bar{\lambda} = \frac{2\lambda\mu}{\lambda + 2\mu}$$

The constitutive equations may be rewritten in terms of the membrane forces, **N**; the resultant moments, **M**; the shear resultants, **Q**; the curvature, κ; the shear strain γ; and the in-plane strain $\bar{\epsilon}$, as:

$$N_{\alpha\beta} = \mathbf{C}^{n}_{\alpha\beta\gamma\delta}\bar{\epsilon}_{\gamma\delta} \tag{2.14a}$$

$$M_{\alpha\beta} = \mathbf{C}^{b}_{\alpha\beta\gamma\delta}\kappa_{\gamma\delta} \tag{2.14b}$$

and

$$\mathbf{Q}_{\alpha} = \alpha\, \mathbf{C}^{s}_{\alpha\beta}\,\gamma_{\beta} \tag{2.14c}$$

where $\mathbf{C}^{n}$ is the elastic coefficients tensor for the membrane effect, given by:

$$\mathbf{C}^{n}_{\alpha\beta\gamma\delta} = h\left[\mu\left(\delta_{\alpha\gamma}\delta_{\beta\delta} + \delta_{\alpha\delta}\delta_{\gamma\delta}\right) + \bar{\lambda}\,\delta_{\alpha\beta}\delta_{\gamma\delta}\right] \tag{2.15}$$

$\mathbf{C}^{b}$ is the elastic coefficients tensor for the bending effect, given by:

$$\mathbf{C}^{b}_{\alpha\beta\gamma\delta} = \frac{h^3}{12}\left[\mu\left(\delta_{\alpha\gamma}\delta_{\beta\delta} + \delta_{\alpha\delta}\delta_{\gamma\delta}\right) + \bar{\lambda}\,\delta_{\alpha\beta}\delta_{\gamma\delta}\right] \tag{2.16}$$

α is a correction factor introduced in order to obtain consistent results with the three-dimensional theory, quadratic variation of the transverse shear along a fiber normal to the mid-surface, (usually $\alpha = \frac{5}{6}$); and $\mathbf{C}^{s}$ is a second order tensor, of the elastic coefficients for shear, given by:

$$\mathbf{C}^{s}_{\alpha\beta} = h\,\mu\,\delta_{\alpha\beta} \tag{2.17}$$

$\bar{\lambda}$ and μ may be eliminated in favor of Young's modulus, E, and Poisson's ratio, ν:*

$$\bar{\lambda} = \frac{\nu E}{1-\nu^2} \quad ; \quad \mu = \frac{E}{2(1+\nu)}$$

2.5 Strong Form

The formal statement of the strong form of the plate bending boundary-value problem is summarized in Box 2.1, and that of the plane stress/strain boundary-value problem is summarized in Box 2.2.

* A plane strain formulation for the membrane part may be obtained by setting h to 1, and replacing $\bar{\lambda}$ by λ, where λ is given by:

$$\lambda = \frac{\nu E}{(1+\nu)(1-2\nu)}$$

Box 2.1: Plate Bending - Strong Form

Given $\bar{M}_\alpha$, $\bar{Q}$, M_n^a, M_{nt}^a, Q_n^a, W^a, θ_n^a and θ_t^a; find w, θ_α, Q_α and $M_{\alpha\beta}$ such that:

$$
\text{in } A \begin{cases}
M_{\alpha\beta,\beta} - Q_\alpha + \bar{M}_\alpha = 0 \\
Q_{\alpha,\alpha} + \bar{Q} = 0 \\
M_{\alpha\beta} = \mathbf{C}^b_{\alpha\beta\gamma\delta}\kappa_{\gamma\delta} \\
Q_\alpha = \alpha\, \mathbf{C}^s_{\alpha\beta}\gamma_\beta \\
\kappa_{\alpha\beta} = -\frac{1}{2}(e_{\alpha\gamma}\theta_{\gamma,\beta} + e_{\beta\gamma}\theta_{\gamma,\alpha}) \\
\gamma_\alpha = e_{\alpha\beta}\theta_\beta + w_{,\alpha}
\end{cases}
$$

$$
\text{on } C_U \begin{cases}
\theta_\alpha = \theta_\alpha^a \\
w = W^a
\end{cases}
$$

$$
\text{on } C_t \begin{cases}
M_n = M_n^a \\
M_{nt} = M_{nt}^a \\
Q_n = Q_n^a
\end{cases}
$$

2.6 Matrix Notation

The plate theory presented above in tensor notation is now rewritten in matrix notation, which is the standard notation used in the finite element method. The following vectors are introduced:

$\mathbf{U}^n$ is the in-plane displacement vector, defined as: $\mathbf{U}^{nT} := < U_1, U_2 >$,

$\mathbf{U}^b$ is the "bending displacement" vector, defined as: $\mathbf{U}^{bT} := < w, \theta_1, \theta_2 >$,

Box 2.2: Plane stress/strain - Strong Form

Given $\bar{N}_\alpha$, N^a_α, and U^a_α; find U_α and $N_{\alpha\beta}$ such that:

$$\text{in } A \begin{cases} N_{\alpha\beta,\beta} + \bar{N}_\alpha = 0 \\ N_{\alpha\beta} = \mathbf{C}^n_{\alpha\beta\gamma\delta}\bar{\epsilon}_{\gamma\delta} \\ \bar{\epsilon}_{\alpha\beta} = \frac{1}{2}(U_{\alpha,\beta} + U_{\beta,\alpha}) \end{cases}$$

$$\text{on } C_U \begin{cases} U_\alpha = U^a_\alpha \end{cases}$$

$$\text{on } C_t \begin{cases} \nu_\beta N_{\alpha\beta} = N^a_\alpha \end{cases}$$

γ is the shear strain vector, defined as: $\gamma^T := <\gamma_1, \gamma_2>$,

κ is the curvature vector, defined as: $\kappa^T := <\kappa_{11}, \kappa_{22}, \kappa_{12}>$,

$\mathbf{P}$ is the membrane strain vector, defined as: $\mathbf{P}^T := <\bar{\epsilon}_{11}, \bar{\epsilon}_{22}, \bar{\epsilon}_{12}>$,

$\mathbf{Q}$ is the shear resultant vector, defined as: $\mathbf{Q}^T := <Q_1, Q_2>$,

$\mathbf{M}$ is the moment resultant vector, defined as: $\mathbf{M}^T := <M_{11}, M_{22}, M_{12}>$, and

$\mathbf{N}$ is the membrane resultant vector, defined as: $\mathbf{N}^T := <N_{11}, N_{22}, N_{12}>$.

The shear strain displacement relation is given by:

$$\gamma = \mathbf{L}^s\, \mathbf{U}^b$$

the curvature displacement relation is given by:

$$\kappa = \mathbf{L}^b\, \mathbf{U}^b$$

and the membrane strain displacement relation is given by:

$$\mathbf{P} = \mathbf{L}^n\, \mathbf{U}^n$$

where $\mathbf{L}^s$ is the shear strain displacement operator, given by:

$$\mathbf{L}^s := \begin{bmatrix} \frac{\partial}{\partial x_1} & 0 & 1 \\ \frac{\partial}{\partial x_2} & -1 & 0 \end{bmatrix} \tag{2.18}$$

$\mathbf{L}^b$ is the curvature displacement operator, given by:

$$\mathbf{L}^b := \begin{bmatrix} 0 & 0 & -\frac{\partial}{\partial x_1} \\ 0 & \frac{\partial}{\partial x_2} & 0 \\ 0 & \frac{\partial}{\partial x_1} & -\frac{\partial}{\partial x_2} \end{bmatrix} \tag{2.19}$$

and $\mathbf{L}^n$ is the membrane strain displacement operator, given by:

$$\mathbf{L}^n := \begin{bmatrix} \frac{\partial}{\partial x_1} & 0 \\ 0 & \frac{\partial}{\partial x_2} \\ \frac{\partial}{\partial x_2} & \frac{\partial}{\partial x_1} \end{bmatrix} \tag{2.20}$$

The constitutive equations relating the shear resultants to the shear strain, in matrix form, are given by:

$$\mathbf{Q} = \mathbf{D}^s \boldsymbol{\gamma}$$

the constitutive equations relating the moment resultants to the curvature, in matrix form, are given by:

$$\mathbf{M} = \mathbf{D}^b \boldsymbol{\kappa}$$

and the constitutive equations relating the membrane resultants to the in-plane strains, in matrix form, are given by:

$$\mathbf{N} = \mathbf{D}^n \mathbf{P}$$

where $\mathbf{D}^s$ is the shear elastic coefficients matrix, given by:

$$\mathbf{D}^s = \frac{\alpha E h}{2(1+\nu)} \begin{bmatrix} 1 & 0 \\ 0 & 1 \end{bmatrix} \tag{2.21}$$

$\mathbf{D}^b$ is the bending elastic coefficients matrix, given by:

$$\mathbf{D}^b = \frac{E h^3}{12(1-\nu^2)} \begin{bmatrix} 1 & \nu & 0 \\ \nu & 1 & 0 \\ 0 & 0 & \frac{1}{2}(1-\nu) \end{bmatrix} \tag{2.22}$$

and $\mathbf{D}^n$ is given by:

$$\mathbf{D}^n = \frac{E h}{1-\nu^2} \begin{bmatrix} 1 & \nu & 0 \\ \nu & 1 & 0 \\ 0 & 0 & \frac{1}{2}(1-\nu) \end{bmatrix} \tag{2.23a}$$

for the case of plane stress and by:

$$\mathbf{D}^n = \frac{E}{(1+\nu)(1-2\nu)} \begin{bmatrix} 1-\nu & \nu & 0 \\ \nu & 1-\nu & 0 \\ 0 & 0 & \frac{1}{2}(1-2\nu) \end{bmatrix} \tag{2.23b}$$

for the case of plane strain.

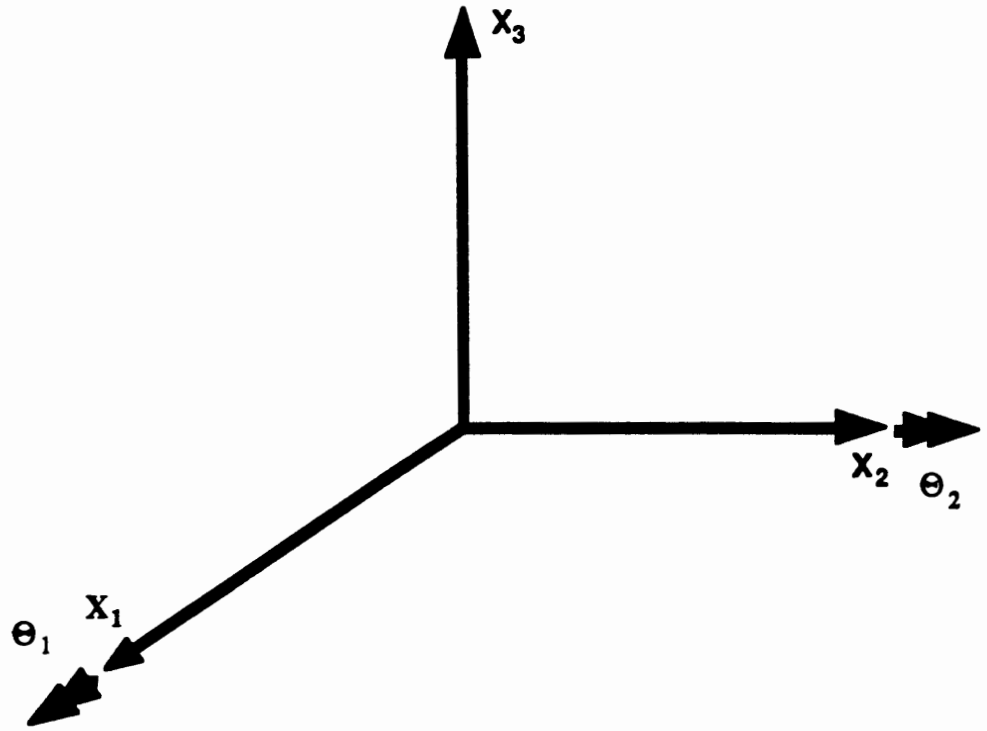

Figure 2.1: Sign convention for rotations, right-hand-rule rotations.

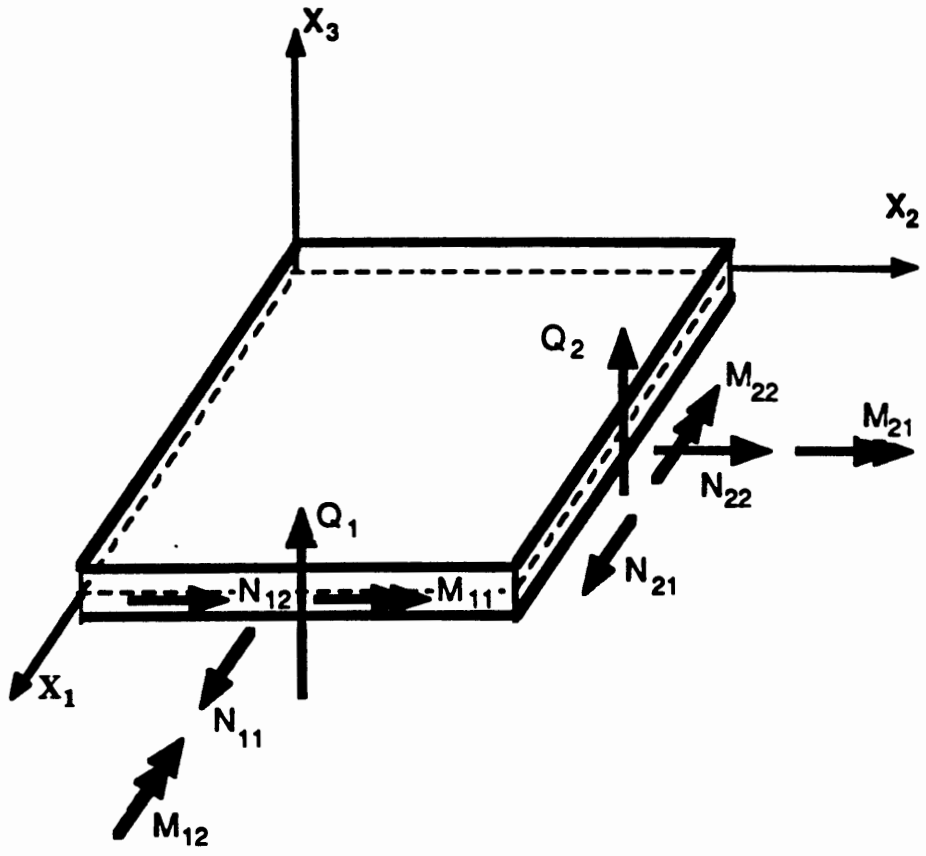

Figure 2.2: Sign convention for stress resultants on positive faces.

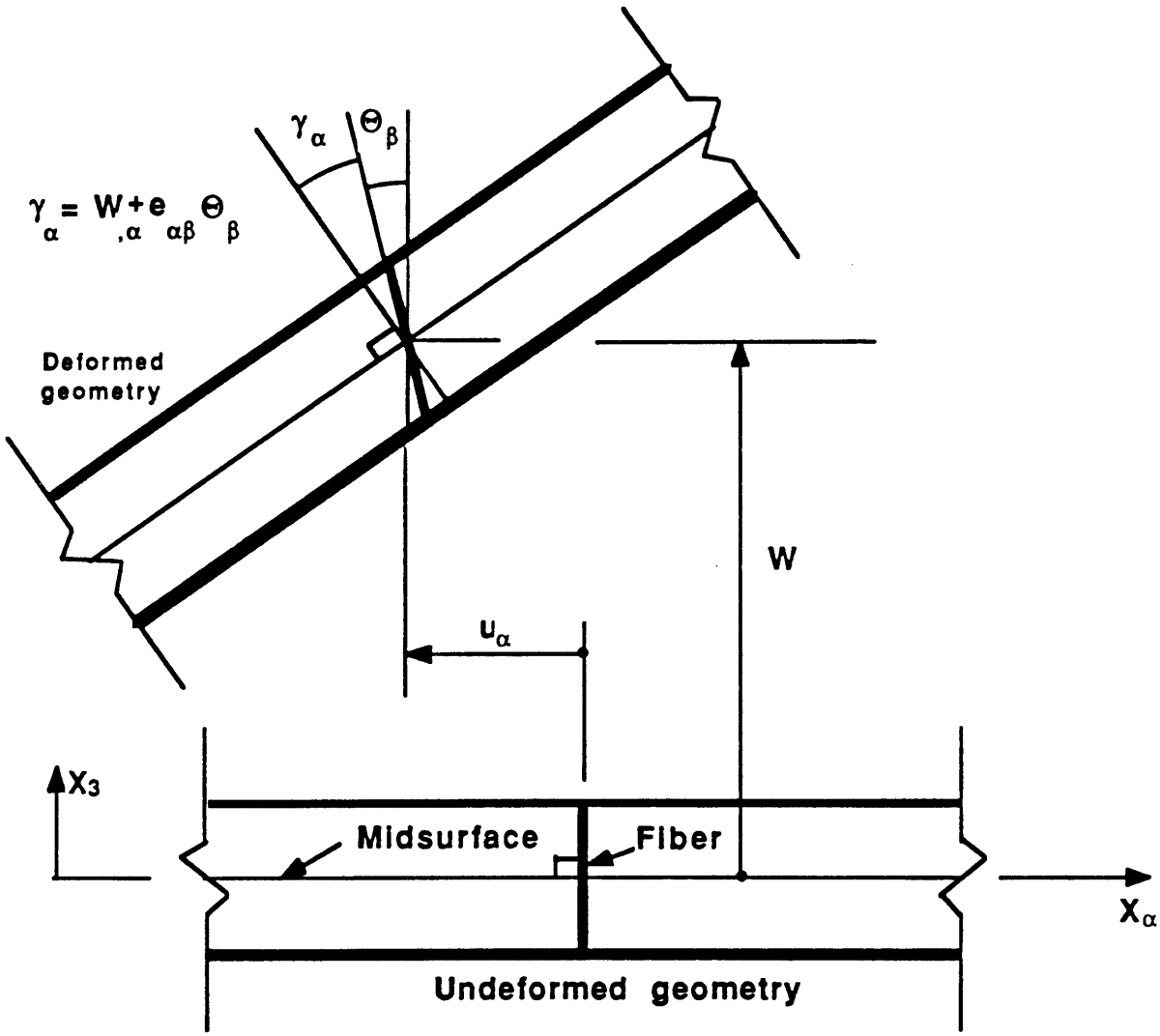

Figure 2.3: Plate kinematics.

CHAPTER 3: MIXED FORMULATIONS FOR PLATE BENDING AND PLATE BOUNDARY-VALUE PROBLEMS

3.1 Introduction

The weak form counterpart of the strong form presented in Chapter 2 is derived, in parallel and independently, from the Hellinger-Reissner and Hu-Washizu mixed variational principles. The weak form is then used to obtain the finite element stiffness matrix and load vector.

In order to emulate the equilibrium equations structure, the following couplings are introduced in the finite element approximations of the stress resultant and strain fields: an explicit coupling between the assumed moment resultant and shear resultant fields, and an explicit coupling between the assumed curvature and shear-strain fields. It will be shown in Chapter 4 that as a consequence of these couplings the resulting plate bending elements do not lock in shear at the thin plate limit. A method to generate the assumed stress resultant and strain fields will be given in Chapter 5.

Because the strong forms of the in-plane and plate bending problems are decoupled (see Chapter 2), the two problems are treated independently. The Hellinger-Reissner and Hu-Washizu variational functionals are used in both cases.

The superscripts b and n on U will be omitted. It will be clear from the context which displacement field is referenced. Furthermore, to avoid cumbersome notations in the finite element approximation subsections, the superscript h denoting the finite element approximation will be omitted with the understanding that the finite element approximations used are all proper subspaces of the corresponding spaces introduced in the weak form subsections.

3.2 Approximation of the Assumed Fields

Both the Hellinger-Reissner and the Hu-Washizu mixed variational principles, which form the theoretical framework for this dissertation, involve the use of assumed independent displacement and stress resultant variables. The Hu-Washizu principle requires in

addition the use of assumed independent strain variables. In this section, the approximation of these fields is introduced and motivated.

3.2.1 Assumed displacement field

The displacement field, U, is approximated by an interpolation between displacements at discrete points, known as nodes in the finite element terminology. The following approximation is used (summation convention is implied):

$$U = N_I(\xi)\, d_I \tag{3.1}$$

where $N_I(\xi)$ is the shape function associated with node I (N_I is a function of the element natural coordinates $\xi^T = <\xi, \eta>$), and d_I is the displacement vector associated with node I, given by:

$$d_I^{bT} = <W_I, \theta_{1I}, \theta_{2I}> \tag{3.2a}$$

for the plate bending problem, and by:

$$d_I^{nT} = <U_{1I}, U_{2I}> \tag{3.2b}$$

for the in-plane problem.

3.2.2 Assumed stress fields

Plate boundary-value problems involve membrane forces, moment resultants and shear resultants. It follows from the governing balance equations, (2.2), that the moment and shear resultant fields are coupled. The coupling is such that it is possible to obtain a state of pure moment but not one of pure shear. Following this observation, the stress field is assumed as:

$$\mathbf{N} := \tilde{\mathbf{N}}(\xi)\, \mathbf{n} \tag{3.3a}$$

$$\mathbf{M} := \tilde{\mathbf{M}}(\xi)\, \mathbf{m} + \mathbf{S}(\xi)\, \mathbf{q} \tag{3.3b}$$

and

$$\mathbf{Q} := \tilde{\mathbf{Q}}(\xi)\, \mathbf{q} \tag{3.3c}$$

where **n** is the membrane force coefficients vector, **m** is the moment resultant coefficients vector, **q** is the shear resultant coefficients vector and the second term in equation (3.3b) is the explicit coupling term introduced in this dissertation. In the finite element approximation, **n**, **q** and **m** will be defined at the element level.

3.2.3 Assumed strain fields

Plate boundary-value problems involve membrane strain, curvature and shear strain. The curvature and shear strain fields are coupled in such a way that a state of pure curvature is possible, but not one of pure shear strain. Following this observation, the strain field is assumed as:

$$\mathbf{P} := \tilde{\mathbf{P}}(\xi)\,\mathbf{p} \tag{3.4a}$$

$$\kappa := \tilde{\kappa}(\xi)\,\mathbf{k} + \mathbf{R}(\xi)\,\mathbf{e} \tag{3.4b}$$

and

$$\gamma := \Gamma(\xi)\,\mathbf{e} \tag{3.4c}$$

where **p** is the membrane strain coefficients vector, **k** is the curvature coefficients vector, **e** is the shear strain coefficients vector and the second term in equation (3.4b) is the coupling term introduced in this dissertation.

3.3 Hellinger-Reissner Mixed Formulation for Plate Bending

3.3.1 The energy functional

The Hellinger-Reissner functional is a two-field principle: the energy functional is stated in terms of displacements and stress resultants as independent fields. For the case of a plate bending boundary-value problem, the energy functional is stated as follows:

$$\Pi_R(\mathbf{M},\mathbf{Q},\mathbf{U}) := \int_A \left\{ -\frac{1}{2}(\mathbf{M}^T(\mathbf{D}^b)^{-1}\mathbf{M} + \mathbf{Q}^T(\mathbf{D}^s)^{-1}\mathbf{Q}) + \mathbf{M}^T\mathbf{L}^b\,\mathbf{U} + \mathbf{Q}^T\mathbf{L}^s\,\mathbf{U} \right\} dA$$

$$- \int_A \mathbf{U}^T\mathbf{F}\,dA - \int_{C_t} \mathbf{U}^T\mathbf{t}\,ds \tag{3.5}$$

where:

$\mathbf{F}^T = <\bar{\mathbf{Q}}, \bar{\mathbf{M}}_1, \bar{\mathbf{M}}_2>$ is the body resultants vector; and

$\mathbf{t}^T = <\bar{\mathbf{Q}}_n^a, \bar{\mathbf{M}}_n^a, \bar{\mathbf{M}}_{nt}^a>$ is the applied boundary traction vector.

3.3.2 Weak form

To define the weak, or variational, form a number of classes of functions must be characterized as follows:

Trial displacement solutions:*

$$U := \left\{ \mathbf{U} \mid \mathbf{U} \in H^1(\bar{\Omega}), \mathbf{U} = \mathbf{U}^a \text{ on } C_U \right\} \tag{3.6}$$

Displacement weighting functions:

$$\bar{U} := \left\{ \mathbf{U} \mid \mathbf{U} \in H^1(\bar{\Omega}), \mathbf{U} = \mathbf{0} \text{ on } C_U \right\} \tag{3.7}$$

Trial moment solutions:

$$M := \left\{ \mathbf{M} \mid \mathbf{M} \in H^0(\bar{\Omega}) \right\} \tag{3.8}$$

and trial shear resultant solutions:

$$Q := \left\{ \mathbf{Q} \mid \mathbf{Q} \in H^0(\bar{\Omega}) \right\} \tag{3.9}$$

Note that the spaces of functions introduced as moments and shear resultant solution spaces may also be used as the spaces for the moment and shear resultant weight functions,

* A function G is said to be a member of H^n if the function and its first n derivatives are members of L_2. A function F is said to be a member of L_2 if it is square-integrable, i.e., $\int_A F^2\,dA < \infty$.

respectively.

The first variation of the energy functional is given by:

$$\delta\Pi_R(\mathbf{M},\mathbf{Q},\mathbf{U}) = \int_A \delta\mathbf{M}^T(\mathbf{L}^b\,\mathbf{U} - (\mathbf{D}^b)^{-1}\mathbf{M})\,dA + \int_A \delta\mathbf{Q}^T(\mathbf{L}^s\,\mathbf{U} - (\mathbf{D}^s)^{-1}\mathbf{Q})\,dA$$

$$+ \int_A \left\{ (\mathbf{L}^b\,\delta\mathbf{U})^T\mathbf{M} + (\mathbf{L}^s\,\delta\mathbf{U})^T\mathbf{Q} - \delta\mathbf{U}^T\mathbf{F} \right\} dA - \int_{C_t} \delta\mathbf{U}^T\mathbf{t}\,ds = 0 \qquad (3.10)$$

The first two terms are the weak form of the constitutive equations. After integration by parts, the last two terms provide the balance of momentum equations for the plate bending problem. The formal statement of the weak form is given in Box 3.1.

Box 3.1: Plate Bending - Hellinger-Reissner Weak Form

Given $\overline{\mathbf{M}}$, $\overline{\mathbf{Q}}$, $\mathbf{M}_n^a$, $\mathbf{M}_{nl}^a$, $\mathbf{Q}_n^a$ and $\mathbf{U}^a$; find $\mathbf{U} \in U$, $\mathbf{M} \in M$ and $\mathbf{Q} \in Q$ such that for every $\delta\mathbf{U} \in \overline{U}$, $\delta\mathbf{M} \in M$ and $\delta\mathbf{Q} \in Q$

$$0 = \int_A \delta\mathbf{M}^T(\mathbf{L}^b\mathbf{U} - (\mathbf{D}^b)^{-1}\mathbf{M})\,dA + \int_A \delta\mathbf{Q}^T(\mathbf{L}^S\mathbf{U} - (\mathbf{D}^s)^{-1}\mathbf{Q})\,dA$$

$$+ \int_A \left\{ (\mathbf{L}^b\delta\mathbf{U})^T\mathbf{M} + (\mathbf{L}^s\delta\mathbf{U})^T\mathbf{Q} - \delta\mathbf{U}^T\mathbf{F} \right\} dA - \int_{C_t} \delta\mathbf{U}^T\mathbf{t}\,ds$$

3.3.3 Finite element stiffness matrix and load vector

The finite element stiffness matrix and load vector may be obtained from the weak form presented in Section 3.3.2. Substituting the finite element approximations of the assumed fields, as presented in Section 3.2, the first variation of the Hellinger-Reissner functional is as follows:

$$\begin{aligned}\delta\Pi_R(\mathbf{m},\mathbf{q},\mathbf{d}) &= \delta\mathbf{m}^T(\mathbf{G}_m^b\,\mathbf{d} - \mathbf{H}_{mm}^b\,\mathbf{m} - \mathbf{H}_{mq}^b\,\mathbf{q}) \\ &+ \delta\mathbf{q}^T(\mathbf{G}_q^b\mathbf{d} + \mathbf{G}^s\,\mathbf{d} - \mathbf{H}_{mq}^{bT}\,\mathbf{m} - \mathbf{H}_{qq}^b\,\mathbf{q} - \mathbf{H}^s\,\mathbf{q}) \\ &+ \delta\mathbf{d}^T(\mathbf{G}_m^{bT}\mathbf{M} + \mathbf{G}_q^{bT}\mathbf{q} + \mathbf{G}^{sT}\,\mathbf{q}) - \delta\mathbf{d}^T\mathbf{f}\end{aligned} \tag{3.11}$$

where $\mathbf{f}$ is the load vector resulting from body forces and boundary tractions, and the following definitions have been introduced:

$$\begin{gathered}\mathbf{H}_{mm}^b := \int_A \tilde{\mathbf{M}}^T(\mathbf{D}^b)^{-1}\tilde{\mathbf{M}}\,dA \quad ; \quad \mathbf{H}_{mq}^b := \int\tilde{\mathbf{M}}^T(\mathbf{D}^b)^{-1}\mathbf{S}\,dA \;; \\ \mathbf{H}_{qq}^b := \int_A \mathbf{S}^T(\mathbf{D}^b)^{-1}\mathbf{S}\,dA \quad ; \quad \mathbf{H}^s := \int_A\tilde{\mathbf{Q}}^T(\mathbf{D}^s)^{-1}\tilde{\mathbf{Q}}\,dA \;; \\ \mathbf{G}_m^b := \int_A\tilde{\mathbf{M}}^T\mathbf{B}^b\,dA \;;\; \mathbf{G}_q^b := \int_A\mathbf{S}^T\mathbf{B}^b\,dA \;;\; \mathbf{G}^s := \int_A\tilde{\mathbf{Q}}^T\mathbf{B}^s\,dA\end{gathered} \tag{3.12}$$

In the above, $\mathbf{B}^b$ is the finite element curvature-displacement relation, defined by:

$$\mathbf{B}_I^b\,\mathbf{d}_I := \mathbf{L}^b\,\mathbf{U} \tag{3.13}$$

where $\mathbf{B}_I^b$ is associated with node I and is given by:

$$\mathbf{B}_I^b := \begin{bmatrix}0 & 0 & -N_{I,1}\\ 0 & N_{I,2} & 0\\ 0 & N_{I,1} & -N_{I,2}\end{bmatrix} \tag{3.14}$$

and $\mathbf{B}^s$ is the finite element shear strain-displacement relation, defined by:

$$\mathbf{B}_I^s\,\mathbf{d}_I := \mathbf{L}^s\,\mathbf{U} \tag{3.15}$$

where $\mathbf{B}_I^s$ is associated with node I and is given by:

$$\mathbf{B}_I^s := \begin{bmatrix}N_{I,1} & 0 & N_I\\ N_{I,2} & -N_I & 0\end{bmatrix} \tag{3.16}$$

In equation (3.11), $\mathbf{H}_{qq}^b$, $\mathbf{H}_{mq}^b$ and $\mathbf{G}_q^b$ reflect the effect of the explicit coupling introduced. In the absence of "loading" terms from the constitutive equations (e.g., thermal terms), the Euler-Lagrange equations may be written as:

$$\begin{bmatrix}-\mathbf{H} & \mathbf{G}\\ \mathbf{G}^T & \mathbf{0}\end{bmatrix}\begin{Bmatrix}\tau\\ \mathbf{d}\end{Bmatrix} = \begin{Bmatrix}\mathbf{0}\\ \mathbf{f}\end{Bmatrix} \tag{3.17}$$

where

$$\mathbf{H} := \begin{bmatrix} \mathbf{H}^b_{mm} & \mathbf{H}^b_{mq} \\ \mathbf{H}^{bT}_{mq} & \mathbf{H}^b_{qq} + \mathbf{H}^s \end{bmatrix} \quad ; \quad \mathbf{G} := \begin{Bmatrix} \mathbf{G}^b_m \\ \mathbf{G}^b_q + \mathbf{G}^s \end{Bmatrix} \quad ; \quad \tau := \begin{Bmatrix} \mathbf{m} \\ \mathbf{q} \end{Bmatrix} \tag{3.18}$$

Elimination of the stress resultant coefficients,τ, for all elements yields:

$$\mathbf{K}\,\mathbf{d} = \mathbf{f} \tag{3.19}$$

where **K** is the finite element stiffness matrix, defined as:

$$\mathbf{K} := \mathbf{G}^T \mathbf{H}^{-1} \mathbf{G} \tag{3.20}$$

and **f** is the load vector, defined as:

$$f_I := \int_A N_I \,\mathbf{F}\, dA + \int_{C_t} N_I \,\mathbf{t}\, ds \tag{3.21}$$

Since stress resultant interpolations are independent in each element, the elimination of τ may be performed at the element level.

In order to satisfy the mixed patch test (Zienkiewicz, Qu, Taylor & Nakazawa [1986]), the following requirements must be satisfied for all admissible boundary conditions on θ_1, θ_2 and w (i.e., d_I):

$$n_m + n_q \geq n_\theta \tag{3.22a}$$

and

$$n_q \geq n_w \tag{3.22b}$$

where n_m and n_q are the number of moment and shear coefficients, respectively, n_θ is the number of rotational degrees of freedom, and n_w is the number of transverse displacement degrees of freedom.

The stress resultant coefficients may be obtained in terms of the nodal displacements, $\mathbf{d}_I$, as follows:

Shear coefficients:

$$\mathbf{q} = \left[\mathbf{H}^b - \mathbf{H}^s\right]^{-1} \left[\mathbf{G}^b - \mathbf{G}^s\right] \mathbf{d} = \mathbf{F}_1 \mathbf{d} \tag{3.23}$$

and, moment coefficients:

$$\mathbf{m} = (\mathbf{H}_{mm}^{b})^{-1}\left[\mathbf{G}_{m}^{b} - \mathbf{H}_{mq}^{b}\,\mathbf{F}_{1}\right]\mathbf{d} = \mathbf{F}_{2}\mathbf{d} \tag{3.24}$$

where

$$\mathbf{H}^{b} := \mathbf{H}_{mq}^{bT}(\mathbf{H}_{mm}^{b})^{-1}\mathbf{H}_{mq}^{b} - \mathbf{H}_{qq}^{b} \tag{3.25}$$

and

$$\mathbf{G}^{b} := \mathbf{H}_{mq}^{bT}(\mathbf{H}_{mm}^{b})^{-1}\mathbf{G}_{m}^{b} - \mathbf{G}_{q}^{b} \tag{3.26}$$

3.4 Hu-Washizu Mixed Formulation for Plate Bending

3.4.1 The energy functional

The Hu-Washizu functional is a three-field variational principle: the functional is stated in terms of assumed independent displacement, stress, and strain fields. For the case of plate bending boundary-value problems, the energy functional is stated as follows:

$$\Pi_{H}(\mathbf{M},\mathbf{Q},\kappa,\gamma,\mathbf{U}) := \int_{A}\left[\frac{1}{2}(\kappa^{T}\mathbf{D}^{b}\,\kappa + \gamma^{T}\mathbf{D}^{s}\,\gamma) - \mathbf{Q}^{T}(\gamma - \mathbf{L}^{s}\mathbf{U})\right.$$

$$\left. - \mathbf{M}^{T}(\kappa - \mathbf{L}^{b}\mathbf{U}) - \mathbf{U}^{T}\mathbf{F}\right]dA - \int_{C_t}\mathbf{U}^{T}\mathbf{t}\,ds \tag{3.27}$$

3.4.2 Weak form

To define the weak form of the Hu-Washizu functional, two additional classes of functions must be characterized, as follows:

Trial curvature solution:

$$\boldsymbol{K} := \left\{\kappa \mid \kappa \in H^{0}(\bar{\Omega})\right\} \tag{3.28}$$

and trial shear strain solution:

$$\boldsymbol{G} := \left\{\gamma \mid \gamma \in H^{0}(\bar{\Omega})\right\} \tag{3.29}$$

Note that the curvature and shear strain trial solution spaces may be used as the spaces for the curvature and shear strain weight functions, respectively.

The first variation of the Hu-Washizu functional is given by:

$$\begin{aligned}\delta\Pi_H(\mathbf{M},\mathbf{Q},\boldsymbol{\kappa},\boldsymbol{\gamma},\mathbf{U}) := & -\int_A \delta\mathbf{M}^T(\boldsymbol{\kappa}-\mathbf{L}^b\mathbf{U})\,dA - \int_A \delta\mathbf{Q}^T(\boldsymbol{\gamma}-\mathbf{L}^s\mathbf{U})\,dA \\ & + \int_A \delta\boldsymbol{\kappa}^T(\mathbf{D}^b\boldsymbol{\kappa}-\mathbf{M})\,dA + \int_A \delta\boldsymbol{\gamma}^T(\mathbf{D}^s\boldsymbol{\gamma}-\mathbf{Q})\,dA \\ & + \int_A (\mathbf{L}^b\delta\mathbf{U})^T\mathbf{M}\,dA + \int_A (\mathbf{L}^s\delta\mathbf{U})^T\mathbf{Q}\,dA \\ & - \int_A \delta\mathbf{U}^T\mathbf{F}\,dA - \int_{C'} \delta\mathbf{U}^T\mathbf{t}\,ds\end{aligned} \tag{3.30}$$

The first two terms relate the assumed independent strain field to the displacement field. The third and fourth terms are the constitutive equations for the mixed plate bending boundary-value problem. The terms in the third and fourth lines, after integration by parts, provide the balance of momentum equations for the plate bending problem.

The formal statement of the weak form for the Hu-Washizu functional is given in Box 3.2.

Box 3.2: Plate Bending - Hu-Washizu Weak Form

Given $\overline{\mathbf{M}}$, $\overline{\mathbf{Q}}$, $\mathbf{M}_n^a$, $\mathbf{M}_{ns}^a$, $\mathbf{Q}^a$ and $\mathbf{U}^a$; find $\mathbf{U} \in U$, $\mathbf{M} \in M$, $\mathbf{Q} \in Q$, $\boldsymbol{\kappa} \in K$ and $\boldsymbol{\gamma} \in G$ such that for every $\delta\mathbf{U} \in \overline{U}$, $\delta\mathbf{M} \in M$, $\delta\mathbf{Q} \in Q$, $\delta\boldsymbol{\kappa} \in K$ and $\delta\boldsymbol{\gamma} \in G$

$$\begin{aligned}0 = & -\int_A \delta\mathbf{M}^T(\boldsymbol{\kappa}-\mathbf{L}^b\mathbf{U})\,dA - \int_A \delta\mathbf{Q}^T(\boldsymbol{\gamma}-\mathbf{L}^s\mathbf{U})\,dA \\ & + \int_A \delta\boldsymbol{\kappa}^T(\mathbf{D}^b\boldsymbol{\kappa}-\mathbf{M})\,dA + \int_A \delta\boldsymbol{\gamma}^T(\mathbf{D}^s\boldsymbol{\gamma}-\mathbf{Q})\,dA \\ & + \int_A (\mathbf{L}^b\delta\mathbf{U})^T\mathbf{M}\,dA + \int_A (\mathbf{L}^s\delta\mathbf{U})^T\mathbf{Q}\,dA - \int_A \delta\mathbf{U}^T\mathbf{p}\,dA - \int_{C_t} \delta\mathbf{U}^T\mathbf{t}\,ds\end{aligned}$$

3.4.3 Finite element stiffness matrix and load vector

The weak form presented in Section 3.4.2 is used to formulate the finite element stiffness matrix and load vector. Substituting the finite element approximation of the assumed fields, as presented in Section 3.2, yields the first variation of the Hu-Washizu variational principle, in matrix notation, as follows:

$$\begin{aligned}\delta\Pi_H(\mathbf{m},\mathbf{q},\mathbf{k},\mathbf{e},\mathbf{d}) := {} & \delta\mathbf{q}^T[\mathbf{G}^b\mathbf{d} + \mathbf{G}_q\mathbf{d} - \mathbf{A}^b_{qk}\mathbf{k} - \mathbf{A}^b_{qe}\mathbf{e} - \mathbf{A}^s_{qe}\mathbf{e}] \\ & + \delta\mathbf{m}^T[\mathbf{G}^b_m\mathbf{d} - \mathbf{A}^b_{mk}\mathbf{k} - \mathbf{A}^b_{me}\mathbf{e}] \\ & + \delta\mathbf{k}^T[\mathbf{H}^b_{kk}\mathbf{k} + \mathbf{H}^b_{ke}\mathbf{e} - \mathbf{A}^{bT}_{mk}\mathbf{m} - \mathbf{A}^{bT}_{qk}\mathbf{q}] \\ & + \delta\mathbf{e}^T[\mathbf{H}^{bT}_{ke}\mathbf{k} + \mathbf{H}^b_{ee}\mathbf{e} + \mathbf{H}^s\mathbf{e} - \mathbf{A}^{sT}_{qe}\mathbf{q} - \mathbf{A}^{bT}_{me}\mathbf{m} - \mathbf{A}^{bT}_{qe}\mathbf{q}] \\ & + \delta\mathbf{d}^T[\mathbf{G}^{sT}\mathbf{q} + \mathbf{G}^{bT}_m\mathbf{m} + \mathbf{G}^{bT}_q\mathbf{q}] - \delta\mathbf{d}^T\mathbf{f}\end{aligned} \tag{3.31}$$

where $\mathbf{f}$ is the force vector resulting from the body forces and boundary tractions, given by equation (3.21), and the following definitions have been introduced:

$$\begin{aligned} \mathbf{H}^b_{kk} &:= \int_A \tilde{\kappa}^T\mathbf{D}^b\tilde{\kappa}\,dA \quad ; \quad \mathbf{H}^b_{ke} := \int_A \tilde{\kappa}^T\mathbf{D}^b\mathbf{R}\,dA \; ; \\ \mathbf{H}^b_{ee} &:= \int_A \mathbf{R}^T\mathbf{D}^b\mathbf{R}\,dA \quad ; \quad \mathbf{H}^s := \int_A \Gamma^T\mathbf{D}^s\Gamma\,dA \; ; \\ \mathbf{A}^s_{qe} &:= \int_A \tilde{\mathbf{Q}}^T\Gamma\,dA \; ; \; \mathbf{A}^b_{mk} := \int_A \tilde{\mathbf{M}}^T\tilde{\kappa}\,dA \; ; \; \mathbf{A}^b_{me} := \int_A \tilde{\mathbf{M}}^T\mathbf{R}\,dA \; ; \\ \mathbf{A}^b_{qk} &:= \int_A \mathbf{S}^T\tilde{\kappa}\,dA \quad ; \quad \mathbf{A}^b_{qe} := \int_A \mathbf{S}^T\mathbf{R}\,dA \; ; \end{aligned} \tag{3.32}$$

and $\mathbf{G}^b_m$, $\mathbf{G}^b_q$ and $\mathbf{G}^s$ are as in equation (3.14).

In (3.31) $\mathbf{H}^b_{ke}$, $\mathbf{H}^b_{ee}$, $\mathbf{A}^b_{qk}$, $\mathbf{A}^b_{me}$, $\mathbf{A}^b_{qe}$ and $\mathbf{G}^b_q$ reflect the effect of the two couplings introduced in Section 3.2. In the absence of "loading" terms from the constitutive equations (e.g., thermal terms), the Euler-Lagrange equations may be written as follows:

$$\begin{bmatrix} \mathbf{H} & -\mathbf{A}^T & \mathbf{0} \\ -\mathbf{A} & \mathbf{0} & \mathbf{G} \\ \mathbf{0} & \mathbf{G}^T & \mathbf{0} \end{bmatrix} \begin{Bmatrix} \mathbf{S}^t \\ \tau \\ \mathbf{d} \end{Bmatrix} = \begin{Bmatrix} \mathbf{0} \\ \mathbf{0} \\ \mathbf{f} \end{Bmatrix} \tag{3.33}$$

where

$$H := \begin{bmatrix} H^b_{kk} & H^b_{ke} \\ H^{bT}_{ke} & H^e_{ee} + H^s \end{bmatrix} \; ; \; \mathbf{A} := \begin{bmatrix} \mathbf{A}^b_{mk} & \mathbf{A}^b_{me} \\ \mathbf{A}^b_{qk} & \mathbf{A}^b_{qe} + \mathbf{A}^s_{qe} \end{bmatrix} \; ; \; \mathbf{S}^t := \begin{Bmatrix} \mathbf{k} \\ \mathbf{e} \end{Bmatrix} \tag{3.34}$$

and $\mathbf{G}$ and τ are defined by equation (3.18).

Elimination of the stress resultant coefficients, τ, and the strain coefficients , $\mathbf{S}^t$, from equation (3.33), for all elements yields:

$$\mathbf{K}\,\mathbf{d} = \mathbf{f}$$

where $\mathbf{K}$ is the finite element stiffness matrix, given by:

$$\mathbf{K} := \mathbf{G}^T \mathbf{A}^{-T} H \mathbf{A}^{-1} \mathbf{G} \tag{3.35}$$

and $\mathbf{f}$ is the load vector, given by equation (3.21).

Since the stress resultant and strain interpolation are independent in each element, the reduction may be performed at the element level.

In order to satisfy the mixed patch test (Zienkiewicz, Qu, Taylor & Nakazawa [1986]), the following requirements must be satisfied for all admissible boundary conditions on w, θ_1 and θ_2 (i.e., $\mathbf{d}_I$):

$$n_e + n_k + n_\theta \geq n_m \tag{3.36a}$$

$$n_e + n_k + n_\theta + n_w \geq n_q \tag{3.36b}$$

$$n_q \geq n_w \tag{3.36c}$$

$$n_m + n_q \geq n_\theta \tag{3.36d}$$

Note that in order to obtain the form given by equation (3.35), $\mathbf{A}$ must be a square matrix. This requirement is met if $n_e = n_q$ and $n_k = n_m$. Consequently, equations (3.36a,b) are identically satisfied.

The stress resultant and strain coefficients may be written in terms of the nodal displacement, $\mathbf{d}$, as follows:

$$\mathbf{e} = \bar{\mathbf{A}}^{-1}[\,\mathbf{G}^s + \mathbf{G}^b_q - \mathbf{A}^b_{qk}\,(\mathbf{A}^b_{mk})^{-1}\mathbf{G}^b_m\,]\,\mathbf{d} = F_1\,\mathbf{d} \tag{3.37}$$

$$\mathbf{k} = (\mathbf{A}^b_{mk})^{-1}[\,\mathbf{G}^b_m - \mathbf{A}^b_{me}\,F_1\,]\,\mathbf{d} = F_2\,\mathbf{d} \tag{3.38}$$

$$\mathbf{q} = \bar{\mathbf{A}}^{-T}\left[\left(H_{ke}^{bT} - H_A\right)F_2 + \left(H_{ee}^{b} + H^{s} - H_A\right)F_1\right]\mathbf{d} = F_3\mathbf{d} \tag{3.39}$$

$$\mathbf{m} = \left(\mathbf{A}_{mk}^{bT}\right)^{-1}\left[H_{kk}^{b}F_2 + H_{ke}^{b}F_1 - \mathbf{A}_{qk}^{bT}F_3\right]\mathbf{d} = F_4\mathbf{d} \tag{3.40}$$

where

$$\bar{\mathbf{A}} := \mathbf{A}_{qe}^{s} - \mathbf{A}_{qk}^{b}\left(\mathbf{A}_{mk}^{b}\right)^{-1}\mathbf{A}_{me}^{b} + \mathbf{A}_{qe}^{b} \tag{3.41}$$

and

$$H_A := \mathbf{A}_{me}^{bT}\left(\mathbf{A}_{mk}^{b}\right)^{-1}H_{kk}^{b} \tag{3.42}$$

3.5 Hellinger-Reissner Mixed Formulation for Plane Stress/Strain

3.5.1 The energy functional

The Hellinger-Reissner functional, in the case of in-plane problems, takes the form:

$$\Pi_R(\mathbf{N},\mathbf{U}) := \int_A \left\{-\frac{1}{2}\mathbf{N}^T(\mathbf{D}^n)^{-1}\mathbf{N} + \mathbf{N}^T\mathbf{L}^n\mathbf{U}\right\} - \int_A \mathbf{U}^T\bar{\mathbf{N}}\,dA - \int_{C_t} \mathbf{U}^T\bar{\mathbf{N}}^a\,ds \tag{3.43}$$

3.5.2 Weak form

To define the weak form a number of classes of functions must be characterized as follows:

Trial displacement solutions:

$$U := \left\{\mathbf{U} \mid \mathbf{U} \in \mathbf{H}^1(\bar{\Omega}), \mathbf{U} = \mathbf{U}^a \text{ on } \mathbf{C}_U\right\} \tag{3.44}$$

Displacement weighting functions:

$$\bar{U} := \left\{\mathbf{U} \mid \mathbf{U} \in \mathbf{H}^1(\bar{\Omega}), \mathbf{U} = \mathbf{0} \text{ on } \mathbf{C}_U\right\} \tag{3.45}$$

and trial membrane forces solution:

$$N := \left\{\mathbf{N} \mid \mathbf{N} \in \mathbf{H}^0(\bar{\Omega})\right\} \tag{3.46}$$

Note that the trial membrane forces solution space may also be used as the membrane forces weight functions space.

The first variation of the energy functional is given by:

$$\delta\Pi_R(\mathbf{N},\mathbf{U}) = \int_A \delta\mathbf{N}^T(\mathbf{L}^n\,\mathbf{U} - (\mathbf{D}^n)^{-1}\mathbf{N})\,dA$$

$$+ \int_A \left\{(\mathbf{L}^n\,\delta\mathbf{U})^T\mathbf{N} - \delta\mathbf{U}^T\bar{\mathbf{N}}\right\} dA - \int_{C_t} \delta\mathbf{U}^T\mathbf{t}\,ds = 0 \qquad (3.47)$$

The first term is the weak form of the constitutive equations. After integration by parts, the last two terms provide the balance of momentum equations for the membrane. The formal statement of the weak form is given in Box 3.3.

Box 3.3: In-Plane - Hellinger-Reissner Weak Form

Given $\bar{\mathbf{N}}$, $\mathbf{N}^a$, and $\mathbf{U}^a$; find $\mathbf{U} \in U$, and $\mathbf{N} \in N$ such that for every $\delta\mathbf{U} \in \bar{U}$, and $\delta\mathbf{N} \in N$

$$0 = \int_A \delta\mathbf{N}^T(\mathbf{L}^n\delta\mathbf{U} - (\mathbf{D}^n)^{-1}\mathbf{N})\,dA + \int_A \left\{(\mathbf{L}^n\delta\mathbf{U})^T\mathbf{N} - \delta\mathbf{U}^T\bar{\mathbf{N}}\right\} dA - \int_{C_t} \delta\mathbf{U}^T\mathbf{t}\,ds$$

3.5.3 Finite element stiffness matrix and load vector

The finite element stiffness matrix and load vector may be obtained from the weak form presented in Section 3.5.2. Substituting the finite element approximation of the assumed fields, as presented in Section 3.2, the first variation of the Hellinger-Reissner functional, in matrix notation, is given by:

$$\delta\Pi_R(\mathbf{N},\mathbf{U}) = \delta\mathbf{n}^T(\mathbf{G}^n\,\mathbf{d} - \mathbf{H}^n\,\mathbf{n}) + \delta\mathbf{d}^T(\mathbf{G}^{nT}\mathbf{N}) - \delta\mathbf{d}^T\mathbf{f} \qquad (3.48)$$

where $\mathbf{f}$ is the load vector resulting from body forces and boundary tractions, and the following definitions have been introduced:

$$\mathbf{H}^n := \int_A \tilde{\mathbf{N}}^T (\mathbf{D}^n)^{-1} \tilde{\mathbf{N}}\, dA \quad ; \quad \mathbf{G}^n := \int_A \tilde{\mathbf{N}}^T \mathbf{B}^n\, dA \tag{3.49}$$

In the above, $\mathbf{B}^n$ is the finite element strain-displacement relation, defined by:

$$\mathbf{B}_I^n \mathbf{d}_I := \mathbf{L}^n \mathbf{U} \tag{3.50}$$

where $\mathbf{B}_I^n$ is associated with node I, and is given by:

$$\mathbf{B}_I^n = \begin{bmatrix} N_{I,1} & 0 \\ 0 & N_{I,2} \\ N_{I,2} & N_{I,1} \end{bmatrix} \tag{3.51}$$

In the absence of "loading" terms from the constitutive equations, the Euler-Lagrange equations may be written as:

$$\begin{bmatrix} -\mathbf{H}^n & \mathbf{G}^n \\ \mathbf{G}^{nT} & 0 \end{bmatrix} \begin{Bmatrix} \mathbf{n} \\ \mathbf{d} \end{Bmatrix} = \begin{Bmatrix} 0 \\ \mathbf{f} \end{Bmatrix} \tag{3.52}$$

Elimination of the membrane forces coefficients, $\mathbf{n}$, for all elements yields:

$$\mathbf{K}\,\mathbf{d} = \mathbf{f}$$

where $\mathbf{K}$ is the finite element stiffness matrix, defined as:

$$\mathbf{K} := \mathbf{G}^{nT} (\mathbf{H}^n)^{-1} \mathbf{G}^n \tag{3.53}$$

and $\mathbf{f}$ is the load vector, defined as:

$$\mathbf{f}_I := \int_A N_I \bar{\mathbf{N}}\, dA + \int_{C_t} N_I\, \mathbf{t}\, ds \tag{3.54}$$

Since stress resultant interpolation is independent in each element, the reduction may be performed at the element level.

In order to satisfy the mixed patch test (Zienkiewicz, Qu, Taylor & Nakazawa [1986]), the following requirement must be satisfied for all admissible boundary conditions on $\mathbf{U}$ (i.e., those excluding rigid body modes).

$$n_N \geq n_U \tag{3.55}$$

where n_N is the number of membrane forces coefficients, and n_U is the number of displacement degrees of freedom.

The membrane forces coefficients may be obtained in terms of the nodal displacements, $\mathbf{d}_I$, as follows:

$$\mathbf{n} = (\mathbf{H}^n)^{-1}\mathbf{G}^n\,\mathbf{d} \tag{3.56}$$

3.6 Hu-Washizu Mixed Formulation for Plane Stress/Strain

3.6.1 The energy functional

The Hu-Washizu functional, in the case of in-plane problems, takes the form:

$$\Pi_H(\mathbf{P},\mathbf{N},\mathbf{U}) := \int_A \left\{ \frac{1}{2}\mathbf{P}^T\mathbf{D}^n\,\mathbf{P} + \mathbf{N}^T(\mathbf{L}^n\mathbf{U} - \mathbf{P}) - \mathbf{U}^T\bar{\mathbf{N}} \right\} dA - \int_{C_t} \mathbf{U}^T\mathbf{N}^a\,ds \tag{3.57}$$

3.6.2 Weak form

To define the weak form an additional class of functions must be characterized as follows:

Trial membrane strain solutions:

$$P := \left\{ \mathbf{P} \mid \mathbf{P} \in \mathbf{H}^0(\bar{\Omega}) \right\} \tag{3.58}$$

Note that the membrane strain solutions space may also be used as the space of membrane strain trial functions.

The first variation of the energy functional is given by:

$$\begin{aligned}\delta\Pi_H(\mathbf{P},\mathbf{N},\mathbf{U}) = &\int_A \delta\mathbf{N}^T(\mathbf{L}^n\,\mathbf{U} - \mathbf{P})\,dA + \int_A \delta\mathbf{P}^T(\mathbf{D}^n\,\mathbf{P} - \mathbf{N})\,dA \\ &+ \int_A \left\{ (\mathbf{L}^n\,\delta\mathbf{U})^T\mathbf{N} - \delta\mathbf{U}^T\bar{\mathbf{N}} \right\} dA - \int_{C_t} \delta\mathbf{U}^T\mathbf{t}\,ds = 0\end{aligned} \tag{3.59}$$

The first term relates the assumed strain field to the symmetric part of the gradient of the displacements in a weak form; the second term is the weak form of the constitutive equations; and the last two terms after integration by parts provide the balance of momentum equations for the membrane. The formal statement of the weak form is given in Box 3.4.

Box 3.4: In-Plane - Hu-Washizu Weak Form

Given $\bar{\mathbf{N}}$, $\mathbf{N}^a$, and $\mathbf{U}^a$; find $\mathbf{U} \in \boldsymbol{U}$, $\mathbf{P} \in \boldsymbol{P}$, and $\mathbf{N} \in \boldsymbol{N}$ such that for every $\delta\mathbf{U} \in \bar{\boldsymbol{U}}$, $\delta\mathbf{P} \in \boldsymbol{P}$, and $\delta\mathbf{N} \in \boldsymbol{N}$

$$0 = \int_A \left\{ \delta\mathbf{N}^T(\mathbf{L}^n\mathbf{U} - \mathbf{P}) + \delta\mathbf{P}^T(\mathbf{D}^n\mathbf{P} - \mathbf{N}) + (\mathbf{L}^n\delta\mathbf{U})^T\mathbf{N} - \delta\mathbf{U}^T\mathbf{F} \right\} dA - \int_{C_t} \delta\mathbf{U}^T\mathbf{t}\, ds$$

3.6.3 Finite element stiffness matrix and load vector

The finite element stiffness matrix and load vector may be obtained from the weak form presented in Section 3.6.2. Substituting the finite element approximations of the assumed fields, as presented in Section 3.2, the first variation of the Hu-Washizu functional, in matrix notations, is given by:

$$\delta\Pi_H(\mathbf{n}, \mathbf{p}, \mathbf{d}) := \delta\mathbf{n}^T[\mathbf{G}^n\mathbf{d} - \mathbf{A}^n\mathbf{p}] + \delta\mathbf{p}^T[H^n\mathbf{p} - \mathbf{A}^{nT}\mathbf{n}] + \delta\mathbf{d}^T[\mathbf{G}^{nT}\mathbf{n} - \mathbf{f}] \tag{3.60}$$

where $\mathbf{f}$ is the force vector resulting from the body forces and boundary tractions, given by equation (3.54), and the following definitions have been introduced:

$$H^n := \int_A \tilde{\mathbf{P}}^T \mathbf{D}^n \tilde{\mathbf{P}}\, dA \tag{3.61a}$$

and

$$\mathbf{A}^n := \int_A \tilde{\mathbf{N}}^T \tilde{\mathbf{P}}\, dA \tag{3.61b}$$

and $\mathbf{G}^n$ is defined by equation (3.49b).

In the absence of "loading" terms from the constitutive equations, the Euler-Lagrange equations may be written as:

$$\begin{bmatrix} H^n & -\mathbf{A}^{nT} & \mathbf{0} \\ -\mathbf{A}^n & \mathbf{0} & G^n \\ \mathbf{0} & \mathbf{G}^{nT} & \mathbf{0} \end{bmatrix} \begin{Bmatrix} \mathbf{p} \\ \mathbf{n} \\ \mathbf{d} \end{Bmatrix} = \begin{Bmatrix} \mathbf{0} \\ \mathbf{0} \\ \mathbf{f} \end{Bmatrix} \tag{3.62}$$

Elimination of the membrane forces coefficients, $\mathbf{n}$, and the membrane strains, $\mathbf{p}$, for all elements yields:

$$\mathbf{K}\,\mathbf{d} = \mathbf{f}$$

where $\mathbf{K}$ is the finite element stiffness matrix, defined as:

$$\mathbf{K} := \mathbf{G}^{nT}\,(\mathbf{A}^{nT})^{-1} H^{n}\,(\mathbf{A}^{n})^{-1}\mathbf{G}^{n} \tag{3.63}$$

and $\mathbf{f}$ is the load vector, defined by equation (3.54). Since stress resultant interpolation is independent in each element, the reduction may be performed at the element level.

In order to satisfy the mixed patch test (Zienkiewicz, Qu, Taylor & Nakazawa [1986]), the following requirements must be satisfied for all admissible boundary conditions on $\mathbf{U}$.

$$n_p + n_U \geq n_N \tag{3.64a}$$

$$n_N \geq n_U \tag{3.64b}$$

where n_N is the number of membrane forces coefficients, n_P is the number of membrane strain coefficients, and n_U is the number of displacement degrees of freedom. Note that in order to obtain the form given by equation (3.63), $\mathbf{A}_n$ must be a square matrix. This requirement is met if $n^p = n_N$. Consequently, equation (3.64a) is identically satisfied.

The membrane strain coefficients may be obtained in terms of the nodal displacements, as follows:

$$\mathbf{p} = (\mathbf{A}^{n})^{-1}\mathbf{G}^{n}\,\mathbf{d} \tag{3.65}$$

and the membrane force coefficients may be obtained, as follows:

$$\mathbf{n} = (\mathbf{A}^{nT})^{-1} H^{n} (\mathbf{A}^{n})^{-1}\mathbf{G}^{n}\,\mathbf{d} \tag{3.66}$$

CHAPTER 4: LOCKING ANALYSIS

4.1 Introduction

This dissertation concerns itself with plate bending and plane stress/strain elements. As is well known, some plate bending elements which are formulated based upon theories that account for shear deformations lock in shear at the thin plate limit. Also well known is the fact that some plane strain elements lock at the nearly incompressible limit. In this chapter these locking mechanisms are investigated.

In Section 4.2 locking at the nearly incompressible limit is discussed. In Section 4.3, it is proved that as a result of the coupling introduced in Chapter 3, shear locking at the thin plate limit is avoided. If the coupling is rank deficient (i.e., not all shear terms are coupled to the bending terms), the proof relies on the constraint count method, which is summarized in Appendix 4.1.

A method to generate stress resultant and strain fields possessing the properties presented in this chapter will be given in Chapter 5.

4.2 Locking at the Nearly Incompressible Limit

Locking at the nearly incompressible limit occurs in plane strain elements as a result of trying to force the trace of the strain to vanish pointwise. Thus, if it is possible to obtain elements in which the number of constraint equations is smaller than the number of degrees-of-freedom, it is possible to obtain elements that will not lock. This is the basis for the constraint count method, which is summarized in Appendix 4.1.

In this dissertation a different avenue of thought is taken. The assumed strain field is designed *a priori* in such a way that as Poisson's ratio, ν, goes to 0.5^-, the trace of the assumed strain field goes to zero pointwise. Consequently, there are no constraints to be enforced, and locking at the nearly incompressible limit will not occur. It must be noted,

however, that the criteria set by the constraint count method, namely, that elements with less constraints than the "optimal" number of constraints per element are too soft, does not apply to the elements presented in this dissertation. It will be shown in Chapter 6 that the assumed strain field for the proposed plane strain elements have indeed the property that at the nearly incompressible limit the trace of the assumed strain vanishes pointwise.

4.3 Shear Locking

Shear locking occurs at the thin plate limit in some elements based upon theories that account for shear deformations. Shear locking is defined as follows:

> Shear locking occurs at the thin plate limit when the shear strain energy becomes large in comparison to the bending strain energy.

Shear locking occurs in elements which become over-constrained at the thin plate limit. Thus, a common criteria for element design is to have the "correct" number of constraints per element, given by the constraint count method (see Appendix 4.1).

In this Chapter it will be shown that due to the couplings introduced in Chapter 3, shear locking is avoided *a priori* at the element level. Furthermore, it will be shown that in cases where the couplings are rank deficient, provided the rank deficiency is smaller than the "optimal" number of constraints per element, shear locking will not occur. Consequently, the coupling introduced reduces the number of constraints per element, and in the best case there are no constraints.

It must be noted that according to the constraint count method, if the element has less constraints than the "optimal" number, it is predicted to be soft. This comment, however, does not apply to the class of elements presented in this dissertation. The comment refers to elements in which all shear strain parameters must be constrained. As will be shown, this is not the case with the formulations proposed in this dissertation.

First, the formulation based upon the Hellinger-Reissner variational principle is investigated in Section 4.3.1. Then the formulation based upon the Hu-Washizu variational principle is investigated in Section 4.3.2.

4.3.1 Hellinger-Reissner formulation

In this section it is proved that as a result of the coupling between the shear and moment resultant fields, elements derived from the Hellinger-Reissner variational principle do not lock in shear. First the coupling is assumed to be of full rank. It is shown, without resorting to the constraint count method, that shear locking at the thin plate limit is avoided. Furthermore, it is proved that the definition given for shear locking holds for elements derived from the Hellinger-Reissner variational principle. In the second part of this section the constraint on the rank of the coupling matrix is relaxed. It is shown that provided the number of shear resultant parameters which are not coupled to the moment field is less than or equal to the number of constraints allowed per element by the constraint count method, results established in the first part of this section hold. Finally it is shown in proposition 4.6 that as the thickness is reduced to zero convergence to the thin plate solution is obtained.

Proposition 4.1: If the stress resultant fields are given by equations (3.3b) and (3.3c), and, furthermore, if $\tilde{\mathbf{M}}$, $\mathbf{S}$, and $\tilde{\mathbf{Q}}$ are of full rank, then, as the thickness is reduced to zero, $\mathbf{F}_1$ and $\mathbf{F}_2$, defined by equations (3.23) and (3.24), respectively, are $O(h^3)$.

Proof: First note that $\mathbf{H}^b_{mm}$, $\mathbf{H}^b_{mq}$, and $\mathbf{H}^b_{qq}$ are $O(h^{-3})$; $\mathbf{H}^s$ is $O(h^{-1})$; and $\mathbf{G}^b_m$, $\mathbf{G}^b_q$, and $\mathbf{G}^s$ are independent of h.

It follows that, as the thickness is reduced to zero, $\mathbf{H}^b - \mathbf{H}^s \approx \mathbf{H}^b$ where $\mathbf{H}^b$ is defined by equation (3.25). Consequently, the desired results follow. ▪

Proposition 4.2: If the stress resultant fields are given by equations (3.3b) and (3.3c), and $\mathbf{F}_1$ and $\mathbf{F}_2$, defined by equations (3.23) and (3.24), respectively, are $O(h^3)$, then, as the thickness is reduced to zero, the shear strain energy becomes negligible in

comparison to the bending strain energy.

Proof: By equation (3.11):

$$\mathbf{m}^T \mathbf{H}^b_{mm} \mathbf{m} = \mathbf{m}^T \mathbf{G}^b_m \mathbf{d} - \mathbf{m}^T \mathbf{H}^b_{mq} \mathbf{q} \tag{4.1}$$

and

$$\mathbf{q}^T \mathbf{G}^b_q \mathbf{d} = \mathbf{q}^T \mathbf{H}^{bT}_{mq} \mathbf{m} + \mathbf{q}^T \mathbf{H}^b_{qq} \mathbf{q} + \mathbf{q}^T \mathbf{H}^s \mathbf{q} - \mathbf{q}^T \mathbf{G}^s \mathbf{d} \tag{4.2}$$

The strain energy part of the Hellinger-Reissner functional, equation (3.5), is given by:

$$\Pi_R(\mathbf{m}, \mathbf{q}, \mathbf{d}) = -\frac{1}{2}[\mathbf{m}^T \mathbf{H}^b_{mm} \mathbf{m} + \mathbf{m}^T \mathbf{H}^b_{mq} \mathbf{q} + \mathbf{q}^T \mathbf{H}^{bT}_{mq} \mathbf{m} + \mathbf{q}^T (\mathbf{H}^b_{qq} + \mathbf{H}^s) \mathbf{q}]$$

$$+ \mathbf{m}^T \mathbf{G}^b_m \mathbf{d} + \mathbf{q}^T \mathbf{G}^b_q \mathbf{d} + \mathbf{q}^T \mathbf{G}^s \mathbf{d} \tag{4.3}$$

Substituting equations (4.1) and (4.2) into equation (4.3) yields:

$$\Pi_R(\mathbf{m}, \mathbf{q}, \mathbf{d}) = \frac{1}{2}(\mathbf{m}^T \mathbf{G}^b_m \mathbf{d} + \mathbf{q}^T \mathbf{H}^{bT}_{mq} \mathbf{m} + \mathbf{q}^T \mathbf{H}^b_{qq} \mathbf{q} + \mathbf{q}^T \mathbf{H}^s \mathbf{q}) \tag{4.4}$$

It follows from the assumptions that as the thickness is reduced to zero, the last term in equation (4.4), which is associated with the shear strain energy, is negligible in comparison to the first three terms, which are associated with the bending strain energy. Consequently, as the thickness is reduced to zero, the shear strain energy becomes negligible in comparison to the bending strain energy. ▪

Proposition 4.3: Shear locking is avoided if and only if the shear strain energy is negligible in comparison to the bending strain energy.

Proof: Assume the shear strain energy is negligible in comparison to the bending strain energy; it follows immediately from the definition of shear locking that shear locking does not occur.

Now assume that shear locking does not occur. Since **M** and **Q** are determined by equilibrium and are $O(h^0)$, it follows that **m** and **q** are $O(h^0)$. Furthermore, $\mathbf{F}_2$, defined by equation (3.24), is $O(h^3)$ independent of the coupling. Consequently, **d** is $O(h^{-3})$. Thus, it follows from equation (4.4) that the shear strain energy is negligible in comparison

to the bending strain energy. ▪

So far, $\tilde{\mathbf{M}}$, $\mathbf{S}$ and $\tilde{\mathbf{Q}}$ were restricted to be fully ranked. The question then arises, what happens when $\mathbf{S}$ is not fully ranked? As a first step, spectral decomposition of $\mathbf{H}^b$, given by equation (3.25), is performed.

$$\mathbf{H}^b = \mathbf{X}^T \Lambda \mathbf{X}$$

where $\mathbf{X}^T \mathbf{X} = \mathbf{I}$, the identity matrix. $\mathbf{H}^s$ is represented in the generalized coordinates ($\mathbf{X}$) as:

$$\mathbf{H}^s = \mathbf{X}^T \mathbf{X} \mathbf{H}^s \mathbf{X}^T \mathbf{X} = \mathbf{X}^T \bar{\mathbf{H}}^s \mathbf{X}$$

By equations (3.12), (3.17) and (3.18):

$$(\Lambda + \bar{\mathbf{H}}^s)\,\bar{\mathbf{q}} = \bar{\mathbf{G}}\mathbf{d} \tag{4.5}$$

where,

$$\bar{\mathbf{q}} = \mathbf{X}\mathbf{q} \qquad \bar{\mathbf{G}} = \mathbf{X}(\mathbf{G}^b - \mathbf{G}^s) \tag{4.6a}$$

$$\Lambda = \begin{bmatrix} \bar{\Lambda} & \mathbf{0} \\ \mathbf{0} & \mathbf{0} \end{bmatrix} \qquad \bar{\mathbf{q}}^T = <\bar{\mathbf{q}}_1, \bar{\mathbf{q}}_2> \qquad \bar{\mathbf{G}}^T = <\bar{\mathbf{G}}_1, \bar{\mathbf{G}}_2> \tag{4.6b}$$

and

$$\bar{\mathbf{H}}^s = \begin{bmatrix} \bar{\mathbf{H}}^s_{11} & \bar{\mathbf{H}}^s_{12} \\ \bar{\mathbf{H}}^s_{21} & \bar{\mathbf{H}}^s_{22} \end{bmatrix} \tag{4.6c}$$

Substituting equations (4.6) into equation (4.5) yields:

$$\begin{bmatrix} (\bar{\mathbf{H}}^s_{11} + \bar{\Lambda}) & \bar{\mathbf{H}}^s_{12} \\ \bar{\mathbf{H}}^s_{21} & \bar{\mathbf{H}}^s_{22} \end{bmatrix} \begin{Bmatrix} \bar{\mathbf{q}}_1 \\ \bar{\mathbf{q}}_2 \end{Bmatrix} = \begin{Bmatrix} \bar{\mathbf{G}}_1 \\ \bar{\mathbf{G}}_2 \end{Bmatrix} \mathbf{d} \tag{4.7}$$

Let $\bar{\mathbf{q}}_1 = \bar{\mathbf{F}}_1 \mathbf{d}$ and $\bar{\mathbf{q}}_2 = \bar{\mathbf{F}}_2 \mathbf{d}$. It follows from equation (4.7) that $\bar{\mathbf{F}}_1$ is $O(h^3)$ while $\bar{\mathbf{F}}_2$ is $O(h^1)$.

Proposition 4.4: Given that the rank deficiency of **S** is less than or equal to the maximum number of constraints allowed per element by the constraint count method, then $\bar{\mathbf{q}}_2$ is $O(h^0)$.

Proof: First note that **d** is $O(h^{-3})$, as in proposition 4.3. Since $\bar{\mathbf{F}}_1$ is $O(h^3)$, it follows that $\bar{\mathbf{q}}_1$ is $O(h^0)$. $\bar{\mathbf{F}}_2$, on the other hand, is $O(h)$; consequently $\bar{\mathbf{q}}_2$ is at worst $O(h^{-2})$.

As a result of meeting the constraint count requirement, shear locking does not occur. It follows from proposition 4.3 together with equation (4.4) that $\bar{\mathbf{q}}$ is $O(h^\alpha)$, where $\alpha > -1$. Recall that **Q** is determined by equilibrium; as a result, **Q** is $O(h^0)$. Consequently, $\alpha = 0$. This result contradicts the previous result for $\bar{\mathbf{q}}_2$.

Let $\mathbf{d} = \sum_{i=0}^{n} h^{i-3}\hat{\mathbf{d}}_i$. The above contradiction is resolved if and only if $\hat{\mathbf{d}}_0$ and $\hat{\mathbf{d}}_1$ are orthogonal to $\bar{\mathbf{q}}_2$. Consequently, $\bar{\mathbf{q}}_2$ is $O(h^0)$. ▪

Proposition 4.5: The vector $\bar{\mathbf{G}}_2\mathbf{d}$ is $O(h^{-1})$ if and only if $\bar{\mathbf{q}}_2$ is $O(h^0)$.

Proof: This result follows immediately from equation (4.7) once it is noted that **d** is $O(h^{-3})$ and $\bar{\mathbf{q}}_2$ is $O(h^0)$. ▪

Proposition 4.6: If **M** and **Q** are $O(h^0)$ and the formulation is based upon the Hellinger-Reissner functional, then the components of the shear strain tensor are $O(h^{-1})$ while the components of the curvature tensor are $O(h^{-3})$.

Proof: The Hellinger-Reissner functional may be viewed as a special case of the Hu-Washizu functional, where the assumed shear strain tensor is given by:

$$\boldsymbol{\gamma} = (\mathbf{C}^s)^{-1}\mathbf{Q}$$

and the assumed curvature tensor is given by:

$$\boldsymbol{\kappa} = (\mathbf{C}^b)^{-1}\mathbf{M}$$

Since both **M** and **Q** are $O(h^0)$, the desired result follows immediately. ▪

Remarks

- It follows from proposition 4.6 that as the thickness is reduced to zero the solution obtained by the proposed formulation converges to the thin plate solution (Kirchhoff theory). It must be noted, however, that the solution converges to the thin plate solution only when the analytical solution obtained for the plate theory used converges to the thin plate solution (e.g., when point loads are considered, the thin plate solution under the load is bounded while the Reissner-Mindlin solution is not).
- Without the coupling between the shear and moment stress resultant fields, $\mathbf{F}_1$ is $O(h)$, while $\mathbf{F}_2$ is $O(h^3)$. Consequently, if the coupling is neglected, then as the thickness is reduced to zero, the first three terms in equation (4.4), associated with the bending strain energy, become negligible in comparison to the last term, associated with the shear strain energy. As a result, by proposition 4.3, the element locks in shear at the element level. Thus, analysis at the global level is required to determine whether shear locking occurs.
- The functional presented in equation (4.4) is not useful in formulating elements since the constitutive equations were used to obtain it; equation (4.4) can be used, however, to obtain bounds on the strain energy.
- It follows from the above propositions that the formulation presented in this dissertation guarantees elements which do not lock in shear (provided $\mathbf{H}$ is invertible and $\mathbf{H}^b$ is of the appropriate rank).
- As $\mathbf{H}^s$ becomes negligible (i.e., numerically zero), the mixed patch test requirement for the full recovery of $\bar{\mathbf{q}}_2$ is $n_w + n_\theta \geq n_{q2}$, where n_{q2} is the number of $\bar{\mathbf{q}}_2$ parameters. In order to maintain a robust implementation for this case $\bar{\mathbf{q}}_2$ would be taken as global variables (i.e., Lagrangian multipliers). When a rectangular mesh of $n \times n$ elements, with clamped boundary conditions, is considered, the number of parameters in $\bar{\mathbf{q}}_2$ is:

$$n_{q2} = \begin{cases} 2n^2 & \text{S1 element} \\ 2n(n+1) & \text{T1 or Dvorkin-Bathe} \\ \leq 2n^2 & \text{for elements presented in Chapter 6 of this dissertation} \end{cases}$$

and the number of displacement parameters is $n_w + n_\theta = 3(n-1)^2$. Hence, a full solution for all variables is achievable only when

$$n = \begin{cases} 6 & - \text{ S1 element} \\ 7 & - \text{ T1 or Dvorkin-Bathe} \\ \leq 6 & - \text{ for elements presented in Chapter 6 of this dissertation} \end{cases}$$

- By introducing the coupling, the S1 element, which represented the best case scenario in comparison with the T1 or Dvorkin-Bathe elements, in terms of locking, is the worst case scenario in comparison with the elements presented in this dissertation.

4.3.2 Hu-Washizu formulation

Following the path established for the Hellinger-Reissner formulation, initially it will be assumed that the coupling introduced in the strain fields as well as that introduced in the stress resultant fields are fully ranked. It will be shown, without resorting to the constraint count method, that shear locking at the thin plate limit is avoided. The constraint on the rank of the coupling matrices will then be relaxed. It will be shown that provided the number of shear strain parameters not coupled into the curvature field and the number of shear resultant parameters not coupled into the moment field are both less than or equal to the number of constraints allowed per element by the constraint count method, results presented in the first part of this section hold. In proposition 4.11 it will be shown that as the thickness is reduced to zero, convergence to the thin plate solution is obtained.

In order to simplify notations and without loss of generality, the plate thickness will be assumed as constant over the element domain. Furthermore, the shear strain assumption introduced in equation (3.4c) is modified as follows:

$$\gamma := h^2 \Gamma \mathbf{e} \tag{4.8}$$

This assumption will be justified in Chapter 5. As a result,

$$\mathbf{A}^s_{qe} := \int_A h^2 \tilde{\mathbf{Q}}^T \Gamma \, dA \tag{4.9a}$$

and

$$H^s := \int_A h^4 \Gamma^T \mathbf{D}^s \Gamma \, dA \tag{4.9b}$$

Proposition 4.7: If the assumed stress resultant field is given by equations (3.3b,c), the assumed strain field is given by equations (3.4b) and (4.8), and if $\tilde{\mathbf{M}}$, $\mathbf{S}$, $\tilde{\mathbf{Q}}$, $\tilde{\kappa}$, $\mathbf{R}$, and Γ are of full rank, then, as the thickness is reduced to zero, $\mathbf{F}_1$ and $\mathbf{F}_2$, defined by equations (3.37) and (3.38), respectively, are $O(h^0)$, while $\mathbf{F}_3$ and $\mathbf{F}_4$, defined by equations (3.39) and (3.40), respectively, are $O(h^3)$.

Proof: First note that H^b_{kk}, H^b_{ke}, and H^b_{ee} are $O(h^3)$; H^s is $O(h^5)$; $\mathbf{G}^b_m$, $\mathbf{G}^b_q$, and $\mathbf{G}^s$ are independent of h; $\mathbf{A}^b_{mk}$, $\mathbf{A}^b_{me}$, $\mathbf{A}^b_{qk}$, and $\mathbf{A}^b_{qe}$ are independent of h; and $\mathbf{A}^s_{qe}$ is $O(h^2)$. It follows that, as the thickness is reduced to zero, $\bar{\mathbf{A}}$, defined by equation (3.41), is given by:

$$\bar{\mathbf{A}} \approx \mathbf{A}^b_{qe} - \mathbf{A}^b_{qk} \left(\mathbf{A}^b_{mk} \right)^{-1} \mathbf{A}^b_{me}$$

Consequently, the desired result follows. ▪

Proposition 4.8: Let the assumed stress resultant and strain fields be as in proposition 4.7. If $\mathbf{F}_1$ and $\mathbf{F}_2$ are $O(h^0)$, and $\mathbf{F}_3$ and $\mathbf{F}_4$ are $O(h^3)$, then, as the element thickness is reduced to zero, the shear strain energy becomes negligible in comparison to the bending strain energy.

Proof: It follows from equation (3.31) that:

$$\mathbf{G}^b_q \mathbf{d} = \mathbf{A}^s_{qe} \mathbf{e} + \mathbf{A}^b_{qk} \mathbf{k} + \mathbf{A}^b_{qe} \mathbf{e} - \mathbf{G}^s \mathbf{d} \tag{4.10a}$$

$$\mathbf{A}^b_{mk} \mathbf{k} = \mathbf{G}^b_m \mathbf{d} - \mathbf{A}^b_{me} \mathbf{e} \tag{4.10b}$$

$$H^b_{ke} \mathbf{e} = \mathbf{A}^{bT}_{mk} \mathbf{m} + \mathbf{A}^{bT}_{qk} \mathbf{q} - H^b_{kk} \mathbf{k} \tag{4.10c}$$

and

$$H^b_{ee} = \mathbf{A}^{sT}_{qe}\mathbf{q} + \mathbf{A}^{bT}_{me} + \mathbf{A}^{bT}_{qe} - H^{bT}_{ke}\mathbf{k} - H^s\mathbf{e} \tag{4.10d}$$

Substituting equations (4.10) into equation (3.27), and neglecting the external work, yields the following expression for the strain energy:

$$\Pi_H(\mathbf{m},\mathbf{q},\mathbf{e},\mathbf{k},\mathbf{d}) = \frac{1}{2}[\mathbf{k}^T\mathbf{A}^{bT}_{mk}\mathbf{m} + \mathbf{k}^T\mathbf{A}^{bT}_{qk}\mathbf{q} + \mathbf{e}^T\mathbf{A}^{bT}_{me}\mathbf{m} + \mathbf{e}^T(\mathbf{A}^{bT}_{qe} + \mathbf{A}^{sT}_{qe})\mathbf{q}] \tag{4.11}$$

It follows from the assumed order of $\mathbf{F}_1$, $\mathbf{F}_2$, $\mathbf{F}_3$, and $\mathbf{F}_4$ that the last term in equation (4.11), associated with the shear strain energy, is negligible in comparison to the first four terms, which are associated with the bending strain energy. Consequently, as the thickness is reduced to zero, the shear strain energy becomes negligible in comparison to the bending strain energy. ▪

Proposition 4.9: Shear locking is avoided if and only if the shear strain energy is negligible in comparison to the bending strain energy.

Proof: Assume the shear strain energy is negligible in comparison to the bending strain energy; it follows from the definition of shear locking that it does not occur.

Now assume that shear locking does not occur. $\mathbf{M}$ and $\mathbf{Q}$ are defined by equilibrium equations and are $O(h^0)$. Furthermore, $\mathbf{F}_4$ is $O(h^3)$ independent of the coupling. It follows that the elements of the vector $\mathbf{d}$ are $O(h^{-3})$. As a result, $\mathbf{e}$ and $\mathbf{k}$ are $O(h^{-3})$, and $\mathbf{m}$ and $\mathbf{q}$ are $O(h^0)$. It follows from equation (4.11) that the shear strain energy becomes negligible in comparison to the bending strain energy as the thickness is reduced to zero. ▪

So far it has been assumed that $\tilde{\mathbf{M}}$, $\mathbf{S}$, $\tilde{\mathbf{Q}}$, $\tilde{\boldsymbol{\kappa}}$, $\mathbf{R}$ and Γ are fully ranked. The question arises, what if $\mathbf{S}$ and $\mathbf{R}$ are not fully ranked? To answer this question, note that the constraint is that the shear strain must vanish pointwise as the thickness is reduced to zero. Consequently, only the rank deficiency of $\mathbf{R}$ is of importance, as long as the rank deficiency of $\mathbf{S}$ is less or equal to the rank deficiency of $\mathbf{R}$. This will be shown below.

Proposition 4.10: $\bar{\mathbf{A}}$ is $O(h^0)$ independent of the coupling introduced between the assumed shear strain and assumed curvature.

Proof: In the case when **R** is rank deficient, the assumed shear strain is given by:

$$\gamma = h^2 \bar{\Gamma}_1 \mathbf{e}_1 + \bar{\Gamma}_2 \mathbf{e}_2 \tag{4.12}$$

where $\mathbf{e}_1$ are the shear strain coefficients coupled into the curvature, and $\mathbf{e}_2$ are the shear strain coefficients not coupled into the curvature. Consequently, the following structure is induced on $\mathbf{A}^s_{qe}$:

$$\mathbf{A}^s_{qe} = \begin{Bmatrix} h^2 \mathbf{A}^s_1 \\ \mathbf{A}^s_2 \end{Bmatrix}$$

The desired result follows. ▪

Remark: The above proof holds as long as the rank deficiency of **S** is less than or equal to the rank deficiency of **R**. This may be seen directly from the structure of $\bar{\mathbf{A}}$. ▪

Let the shear coefficients **q** be given by:

$$\mathbf{q}^T = < \bar{\mathbf{q}}_1 , \bar{\mathbf{q}}_2 > \tag{4.13}$$

and let the displacement vector **d** be given by:

$$\mathbf{d} = \sum_{i=0}^{n} h^{i-3} \hat{\mathbf{d}}_i \tag{4.14}$$

where $\hat{\mathbf{d}}_i$ are independent of h.

Proposition 4.11: If the rank deficiency of **R** is less than or equal to the maximum number of constraints allowed per element by the constraint count method, and provided the rank deficiency of **S** is less than or equal to the rank deficiency of **R**, then, $\bar{\mathbf{q}}_2$ is $O(h^0)$ and the shear strain, γ, is $O(h^{-1})$.

Proof: First note that by proposition 4.10 $\bar{\mathbf{A}}$ is $O(h^0)$. Secondly, note that it follows from proposition 4.10 that $\mathbf{F}_1$ and $\mathbf{F}_2$ are $O(h^0)$.

It follows from the structure of equation (3.39) that $\bar{\mathbf{q}}_1 = \bar{\mathbf{F}}_{31}\mathbf{d}$ and $\bar{\mathbf{q}}_2 = \bar{\mathbf{F}}_{32}\mathbf{d}$, where $\bar{\mathbf{F}}_{31}$ is $O(h^3)$, and $\bar{\mathbf{F}}_{32}$ is $O(h^1)$. Hence, there is a contradiction. **Q** is determined by equilibrium, and thus is $O(h^0)$. It follows that the contradiction is resolved if and only if **d** is $O(h^{-3})$, and $\bar{\mathbf{F}}_{32}$ is orthogonal to $\hat{\mathbf{d}}_0$ and $\hat{\mathbf{d}}_1$. Consequently, $\bar{\mathbf{q}}_2$ is $O(h^0)$.

The assumption on the number of constraints implies that shear locking does not occur. Consequently, by proposition 4.9, the shear strain energy becomes negligible in comparison to the bending strain energy at the thin plate limit. Therefore, by equation (4.11) $\mathbf{e}_2$ must be $O(h^{\alpha})$ with $\alpha > -3$.

Let $\mathbf{e}_2 = \bar{\mathbf{F}}_{12}\mathbf{d}$ and $\mathbf{e}_1 = \bar{\mathbf{F}}_{11}\mathbf{d}$. Now, in order for $\bar{\mathbf{F}}_{32}$ to be orthogonal to $\hat{\mathbf{d}}_0$ and $\hat{\mathbf{d}}_1$, $\bar{\mathbf{F}}_{12}$ must be orthogonal to both $\hat{\mathbf{d}}_0$ and $\hat{\mathbf{d}}_1$. Consequently, since $\mathbf{F}_1$ is $O(h^0)$, and, noting equation (4.12), the assumed shear strain is $O(h^{-1})$. ▪

Remarks:

- It follows from proposition 4.11 that the solution obtained by this formulation converges to the thin plate solution as the thickness is reduced to zero. It must be noted, however, that this convergence will be obtained only when the solution of the plate theory used converges to the thin plate solution.
- The energy functional presented in equation (4.11) is not useful in formulating elements. It may be used, however, to obtain bounds on the strain energy.
- The last two remarks made for the Hellinger-Reissner formulation are also applicable to the Hu-Washizu formulation, provided n_{e2} as well as n_{q2} are taken as global variables, where n_{e2} is the number of shear strain parameters that are not coupled into the curvature. ▪

Appendix 4.1: The Constraint Count Method

The constraint count method is a heuristic approach for determining the ability of an element to perform well when subjected to a set of constraints. While it is not a precise mathematical method for evaluating element performance, it is a quick and simple tool for obtaining an indication of the element performance when subjected to constraints. It does have, however, the ability to predict a tendency for locking, which is the issue at hand.

Let n_{eq} represent the total number of active equations in the given mesh (i.e., after boundary conditions have been imposed), and let n_c represent the total number of constraints in the mesh. The constraint ratio, r, is defined by:

$$r := \frac{n_{eq}}{n_c} \tag{4.15}$$

The idea is that the r should imitate the behavior of the number of equilibrium equations divided by the number of constraints for the governing partial differential equations. In the case of in-plane problems subjected to incompressibility constraint, these numbers are 2 and 1, respectively, and in the case of plate bending problems these numbers are 3 and 2, respectively. Consequently, the optimal ratios are 2 and 1.5 for the incompressible and plate bending problems, respectively.

Let a standard mesh, illustrated in Figure 4.1, be introduced. The motivation for the constraint count method is: can the "optimal" ratio be approached asymptotically as the number of elements per side in the standard mesh approaches infinity? The predictions that can be made based upon the constraint count method are summarized in Box 4.1.

It must be pointed out, however, that while these predictions regarding behavior for the incompressible problem are very successful, this is not so for the plate bending problem. Specifically, some plate bending elements which are predicted to be flexible or stiff were shown to perform well. For further elaboration regarding this topic, see Hughes [1987].

Box 4.1: Constraint Count Prediction

$r > r_{optimal}$	too few constraints,
$r = r_{optimal}$	optimal,
$r < r_{optimal}$	too many constraints, and
$r \leq 1$	locking.

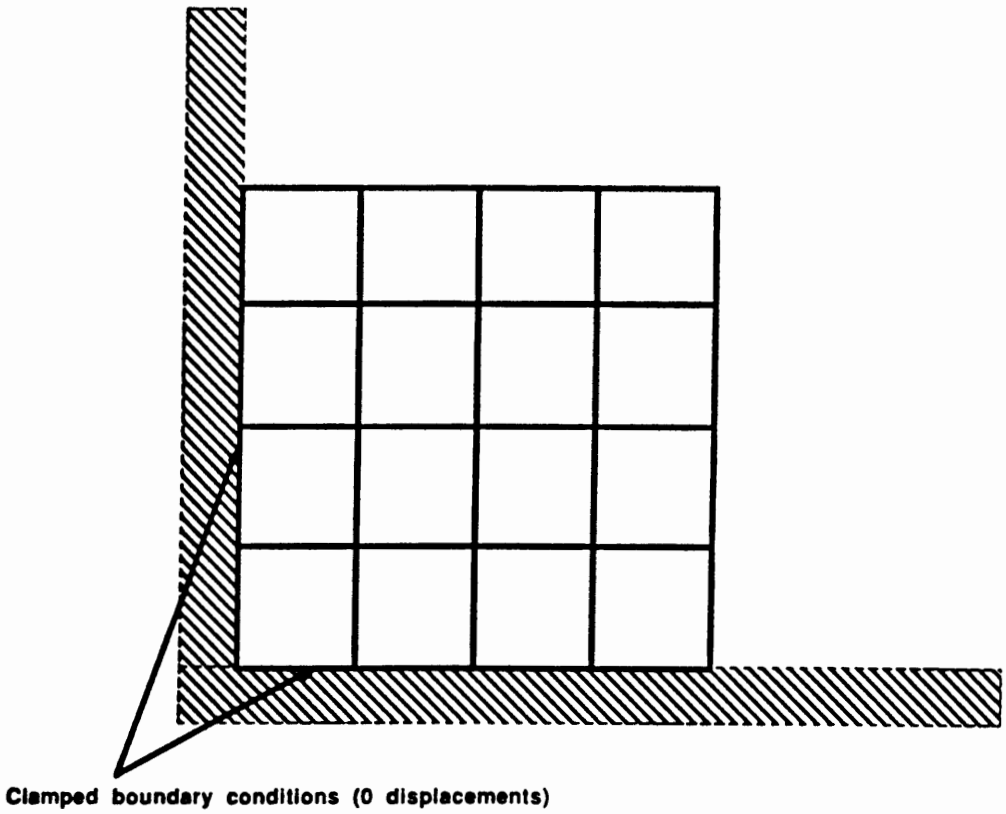

Figure 4.1: Standard mesh.

CHAPTER 5: A METHOD TO GENERATE STRESS RESULTANT AND STRAIN FIELDS

5.1 Introduction

The formulations presented in Chapter 3 rely upon the use of assumed stress resultant and strain fields. In Chapter 4 it was argued that these fields must satisfy some requirements if the resulting elements are to avoid locking. A method that can be applied to both the plate bending and in-plane problems is presented in this chapter.

In order to develop a basis upon which appropriate stress resultant and strain field interpolations possessing the desired properties (as presented in Chapter 4) may be derived, the Hu-Washizu variational principle is modified to account for assumed "incompatible" strains, while retaining the assumed "compatible" strains. The method may also be applied, with no modifications, in cases where the Hellinger-Reissner variational principle is used.

The method presented is a precursor for the finite element method, and should not be confused as being a part of it. It must be noted, however, that in the case where the material properties are constant over the element domain, the formulation presented in this chapter is in agreement with the corresponding variational principle (i.e., Hellinger-Reissner or Hu-Washizu functionals). In this case, the classical form of the variational principle evolves naturally and no distinction is made between the formulation presented and the classical variational principle. Since a state of constant material properties over the element domain is the limit case under mesh refinement, the formulation presented here will always be, in the limit case, a natural precursor for generating the assumed stress and strain fields for mixed finite element methods.

The method relies on the introduction of assumed incompatible strains that are obtained from assumed "incompatible" displacements. The displacement field, however, is

assumed as a compatible field. The incompatible strains are used to reduce the number of independent parameters in the stress and assumed compatible strain fields. The desired couplings in the plate bending problem arise naturally from this method. Furthermore, in the case of constant thickness over the element domain, the assumption introduced in equation (4.8) is recovered. In Chapter 6 it will be proved that the plane strain elements presented in this dissertation possess the property that as the nearly incompressible limit is approached, the trace of the strain goes to zero pointwise.

First, the method is formulated for a general three-dimensional body in Section 5.2. The reduction to the in-plane problem is straightforward, and is stated in Section 5.3. The formulation for plate bending is presented in Section 5.4. In Section 5.5, the formulation for axisymmetric problems is introduced, thus showing applicability to all types of problems arising in mechanics of solids. In Section 5.6, a set of requirements for the assumed incompatible displacements is presented.

In Chapter 6 the method will be applied to generate four-node quadrilateral plane stress/strain and plate bending elements.

5.2 Three-Dimensional Formulation

The starting point for the method presented here is the Hu-Washizu variational principle, which is stated in terms of an assumed stress field, σ, an assumed strain field, ϵ, and an assumed displacement field U. In the case of linearly elastic materials undergoing small deformations in an isothermal state, the Hu-Washizu energy functional is given by:

$$\Pi_H(\epsilon,\sigma,\mathbf{U}) = \int_{\Omega} \left\{ \frac{1}{2}\epsilon^T \mathbf{D}\epsilon + \sigma^T (\mathbf{L}\mathbf{U} - \epsilon) \right\} d\Omega - \Pi_{ext} \tag{5.1}$$

where,

D is the elastic coefficients matrix;

L is the strain displacement operator, given by:

$$\mathbf{L} = \begin{bmatrix} \frac{\partial}{\partial x_1} & 0 & 0 \\ 0 & \frac{\partial}{\partial x_2} & 0 \\ 0 & 0 & \frac{\partial}{\partial x_3} \\ 0 & \frac{\partial}{\partial x_3} & \frac{\partial}{\partial x_2} \\ \frac{\partial}{\partial x_3} & 0 & \frac{\partial}{\partial x_1} \\ \frac{\partial}{\partial x_2} & \frac{\partial}{\partial x_1} & 0 \end{bmatrix} \tag{5.2}$$

and Π_{ext} is the external work.

Let the assumed strain field be given by:

$$\epsilon = \epsilon^c + \epsilon^i \tag{5.3}$$

where ϵ^c is an assumed compatible strain field (in the case of Hellinger-Reissner formulations $\epsilon^c = \mathbf{D}^{-1}\sigma$), ϵ^i are the incompatible strains given by:

$$\epsilon^i = \mathbf{L}\mathbf{U}^i \tag{5.4}$$

and $\mathbf{U}^i$ are the assumed incompatible displacements.

The proposed method consists of constraining the assumed stress fields and the compatible strain fields. These constraints are presented in Box 5.1.

where $\bar{\mathbf{D}}$ is the mean value of $\mathbf{D}$, defined by:

$$\bar{\mathbf{D}} := \frac{\int_\Omega \mathbf{D}\, d\Omega}{\int_\Omega d\Omega}$$

and $\bar{\mathbf{D}}$ is assumed to be positive definite.

Box 5.1: Constraint Equations

$$\int_\Omega \mathbf{U}^i_{,j}\, d\Omega = 0$$

$$\int_\Omega \sigma^T \epsilon^i\, d\Omega = 0$$

$$\int_\Omega \epsilon^{cT} \bar{\mathbf{D}}\, \epsilon^i\, d\Omega = 0$$

The first constraint is introduced in order to pass the constant strain patch test. The motivation is as follows: if the assumed stress field, σ, and the compatible strain field, ϵ^c, can represent a state of constant stresses/strains, then by introducing the first constraint on the incompatible displacements, and noting the particular choice of the incompatible strains, this property of the assumed stress and assumed strain fields is preserved.

The second constraint is introduced in order to force the internal complimentary energy resulting from the assumed stress and assumed incompatible strains to vanish in a weak sense.

The motivation for the third constraint will become clear from subsequent discussion. For now, it may be viewed as a stronger counterpart of the second constraint.

Substituting the assumed strain field, equation (5.3), into the energy functional, equation (5.1), and replacing $\mathbf{D}$ by $\bar{\mathbf{D}}$ yields:

$$\Pi_H(\epsilon, \sigma, \mathbf{U}) = \int_\Omega \left\{ \frac{1}{2}(\epsilon^c + \epsilon^i)^T \bar{\mathbf{D}}(\epsilon^c + \epsilon^i) + \sigma^T(\mathbf{L}\mathbf{U} - \epsilon^c - \epsilon^i) \right\} d\Omega - \Pi_{ext} \tag{5.5}$$

Subjecting equation (5.5) to the last two constraint equations in Box 5.1, it is reduced to:

$$\Pi_H(\epsilon, \sigma, \mathbf{U}) = \int_\Omega \left\{ \frac{1}{2}(\epsilon^{cT} \bar{\mathbf{D}} \epsilon^c + \epsilon^{iT} \bar{\mathbf{D}} \epsilon^i) + \sigma^T(\mathbf{L}\mathbf{U} - \epsilon^c) \right\} d\Omega - \Pi_{ext} \tag{5.6}$$

Let the $\delta\epsilon^i$ denote a virtual incompatible strain field. The first variation of the energy functional Π_H with respect to ϵ^i is given by:

$$D\,\Pi_H \cdot \delta\epsilon^i = \int_{\Omega} \delta\epsilon^i \bar{\mathbf{D}}\, \epsilon^i \, d\Omega = 0 \tag{5.7}$$

It follows from the assumption concerning the positive definiteness of $\bar{\mathbf{D}}$ that, provided all the terms in (5.4) are linearly independent, ϵ^i is zero pointwise. Thus, the incompatible strain vanishes when the material properties are constant over the element. Consequently, a special structure has been induced on the assumed stress and compatible strain fields, and, noting equation (5.7), no incompatible strains are present in equation (5.6) for this case. Furthermore, the functional presented in equation (5.6) is identical to the one presented in equation (5.1). Hence, the starting point for the finite element method is equation (5.1), but the assumed stress field σ, and the assumed strain field $\epsilon \equiv \epsilon^c$ satisfy the constraints summarized in Box 5.1.

5.3 In-Plane Formulation

The reduction of the procedure presented above to the in-plane problem is straightforward. The strain displacement operator, $\mathbf{L}$, is now given by equation (2.20), and the volume integrals are replaced by area integrals. With these exceptions, the procedure is identical to that presented for the three-dimensional body. The constraint equations on the assumed membrane stress field, $\mathbf{N}$, in an explicit form, are given by:

$$\int_A \left\{ \mathbf{N}_{11} U^i_{1,1} + \mathbf{N}_{12} U^i_{1,2} \right\} dA = 0 \tag{5.8a}$$

and

$$\int_A \left\{ \mathbf{N}_{12} U^i_{2,1} + \mathbf{N}_{22} U^i_{2,2} \right\} dA = 0 \tag{5.8b}$$

and the constraint equations on the compatible strain field are given by:

$$\int_A \left\{ (\mathbf{P}^c_{11}\bar{\mathbf{D}}^n_{11} + \mathbf{P}^c_{22}\bar{\mathbf{D}}^n_{21})\,U^i_{1,1} + \mathbf{P}^c_{12}\bar{\mathbf{D}}^n_{33}U^i_{1,2} \right\} dA = 0 \tag{5.9a}$$

and

$$\int_A \left\{ \mathbf{P}^c_{12}\bar{\mathbf{D}}^n_{33}U^i_{2,1} + (\mathbf{P}^c_{11}\bar{\mathbf{D}}^n_{12} + \mathbf{P}^c_{22}\bar{\mathbf{D}}^n_{22})\,U^i_{2,2} \right\} dA = 0 \tag{5.9b}$$

where $\bar{\mathbf{D}}^n$ is the mean value of $\mathbf{D}^n$, given by equation (2.23).

5.4 Plate Bending Formulation

The plate bending problem is formulated in resultant form. Consequently, the last two constraints introduced in Box 5.1 must be reformulated in resultant form. The resulting constraint equations are presented in Box 5.2.

Box 5.2: Constraint Equations: Plate Bending

$$\int_A \mathbf{U}^i_{,\alpha}\, dA = 0$$

$$\int_A \left[\mathbf{M}^T \boldsymbol{\kappa}^i + \mathbf{Q}^T \boldsymbol{\gamma}^i\right] dA = 0$$

$$\int_A \left[\boldsymbol{\kappa}^c \bar{\mathbf{D}}^b \boldsymbol{\kappa}^i + \boldsymbol{\gamma}^c \bar{\mathbf{D}}^s \boldsymbol{\gamma}^i\right] dA = 0$$

where $\bar{\mathbf{D}}^b$ is the mean value of $\mathbf{D}^b$, given by equation (2.22), and $\bar{\mathbf{D}}^s$ is the mean value of $\mathbf{D}^s$, given by equation (2.21).

In the above constraints the assumed incompatible strains are obtained by:

$$\boldsymbol{\kappa}^i = \mathbf{L}^b\mathbf{U}^i \quad ; \quad \boldsymbol{\gamma}^i = \mathbf{L}^s\mathbf{U}^i \tag{5.10}$$

where $\mathbf{L}^b$ is given by equation (2.19), and $\mathbf{L}^s$ is given by equation (2.18).

The structure of the constraint equations presented in Box 5.2 is such that the coupling structure introduced in Chapter 3 between the assumed moment and the assumed shear stress resultant fields is imposed. Also imposed is the coupling between the assumed curvature and assumed shear strain fields. Consequently, as was shown in Chapter 4, shear locking in elements formulated by this method is avoided at the element level. Furthermore, note that the assumption used in Chapter 4 on the assumed shear strain field (i.e., Γ is $O(h^2)$) follows naturally from the structure of the last equation in Box 5.2.

In the previous discussion of the two- and three-dimensional problems it was pointed out that the first constraint introduced in Box 5.1 was necessary in order to obtain elements which pass the constant strain patch test. In the plate bending formulation, however, the displacement itself, $\mathbf{U}^i$, appears explicitly in the constraint equations through the appearance of the incompatible shear strains. The question arises, therefore, do elements formulated by the proposed method pass the constant strain patch test? In order to obtain a better understanding, the constraint equations are now written in an explicit form. The constraint equations on the assumed stress resultant field are given by:

$$\int_A \left\{ q_1 w^i_{,1} + q_2 w^i_{,2} \right\} dA = 0 \tag{5.11a}$$

$$\int_A \left\{ M_{22} \theta^i_{1,2} + M_{12} \theta^i_{1,1} - q_2 \theta^i_1 \right\} dA = 0 \tag{5.11b}$$

and

$$\int_A \left\{ M_{11} \theta^i_{2,1} + M_{12} \theta^i_{2,2} - q_1 \theta^i_2 \right\} dA = 0 \tag{5.11c}$$

and the constraint equations on the assumed compatible strain are given by:

$$\int_A \left\{ \gamma^c_1 \bar{\mathbf{D}}^s_{11} w^i_{,1} + \gamma^c_2 \bar{\mathbf{D}}^s_{22} w^i_{,2} \right\} dA = 0 \tag{5.12a}$$

$$\int_A \left\{ (\kappa^c_{11} \bar{\mathbf{D}}^b_{12} + \kappa^c_{22} \bar{\mathbf{D}}^b_{22}) \theta^i_{1,2} + \kappa^c_{12} \bar{\mathbf{D}}^b_{33} \theta^i_{1,1} - \gamma^c_2 \bar{\mathbf{D}}^s_{22} \theta^i_1 \right\} dA = 0 \tag{5.12b}$$

and

$$\int_A \left\{ (\kappa_{11}^c \bar{\mathbf{D}}_{11}^b + \kappa_{22}^c \bar{\mathbf{D}}_{21}^b)\,\theta_{2,1}^i + \kappa_{12}^c \bar{\mathbf{D}}_{33}^b \theta_{2,2}^i - \gamma_1^c \bar{\mathbf{D}}_{11}^s \theta_2^i \right\} dA = 0 \qquad (5.12c)$$

A close examination of equations (5.11) reveals that the equation used to reduce the assumed shear resultant field, equation (5.11a), involves the derivatives of the assumed incompatible transverse displacement. The equations used to reduce the assumed moment field, equations (5.11b,c), involve derivatives of the assumed incompatible rotations on which the moments perform work, and the incompatible rotations on which the shear resultants perform work. Similar results are obtained for the constraint equations on the assumed curvature and shear strain field, equations (5.12). Consequently, the structure of the constrained fields is such that constant moment/curvature (i.e., shear resultants/shear strains are zero pointwise), as well as a state of constant shear stress/strain are possible. As a result, elements formulated by the proposed method pass the patch test, provided the assumed displacement field can model the associated state of deformations.

5.5 Axisymmetric Formulation

When considering this case, it is not clear why the first constraint introduced in Box 5.1 should be satisfied in the radial direction. Furthermore, examining the strain displacement operator, which in a cylindrical coordinate system is given by:

$$\mathbf{L}^A = \begin{bmatrix} \frac{\partial}{\partial r} & 0 \\ 0 & \frac{\partial}{\partial z} \\ \frac{\partial}{\partial z} & \frac{\partial}{\partial r} \\ \frac{1}{r} & 0 \end{bmatrix} \qquad (5.13)$$

reveals that the circumferential strain, $\epsilon_{\theta\theta}$, is a function of the radial displacement. Consequently, applying the method as presented in Box 5.1 would lead to coupling of the

circumferential stress and strain into the radial stress and strain, respectively. While conceptually this result does not pose any difficulty, from a computational point of view it is undesirable. It was shown by Weissman & Taylor [1988] that excellent results can be obtained when the radial and circumferential stresses are decoupled. Consequently, in order to obtain decoupled circumferential stress and strain, as well as to be able to use the same type of incompatible displacements as in the plane case (the functions used in the plane case divided by the radial coordinate, r, may be used), the strain displacements operator, used to generate the assumed incompatible strains from the assumed incompatible displacements, is modified as follows:

$$\bar{\mathbf{L}}^{A} = \begin{bmatrix} \frac{\partial}{\partial r} & 0 & 0 \\ 0 & \frac{\partial}{\partial z} & 0 \\ \frac{\partial}{\partial z} & \frac{\partial}{\partial r} & 0 \\ 0 & 0 & \frac{1}{r}\left(\frac{\partial}{\partial r} + \frac{\partial}{\partial z}\right) \end{bmatrix} \tag{5.14}$$

Using $\bar{\mathbf{L}}^{A}$ implies the introduction of an assumed incompatible displacement in the circumferential direction. Note, however, that this displacement is such that its integral over the element area vanishes. Since this is an assumed field, it is legitimate to do so provided the resulting strains are contained in the admissible strain space (i.e., are in H^0). Furthermore, the circumferential displacement which is zero pointwise in the strong statement of the problem, is zero in a weak sense if the method presented here is used; in the case of constant material properties over the element domain, this displacement is identically zero pointwise.

5.6 Criteria for the Assumed Incompatible Displacements

The methodology presented above involves the use of incompatible displacements used to generate incompatible strains. A set of properties that these displacements must possess are presented in Box 5.3, and motivated below.

Box 5.3: Properties of the Incompatible Displacements

- Frame invariant,
- Do not artificially bias the element in any direction,
- The functions should be as simple as possible (i.e., lowest order of polynomial possible),
- The assumed incompatible displacements must be of higher order than the assumed compatible displacement (e.g., for the bilinear elements, the assumed incompatible displacements must be at least quadratic),
- The first derivative with respect to the coordinates vanishes (first constraint in Box 5.1), and
- Preserve the sign convention used in the strong form (plates, shells and beams).

The first three requirements are obvious, and are primary objectives for every finite element development.

The fourth requirement is introduced in order to obtain stability of the algorithm. If the order of the incompatible function would not be higher than the compatible functions, the orthogonalization procedure introduced will render nonstable elements. This is because the null kernel of the **G** matrix with respect to the solution space will be augmented by the incompatible functions. By requiring the incompatible functions to be of higher order polynomials, the null kernel with respect to the solution space is not modified.

The fifth requirement is introduced in order to pass the patch test as was explained above.

To obtain a grasp on the last requirement, consider the case of a plate element with constant shear in one direction (e.g., a cantilever beam with end shear). In this case, this requirement must be met in order for the contribution of the shear to the moment (from the explicit coupling introduced) to be of the correct sign.

Using the requirements as put forth in Box 5.3, the incompatible displacements can be defined up to within a constant. This constant does not play any role in the two- and three-dimensional cases as well as in the axisymmetric case, as the incompatible strains are derivatives of the incompatible displacements (see equations (2.20), (5.2) and (5.14), respectively). In the case of plate bending, however, this constant appears explicitly in the incompatible strain, equation (5.10), and is important to the couplings produced, as shown in equations (5.11b,c) and (5.12b,c). Consequently, a method to determine its value must be presented.

The last of the property requirements for the incompatible displacements puts a constraint on the values this constant may take. A unique value for this constant may be obtained if the incompatible displacements are required to integrate to the element area. This may be viewed as a normalization procedure. The constant obtained, however, will depend on the element geometry. As a result, the incompatible displacements will be element dependent. This result may be avoided if it is noted that the range of values that the constant may take is bounded from above and below (assuming the Jacobian to be non-zero at all points in the element). Consequently, a unique value independent of element geometry may be obtained. While for a very coarse mesh, results obtained will not be as good as those obtained by using an element dependent constant, results will converge quickly and, for reasonable meshes, they will be practically insensitive to the constant value (provided the value used is in the allowable range).

CHAPTER 6: PROPOSED ELEMENTS

6.1 Introduction

Four-node quadrilateral plane stress/strain and plate bending elements are presented in this Chapter as an illustration of the methodology developed in Chapters 3 and 5. In Section 6.2, the assumed displacement field is presented. The assumed stress resultant fields are presented in Section 6.3. The assumed compatible strains are presented in Section 6.4. The incompatible displacements used to generate the assumed incompatible strains are presented in Section 6.5. Finally, the proposed elements are presented in Section 6.6.

6.2 Assumed Displacement Field

The assumed displacement field used in the four-node elements presented in this chapter is presented in this section. The in-plane displacement field is assumed as a standard isoparametric field and is presented in Section 6.2.1. The rotation field and transverse displacement field are presented in Section 6.2.2. The rotation field is assumed as a standard isoparametric field. In order to be able to represent exactly a state of constant curvature, characterized by a biquadratic transverse displacement field, the bilinear isoparametric interpolation, used in four-node elements, must be substituted by a biquadratic one. To avoid the addition of degrees of freedom, the transverse displacement field is enhanced by interpolating it in terms of the nodal rotations as well as in terms of the nodal transverse displacement.

6.2.1 Plane stress/strain

The assumed displacement field is a standard isoparametric field; the displacements are given by equation (3.1), which is restated here:

$$\mathbf{U} = N_I \, d_I \tag{6.1}$$

where N_I is the shape function associated with node I, and d_I is the displacement vector given by equation (3.2). In the case of four-node quadrilateral elements, the shape functions are given by:

$$N_I(\xi,\eta) = \frac{1}{4}(1+\xi_I\xi)(1+\eta_I\eta) \tag{6.2}$$

where ξ and η are the element natural coordinates, on the interval [-1,1], and ξ_I and η_I are the values of the natural coordinates at the node I.

6.2.2 Plate bending

Plate bending elements are required to be able to represent exactly constant curvature and constant shear. The former is characterized by a state of biquadratic transverse displacements and bilinear rotation fields (no shear deformations), while the latter is characterized by a state of bicubic transverse displacements and biquadratic rotation fields.

Current four-node element technology (e.g., T1 and Bathe & Dvorkin [1985] elements) is able to model exactly constant curvature for an arbitrarily-shaped quadrilateral. Constant shear strain, however, can be modeled exactly only when the elements are in the form of a parallelogram, but the displacements are not exact at the nodes. This behavior is due to the order of interpolation used for the rotations and transverse shear deformation in four-node elements. In the case of four-node plate bending elements the rotations must be interpolated by standard isoparametric interpolation. The transverse displacement, on the other hand, may be enhanced by expressing it in terms of nodal rotations as well as in terms of the nodal transverse displacement. The enhancement procedure may be done explicitly (e.g., Morris [1986]) or implicitly by modifying the shear strain displacement relations (e.g., T1 and Bathe & Dvorkin [1985] elements). In this dissertation the first approach is taken. A simple and efficient method to explicitly enhance the assumed transverse displacement to a biquadratic field is presented.

The rotation field is assumed as a standard isoparametric field. Consequently, the assumed rotation field is given by:

$$\theta_\alpha = N_I \, \theta_{\alpha I} \tag{6.3}$$

where $\theta_{\alpha I}$ is the rotation θ_α at the node I and N_I is the shape function associated with node I, given by equation (6.2).

A state of constant curvature is characterized by zero shear strain, pointwise. Consequently, it follows from the shear strain displacement relation, equation (2.4a), that $w_{,\alpha} = -e_{\alpha\beta}\,\theta_\beta$. As a result, if the transverse displacement at a point a is known, and if the rotation field is known, too, then the transverse displacement at a point b can be computed as follows:

$$w_b = w_a + \int_a^b \theta_n(\xi, \eta)\, ds \tag{6.4}$$

where w_b is the transverse displacement at point b, w_a is the transverse displacement at point a and θ_n is the rotation about the normal to the line ab connecting points a and b. θ_n is given by:

$$\theta_n(\xi, \eta) = \nu_\alpha(\xi, \eta)\; \theta_\alpha(\xi, \eta) \tag{6.5}$$

where ν_1 and ν_2 are the components of the unit normal vector to the line ab in the x_1 and x_2 directions, respectively.

Using the relations given by equations (6.4) and (6.5), the transverse displacements at the element mid-edge points can be computed as follows:

$$w_{i+4} = \frac{1}{2}\left(w_i + w_k + \int_i^{i+4} \theta_{ni}\, ds - \int_{i+4}^{k} \theta_{ni}\, ds \right) \tag{6.6}$$

where i=1,2,3,4; and k = (i+4) modulo 4. The "node" numbering and the normals to the paths used are presented in Figure 6.1. The transverse displacement at the element center ($\xi = \eta = 0$) can be computed as follows:

$$w_9 = \frac{1}{4}\sum_{i=5}^{8}\left(w_i + \int_i^9 \theta_{ni}\, ds\right) \tag{6.7}$$

Using the procedure outlined above, the transverse displacement field can be interpolated by the nine-node Lagrangian element shape functions. The shape functions associated with the corner nodes (nodes 1,2,3 and 4) are given by:

$$\tilde{N}_I = \frac{1}{4}\xi\eta\,(\xi + \xi_I)(\eta + \eta_I) \tag{6.8}$$

the shape functions associated with the mid-edge points 5 and 7 are given by:

$$\tilde{N}_I = \frac{1}{2}\eta\,(1-\xi^2)(\eta + \eta_I) \tag{6.9}$$

the shape functions associated with the mid-edge points 6 and 8 are given by:

$$\tilde{N}_I = \frac{1}{2}\xi\,(1-\eta^2)(\xi + \xi_I) \tag{6.10}$$

and the shape function associated with the center point is given by:

$$\tilde{N}_9 = (1-\xi^2)(1-\eta^2) \tag{6.11}$$

Consequently, the assumed quadratic transverse displacement field is given by:

$$w(\xi,\eta) = \sum_{I=1}^{9} \tilde{N}_I(\xi,\eta)\, w_I \tag{6.12}$$

Remarks:

- The consistent loading and consistent mass matrix must be modified to account for the enhanced interpolation used for the transverse displacement.
- When the simply supported boundary condition is specified as $w = M_n = M_{nt} = 0$ (the so called SS1 boundary condition), as a result of the enhanced interpolation used on the transverse displacement, the $w = 0$ condition is satisfied only at the nodes. w converges pointwise to zero, however, under mesh refinement.
- It must be emphasized that without the enhanced interpolation used for the transverse displacement, the proposed elements will not lock in shear. The enhanced transverse

displacement is introduced only in order to be able to represent a state of constant curvature/moment for elements distorted from a parallelogram shape.

- An error is introduced in the values computed for the transverse displacements at the mid-edge and center points when the shear strain is not zero pointwise and/or the rotation field cannot be represented exactly by a bilinear field. Consequently, the interpolation used for the transverse displacement is not, in general, identical to the nine-node element interpolation.
- The general constant strain patch test requirement for plate bending elements necessitates the ability to exactly represent a state of constant shear strain/stress as well as that of constant curvature/moment. The scheme outlined above will not yield elements that can model a state of constant shear if the element is perturbed from a parallelogram shape. This remark, however, is true for all known four-node plate bending elements (e.g., T1 and Bathe & Dvorkin [1985] elements).
- It is common practice in the finite element literature to replace the constant shear strain patch test, as stated above, by a test in which the nodal rotations are constrained to be zero (i.e., shear deformation only). Indeed, the transverse displacement field for this case is bilinear. Consequently, all four-node elements can represent this case exactly. The plate bending elements presented in this dissertation contain coupling between the shear strain and the curvature. Consequently, the curvature is not zero unless body couples are introduced. The shear strain, however, is exact. ▪

6.3 Assumed Stress Resultant Fields

The assumed membrane, moment and transverse shear resultant fields are formulated in the element natural coordinates and then transformed into the physical domain by means of a transformation identical to the one used to transform second Piola-Kirchhoff stresses into Cauchy stresses. However, in order to pass the patch test and in order to maintain frame invariance, the transformation is based on values at the center of the

element (Pian & Sumihara [1984]).

6.3.1 Assumed membrane resultant field

The assumed membrane resultant field is a complete linear field* in the element natural coordinates and is expressed as:

$$\mathbf{N}^* = \begin{Bmatrix} N^*_{\xi\xi} \\ N^*_{\eta\eta} \\ N^*_{\xi\eta} \end{Bmatrix} = \begin{bmatrix} 1 & \xi & \eta & 0 & 0 & 0 & 0 & 0 & 0 \\ 0 & 0 & 0 & 1 & \xi & \eta & 0 & 0 & 0 \\ 0 & 0 & 0 & 0 & 0 & 0 & 1 & \xi & \eta \end{bmatrix} \begin{Bmatrix} n^*_1 \\ n^*_2 \\ \cdot \\ \cdot \\ n^*_9 \end{Bmatrix} \tag{6.13}$$

Since complete polynomials are used to express the membrane forces, equation (6.13) could be used for $\mathbf{N}^*$ directly. However, the reduction to satisfy the constraints introduced in Chapter 5 would require selection of different parameters in each element (i.e., there would be a dependence on element orientation of ξ and η with respect to x_1 and x_2). This dependence may be avoided by using the transformation procedure described below.

The following definitions are introduced:

$$xs = \frac{1}{4}\xi_I x_{1I} \;\; ; \;\; xt = \frac{1}{4}\eta_I x_{1I} \;\; ; \;\; xh = \frac{1}{4}(\xi\eta)_I x_{1I}$$

$$ys = \frac{1}{4}\xi_I x_{2I} \;\; ; \;\; yt = \frac{1}{4}\eta_I x_{2I} \;\; ; \;\; yh = \frac{1}{4}(\xi\eta)_I x_{2I}$$

Following Zienkiewicz & Taylor [1989], the Jacobian of the coordinate transformation from the (ξ, η) space to the (x_1, x_2) space is given by:

$$J = J_0 + J_1\xi + J_2\eta \tag{6.14}$$

where,

$$J_0 = xs \cdot yt - xt \cdot ys \tag{6.15a}$$

* The stress resultant and strain fields are assumed as complete linear fields since this is the best assumption that may be used in conjunction with a bilinear displacement field.

$$J_1 = xs \cdot yh - xh \cdot ys \tag{6.15b}$$

$$J_2 = xh \cdot yt - xt \cdot yh \tag{6.15c}$$

The membrane forces in the physical space are obtained by using the following transformation:

$$N_{ij} = \frac{1}{J_0} F_{iI} F_{jJ} N^*_{IJ} \tag{6.16}$$

where both i and j take the values x_1 or x_2, and both I and J take the values ξ or η, and $F_{x_i\xi} = \frac{\partial x_1}{\partial \xi}$, etc.

At the center of the element, F is given by:

$$F_{x_1\xi} = xs \quad ; \quad F_{x_1\eta} = xt \tag{6.17a}$$

$$F_{x_2\xi} = ys \quad ; \quad F_{x_2\eta} = yt \tag{6.17b}$$

After redefining the independent coefficients, the assumed moment resultant field is given by:

$$\mathbf{N} = \begin{Bmatrix} N_{11} \\ N_{22} \\ N_{12} \end{Bmatrix} = \begin{bmatrix} 1 & 0 & 0 & xs^2\eta & xt^2\xi & xs^2\xi & xt^2\eta & 2xs\,xt\,\xi & 2xs\,xt\,\eta \\ 0 & 1 & 0 & ys^2\eta & yt^2\xi & ys^2\xi & yt^2\eta & 2ys\,yt\,\xi & 2ys\,yt\,\eta \\ 0 & 0 & 1 & xs\,ys\,\eta & xt\,yt\,\xi & xs\,ys\,\xi & xt\,yt\,\eta & A\,\xi & A\,\eta \end{bmatrix} \begin{Bmatrix} n_1 \\ n_2 \\ \cdot \\ \cdot \\ n_9 \end{Bmatrix} \tag{6.18}$$

where,

$$A = xs \cdot yt + xt \cdot ys$$

$$n_1 = \frac{1}{J_0}(xs^2 n_1^* + xt^2 n_4^* + 2xs\,xt\,n_7^*)$$

$$n_2 = \frac{1}{J_0}(ys^2 n_1^* + yt^2 n_4^* + 2ys\,yt\,n_7^*)$$

$$n_3 = \frac{1}{J_0}(xs\,ys\,n_1^* + xt\,yt\,n_4^* + A\,n_7^*)$$

$$n_i = \frac{1}{J_0} n_j^*$$

with

$$(i,j) \in \left\{ (4,3),(5,5),(6,2),(7,6),(,8,8),(9,9) \right\}$$

It is convenient to write **N** in the following form:

$$\mathbf{N} = \left[\hat{N}_1 \,|\, \hat{N}_2 \right] \begin{Bmatrix} \hat{n}_1 \\ \hat{n}_2 \end{Bmatrix}$$

where,

$$\hat{n}_1^T = < n_1, n_2, n_3, n_4, n_5 > \; ; \; \hat{n}_2^T = < n_6, n_7, n_8, n_9 >$$

With the above construction, the parameter set $\hat{n}_2$ may always be selected as the set to be eliminated in satisfying equation (5.8).

6.3.2 Assumed moment resultant field

The moment resultant field is constructed in a manner identical to that described above for the assumed membrane forces. Accordingly, following the procedure presented for the assumed membrane field, the assumed moment resultant field, in the physical space, is given by:

$$\mathbf{M} = \begin{Bmatrix} M_{11} \\ M_{22} \\ M_{12} \end{Bmatrix} = \begin{bmatrix} 1 & 0 & 0 & xs^2\eta & xt^2\xi & xs^2\xi & xt^2\eta & 2\,xs\,xt\,\xi & 2\,xs\,xt\,\eta \\ 0 & 1 & 0 & ys^2\eta & yt^2\xi & ys^2\xi & yt^2\eta & 2\,ys\,yt\,\xi & 2\,ys\,yt\,\eta \\ 0 & 0 & 1 & xs\,ys\,\eta & xt\,yt\,\xi & xs\,ys\,\xi & xt\,yt\,\eta & A\,\xi & A\,\eta \end{bmatrix} \begin{Bmatrix} m_1 \\ m_2 \\ \cdot \\ \cdot \\ m_9 \end{Bmatrix} \qquad (6.19)$$

It is convenient to write **M** in the following form:

$$\mathbf{M} = \left[\hat{M}_1 \,|\, \hat{M}_2 \right] \begin{Bmatrix} \hat{m}_1 \\ \hat{m}_2 \end{Bmatrix}$$

where,

$$\hat{m}_1^T = < m_1, m_2, m_3, m_4, m_5 > \; ; \; \hat{m}_2^T = < m_6, m_7, m_8, m_9 >$$

With the above construction, the parameter set $\hat{m}_2$ may always be selected as the set to be eliminated in satisfying equation (5.11).

6.3.3 Assumed shear resultant field

The shear resultant field is constructed in a manner similar to that described above for the membrane and moment resultant fields. Accordingly, let the assumed linear resultant field in the element natural space be given by:

$$\mathbf{Q}^* = \begin{Bmatrix} Q^*_\xi \\ Q^*_\eta \end{Bmatrix} = \begin{bmatrix} 1 & \xi & \eta & 0 & 0 & 0 \\ 0 & 0 & 0 & 1 & \xi & \eta \end{bmatrix} \begin{Bmatrix} q^*_1 \\ q^*_2 \\ \cdot \\ \cdot \\ q^*_6 \end{Bmatrix} \tag{6.20}$$

The shear resultant field in the physical space is obtained by means of the following transformation:

$$Q_i = \frac{1}{J_0} F_{iI} Q^*_I \tag{6.21}$$

where i takes the values x_1 or x_2, and I takes the values ξ or η. After redefining the independent shear coefficients, the assumed shear resultant field in the physical space is given by:

$$\mathbf{Q} = \begin{Bmatrix} Q_1 \\ Q_2 \end{Bmatrix} = \begin{bmatrix} 1 & 0 & xs\,\eta & xt\,\xi & xs\,\xi & xt\,\eta \\ 0 & 1 & ys\,\eta & yt\,\xi & ys\,\xi & yt\,\eta \end{bmatrix} \begin{Bmatrix} q_1 \\ q_2 \\ \cdot \\ \cdot \\ q_6 \end{Bmatrix} \tag{6.22}$$

where,

$$q_1 = \frac{1}{J_0}(xs\, q^*_1 + xt\, q^*_4)$$

$$q_2 = \frac{1}{J_0}(ys\, q^*_1 + yt\, q^*_4)$$

$$q_i = \frac{1}{J_0} q_j^*$$

with

$$(i,j) \in \left\{ (3,3),(4,5),(5,2),(6,6) \right\}$$

It is convenient to write **Q** in the following form:

$$\mathbf{Q} = \left[\hat{Q}_1 \mid \hat{Q}_2 \right] \begin{Bmatrix} \hat{q}_1 \\ \hat{q}_2 \end{Bmatrix}$$

where,

$$\hat{q}_1^T = < q_1, q_2, q_3, q_4 > \ ; \ \hat{q}_2^T = < q_5, q_6 >$$

With the above construction, the parameter set $\hat{q}_2$ may always be selected as the set to be eliminated in satisfying equation (5.11).

6.4 Assumed Strain Fields

The assumed membrane strain, curvature and shear strain fields are formulated in the element natural coordinates, and then transformed into the physical domain. Two types of transformations can be used:

- The same transformation as used for the corresponding stress fields.
- The inverse to the transformation used for the corresponding stress fields.

The motivation for the first approach is to have the same "shape functions," or interpolation, for the strain fields as for the corresponding stress fields. The second approach is motivated by the invariance of the complementary energy ($\sigma_{ij}\,\epsilon_{ij}$) under coordinate transformation. Accordingly, the transformation of a tensor of order two is given by:*

$$T_{ij} = J\, F_{Ii}^{-1} F_{Jj}^{-1} T_{IJ}^* \tag{6.23}$$

* In direct notation, equation (6.23) would read: $T = J\, F^{-1}\, T^*\, F^{-T}$

and the transformation for a tensor of order one is given by:

$$Z_i = J\, F_{Ii}^{-1} Z_I^* \tag{6.24}$$

A similar approach was taken by Simo & Rifai [1989].

6.4.1 Assumed membrane strain field

Following the path established in the assumed stress fields, the membrane strain field is assumed as a complete linear field in the element natural coordinates, and then transformed into the physical space. Using the transformation given by equation (6.16) yields:

$$\mathbf{P} = \begin{Bmatrix} P_{11} \\ P_{22} \\ P_{12} \end{Bmatrix} = \begin{bmatrix} 1 & 0 & 0 & xs^2\eta & xt^2\xi & xs^2\xi & xt^2\eta & 2\,xs\,xt\,\xi & 2\,xs\,xt\,\eta \\ 0 & 1 & 0 & ys^2\eta & yt^2\xi & ys^2\xi & yt^2\eta & 2\,ys\,yt\,\xi & 2\,ys\,yt\,\eta \\ 0 & 0 & 1 & xs\,ys\,\eta & xt\,yt\,\xi & xs\,ys\,\xi & xt\,yt\,\eta & A\,\xi & A\,\eta \end{bmatrix} \begin{Bmatrix} p_1 \\ p_2 \\ \cdot \\ \cdot \\ p_9 \end{Bmatrix} \tag{6.25a}$$

and using the inverse transformation, equation (6.23), yields:

$$\mathbf{P} = \begin{bmatrix} 1 & 0 & 0 & yt^2\eta & xt^2\xi & yt^2\xi & xt^2\eta & -2\,yt\,xt\,\xi & -2\,yt\,xt\,\eta \\ 0 & 1 & 0 & ys^2\eta & xs^2\xi & ys^2\xi & xs^2\eta & -2\,ys\,xs\,\xi & -2\,ys\,xs\,\eta \\ 0 & 0 & 1 & -yt\,ys\,\eta & -xt\,xs\,\xi & -yt\,ys\,\xi & -xt\,xs\,\eta & A\,\xi & A\,\eta \end{bmatrix} \begin{Bmatrix} p_1 \\ p_2 \\ \cdot \\ \cdot \\ p_9 \end{Bmatrix} \tag{6.25b}$$

It is convenient to write $\mathbf{P}$ in the following form:

$$\mathbf{P} = \left[\hat{P}_1 \mid \hat{P}_2\right] \begin{Bmatrix} \hat{p}_1 \\ \hat{p}_2 \end{Bmatrix}$$

where,

$$\hat{p}_1^T = <p_1, p_2, p_3, p_4, p_5> \;;\; \hat{p}_2^T = <p_6, p_7, p_8, p_9>$$

With the above construction, the parameter set $\hat{p}_2$ may always be selected as the set to be eliminated in satisfying equation (5.9).

6.4.2 Assumed curvature field

An identical procedure to the one used to obtain the assumed membrane strain field in the physical space is repeated for the assumed curvature field. Accordingly, the assumed curvature field in the physical space, using equation (6.16), is given by:

$$\kappa = \begin{Bmatrix} \kappa_{11} \\ \kappa_{22} \\ \kappa_{12} \end{Bmatrix} = \begin{bmatrix} 1 & 0 & 0 & xs^2\eta & xt^2\xi & xs^2\xi & xt^2\eta & 2\,xs\,xt\,\xi & 2\,xs\,xt\,\eta \\ 0 & 1 & 0 & ys^2\eta & yt^2\xi & ys^2\xi & yt^2\eta & 2\,ys\,yt\,\xi & 2\,ys\,yt\,\eta \\ 0 & 0 & 1 & xs\,ys\,\eta & xt\,yt\,\xi & xs\,ys\,\xi & xt\,yt\,\eta & A\,\xi & A\,\eta \end{bmatrix} \begin{Bmatrix} k_1 \\ k_2 \\ \cdot \\ \cdot \\ k_9 \end{Bmatrix} \qquad (6.26a)$$

and using the inverse transformation, equation (6.23), the assumed curvature field in the physical space is given by:

$$\kappa = \begin{bmatrix} 1 & 0 & 0 & yt^2\eta & xt^2\xi & yt^2\xi & xt^2\eta & -2\,yt\,xt\,\xi & -2\,yt\,xt\,\eta \\ 0 & 1 & 0 & ys^2\eta & xs^2\xi & ys^2\xi & xs^2\eta & -2\,ys\,xs\,\xi & -2\,ys\,xs\,\eta \\ 0 & 0 & 1 & -yt\,ys\,\eta & -xt\,xs\,\xi & -yt\,ys\,\xi & -xt\,xs\,\eta & A\,\xi & A\,\eta \end{bmatrix} \begin{Bmatrix} k_1 \\ k_2 \\ \cdot \\ \cdot \\ k_9 \end{Bmatrix} \qquad (6.26b)$$

It is convenient to write κ in the following form:

$$\kappa = \left[\hat{\kappa}_1 \mid \hat{\kappa}_2 \right] \begin{Bmatrix} \hat{k}_1 \\ \hat{k}_2 \end{Bmatrix}$$

where,

$$\hat{k}_1^T = < k_1, k_2, k_3, k_4, k_5 > \; ; \; \hat{k}_2^T = < k_6, k_7, k_8, k_9 >$$

With the above construction, the parameter set $\hat{k}_2$ may always be selected as the set to be eliminated in satisfying equation (5.12).

6.4.3 Assumed shear strain field

The shear strain field is constructed in a manner similar to that described above for the membrane strain field. Accordingly, the assumed shear strain field in the physical space, using equation (6.16), is given by:

$$\gamma = \begin{Bmatrix} \gamma_1 \\ \gamma_2 \end{Bmatrix} = \begin{bmatrix} 1 & 0 & xs\,\eta & xt\,\xi & xs\,\xi & xt\,\eta \\ 0 & 1 & ys\,\eta & yt\,\xi & ys\,\xi & yt\,\eta \end{bmatrix} \begin{Bmatrix} e_1 \\ e_2 \\ \cdot \\ \cdot \\ e_6 \end{Bmatrix} \tag{6.27a}$$

and when using the inverse transformation, equation (6.24), the shear strain field in the physical space is given by:

$$\gamma = \begin{bmatrix} 1 & 0 & yt\,\eta & -xt\,\xi & yt\,\xi & -xt\,\eta \\ 0 & 1 & -ys\,\eta & xs\,\xi & -ys\,\xi & xs\,\eta \end{bmatrix} \begin{Bmatrix} e_1 \\ e_2 \\ \cdot \\ \cdot \\ e_6 \end{Bmatrix} \tag{6.27b}$$

It is convenient to write γ in the following form:

$$\gamma = \left[\hat{\gamma}_1 \mid \hat{\gamma}_2 \right] \begin{Bmatrix} \hat{e}_1 \\ \hat{e}_2 \end{Bmatrix}$$

where

$$\hat{e}_1^T = < e_1, e_2, e_3, e_4 > \;\; ; \;\; \hat{e}_2^T = < e_5, e_6 >$$

With the above construction, the parameter set $\hat{e}_2$ may always be selected as the set to be eliminated in satisfying equation (5.12).

6.5 Assumed Incompatible Displacements

The assumed incompatible displacements used in the constraint equations are presented here. To pass the constant strain patch test (see Section 5.2), the first derivative with respect to x_1 and x_2 coordinates must vanish in a weak sense (i.e., their integral over the area should vanish). To demonstrate the rules set up in Chapter 5 for selecting these displacements, two functions are used. The first was presented by Wu, *et. al.* [1987]. These functions do not satisfy the last condition presented in Box 5.3. The second function was presented by Taylor, *et. al.* [1986]. These functions satisfy all the criteria set in

Box 5.3.

6.5.1 Plane displacements

Let the assumed incompatible displacements for the plane case be given by:

$$U_1^i = N_1^i \lambda_1 + N_2^i \lambda_2 \tag{6.28a}$$

and

$$U_2^i = N_1^i \lambda_3 + N_2^i \lambda_4 \tag{6.28b}$$

where λ_1, λ_2, ..., and λ_4 are the independent incompatible displacement parameters, and N_α^i are the incompatible shape functions.

6.5.2 Plate bending displacements

Similarly, let the assumed incompatible displacements for the plate bending case be given by:

$$\theta_1^i = N_1^i \lambda_3 + N_2^i \lambda_4 \tag{6.29a}$$

$$\theta_2^i = N_1^i \lambda_5 + N_2^i \lambda_6 \tag{6.29b}$$

and

$$w^i = N_3^i \lambda_1 + N_4^i \lambda_2 \tag{6.29c}$$

where λ_1, λ_2, ..., and λ_6 are the independent incompatible displacement parameters.

Remark: Different incompatible shape functions are used for the assumed incompatible transverse displacement since a higher order interpolation is used to model the transverse displacement (Section 6.2.2). If isoparametric interpolation was used for the assumed transverse displacement, too, the same shape functions used for the rotations could be used for the transverse displacement. ▪

6.5.3 Assumed incompatible shape functions

As was stated above, two options are selected for the incompatible shape functions N_1^i and N_2^i. The first set of incompatible shape functions were presented by Wu, *et al.* [1987]. The functions are given by:

$$N_1^i = \xi^2 - \frac{2J_1}{3J_0}\xi + \frac{2J_2}{3J_0}\eta \tag{6.30a}$$

and

$$N_2^i = \eta^2 + \frac{2J_1}{3J_0}\xi - \frac{2J_2}{3J_0}\eta \tag{6.30b}$$

The second set of incompatible shape functions was presented by Taylor, *et al.* [1986]. In order to obtain a more compact form, the incompatible modes given below are a linear combination of the modes originally presented. The functions are given by:

$$N_1^i = (1 - \frac{J_2}{J_0}\eta)(1-\xi^2) + \frac{J_1}{J_0}\xi(1-\eta^2) \tag{6.31a}$$

and

$$N_2^i = (1 - \frac{J_1}{J_0}\xi)(1-\eta^2) + \frac{J_2}{J_0}\eta(1-\xi^2) \tag{6.31b}$$

Note that the second set of incompatible modes is zero (compatible) at the nodal points while the first set is not.

The incompatible shape functions N_3^i and N_4^i used in the incompatible transverse displacement were proposed by Wu, *et al.* [1987], and are given by:

$$N_3^i = \xi^4 - \frac{4J_1}{5J_0}\xi + \frac{4J_2}{5J_0}\eta \tag{6.32a}$$

and

$$N_4^i = \eta^4 + \frac{4J_1}{5J_2}\xi - \frac{4J_2}{5J_0}\eta \tag{6.32b}$$

Remark: The functions given by equations (6.32a,b) are used in equations (5.11a) and (5.12b) and thus, it is not necessary to meet the last criteria set in Box 5.3 . ▪

6.6 Proposed Elements

A number of plane stress/strain and plate bending elements are proposed as an illustration and test of the formulation proposed in Chapters 3 and 5. These elements are also designed to test the sensitivity of the formulation to the particular choice of the assumed incompatible displacement fields.

Six four-node quadrilateral plane stress/strain elements are proposed. Two are formulated via the Hellinger-Reissner variational principle, and four via the Hu-Washizu variational principle. The class of elements developed here is labeled Plane Stress/Strain (PSS).

In addition, six four-node quadrilateral plate bending elements are proposed. Again, two are formulated via the Hellinger-Reissner variational principle, and four via the Hu-Washizu variational principle. The class of elements developed here is labeled Coupled Resultants Bending (CRB).

The two sets of incompatible shape functions for the incompatible displacements presented above, equations (6.30) and (6.31), are used in both the plane and plate bending cases. The first of these sets of functions satisfies all the requirements presented in Chapter 5, with the exception of the last requirement set in Box 5.3. The second set satisfies all criteria stated in Box 5.3. Thus, it is anticipated that the plane elements presented should not, to any degree, be sensitive to the type of incompatible shape functions used since they depend on the derivatives of the shape functions only (this result is also true for the three-dimensional and axisymmetric formulations). For very coarse meshes the plate bending elements presented are expected to show some sensitivity to the particular incompatible shape functions used. The stress resultants recovered for the plate elements are expected to be more sensitive than the displacements to the type of incompatible shape functions used.

The incompatible displacements used represent, in effect, the extreme cases of possible choices for the incompatible displacements (see Section 5.6 - normalization of the incompatible displacements). Consequently, if the results will be shown to be insensitive to the particular choice of incompatible shape functions for reasonable meshes, the full robustness of the method will be revealed.

6.6.1 Plane stress/strain elements: Hellinger-Reissner formulation

The displacement field presented in equations (6.1) together with the assumed membrane forces presented in equation (6.18) form the independent fields for the Hellinger-Reissner based elements. The two elements presented differ only by the incompatible displacements used to reduce the assumed membrane force field. It must be noted that in the case of a constant Jacobian element (e.g., equation (6.14) is constant) the two elements are identical. The element associated with the incompatible shape functions given by equations (6.30) is PSS1, and the element associated with the incompatible shape functions given by equations (6.31) is PSS2.

In Chapter 4 it was argued that if the assumed strain field can model a state of strains in which the trace of the strain vanishes, no locking at the nearly incompressible limit will occur. A proof that the elements presented meet this requirement is given in proposition 6.1.

Proposition 6.1: The Hellinger-Reissner elements presented above can, in the case of plane strain, model a state in which the trace of the strain goes to zero pointwise as ν goes to 0.5^{-}.

Proof: Recall that in the case of the Hellinger-Reissner variational principle the assumed strain field is obtained from the assumed independent stress field. Consequently, in the case of plane strain the membrane strain $\mathbf{P}$ is given by:

$$\mathbf{P} = (\mathbf{D}^{n})^{-1}\mathbf{N} \tag{6.33}$$

where $(\mathbf{D}^n)^{-1}$ is given by:

$$(\mathbf{D}^n)^{-1} = \frac{1}{\alpha}\begin{bmatrix} \lambda + 2\mu & -\lambda & 0 \\ -\lambda & \lambda + 2\mu & 0 \\ 0 & 0 & \frac{\alpha}{\mu} \end{bmatrix} \tag{6.34}$$

with,

$$\alpha = 4\mu(\mu + \lambda)$$

As Poisson's ratio, ν, goes to 0.5^-, λ goes to infinity while μ remains bounded. It follows that, at the limit, the following relation is obtained:

$$(\mathbf{D}^n)_{11}^{-1} = (\mathbf{D}^n)_{22}^{-1} = -(\mathbf{D}^n)_{12}^{-1} = -(\mathbf{D}^n)_{21}^{-1} \tag{6.35}$$

After imposing the constraint equations introduced in Chapter 5, the assumed membrane stress field presented in equation (6.18) is reduced to the general form:

$$\mathbf{N} = \begin{Bmatrix} N_{11} \\ N_{22} \\ N_{12} \end{Bmatrix} = \begin{bmatrix} 1 & 0 & 0 & a_1\eta + b_1\xi & a_4\xi + b_4\eta \\ 0 & 1 & 0 & a_2\eta + b_2\xi & a_5\xi + b_5\eta \\ 0 & 0 & 1 & a_3\eta + b_3\xi & a_6\xi + b_6\eta \end{bmatrix} \begin{Bmatrix} n_1 \\ n_2 \\ \cdot \\ \cdot \\ n_5 \end{Bmatrix} \tag{6.36}$$

where a_1, a_2, ..., and a_6, and b_1, b_2, ..., and b_6 are constants to be determined by the procedure presented in Chapter 5.

Substituting equations (6.34) and (6.36) into equation (6.33) and taking notice of equation (6.35) yields the desired result. ▪

6.6.2 Plane stress/strain elements: Hu-Washizu formulation

The displacement field presented in equations (6.1) together with the assumed membrane forces presented in equations (6.18) and the assumed membrane strains presented in either equation (6.25a) or equation (6.25b) form the independent fields for the Hu-Washizu based elements. The four elements presented differ by the incompatible

displacements used to reduce the assumed membrane forces and strains, and by the strain field used. The elements associated with the incompatible shape functions given by equations (6.30) are PSS3 (strain field given by equation (6.25a)) and PSS5 (strain field given by equation (6.25b)); the elements associated with the incompatible shape functions given by equations (6.31) are PSS4 (strain field given by equation (6.25a)) and PSS6 (strain field given by equation (6.25b)).

Once again it is necessary to prove that the trace of the assumed membrane strain field vanishes as Poisson's ratio, ν, goes to 0.5^-. This is done in proposition 6.2.

Proposition 6.2: The trace of the assumed shear strain field, in plane strain elements, goes to zero pointwise as ν goes to 0.5^-.

Proof: After constraining the assumed membrane strain field introduced in equations (6.25), the reduced field is given in a general form by:

$$\mathbf{P} = \begin{Bmatrix} P_{11} \\ P_{22} \\ P_{12} \end{Bmatrix} = \begin{bmatrix} 1 & 0 & 0 & a_1\eta + b_1\xi & a_4\xi + b_4\eta \\ 0 & 1 & 0 & a_2\eta + b_2\xi & a_5\xi + b_5\eta \\ 0 & 0 & 1 & a_3\eta + b_3\xi & a_6\xi + b_6\eta \end{bmatrix} \begin{Bmatrix} p_1 \\ p_2 \\ \cdot \\ \cdot \\ p_5 \end{Bmatrix} \tag{6.37}$$

The structure imposed by the constraint equations is such that the following relations are obtained, as ν goes to 0.5^-, between the a_1, a_2, ..., and a_6 and b_1, b_2, ..., b_6 coefficients:

$$a_1 + a_2 = 0 \quad ; \quad a_4 + a_5 = 0 \tag{6.38a}$$

and

$$b_1 + b_2 = 0 \quad ; \quad b_4 + b_5 = 0 \tag{6.38b}$$

A formal proof for equations (6.38) can be obtained. This proof, however, is very cumbersome and tedious, and does not yield a better understanding of the formulation. For these reasons, a numerical "proof" will be given. To obtain a more compact form, an equivalent form to equations (6.38) is given. Namely, the values of

$(a_1+a_2)\eta+(b_1+b_2)\xi$ and $(a_4+a_5)\xi+(b_4+b_5)\eta$ are reported at the Gauss points. First, a square element (see Figure 6.2a) is examined. The values for the first Gauss point are reported in Table 6.1. Values for other Gauss points may be obtained as follows: given that the value at the first point is v, then, at the other points it is - sign(ξ) * v, where sign(ξ) is the sign of the ξ/η coordinate at the given Gauss point (η for the first column and ξ for the second column).

Table 6.1 Square element

ν	$(a_1+a_2)\eta+(b_1+b_2)\xi$	$(a_4+a_5)\xi+(b_4+b_5)\eta$
0.	-0.144338	-0.144338
0.3	-0.082479	-0.082479
0.49	-0.005661	-0.005661
0.499	-0.000577	-0.000577
0.4999	-0.000058	-0.000058

Secondly, an element distorted from a parallelogram shape (see Figure 6.2b) is examined. In this case the values at the first and second Gauss points are reported. The value for the third Gauss point is minus the value at the second Gauss point, and the value at the forth Gauss point is minus the value at the second Gauss point. Results are summarized in Tables 6.2 and 6.3.

Table 6.2 Distorted element

ν	point	$(a_1+a_2)\eta+(b_1+b_2)\xi$			
		PSS3	PSS4	PSS5	PSS6
0.	1	-0.138299	-0.136318	-0.239751	-0.166003
	2	-0.142666	-0.145547	-0.234665	-0.224427
0.3	1	-0.074126	-0.072729	-0.2255061	-0.231639
	2	-0.077283	-0.079388	-0.204323	-0.169421
0.49	1	-0.004723	-0.004612	-0.051700	-0.037454
	2	-0.004982	-0.005156	-0.055967	-0.042924
0.499	1	-0.000479	-0.000467	-0.006410	-0.004384
	2	-0.000505	-0.000523	-0.006890	-0.004980
0.4999	1	-0.000048	-0.000047	-0.000650	-0.000446
	2	-0.000051	-0.000052	-0.000700	-0.000506

The results summarized in Tables 6.1, 6.2 and 6.3 "prove" equations (6.38).

Table 6.3 Distorted element					
ν	point	$(a_4+a_5)\xi+(b_4+b_5)\eta$			
		PSS3	PSS4	PSS5	PSS6
0.	1	-0.099318	-0.096704	-0.386263	-0.414609
	2	+0.102311	+0.103024	+0.388999	+0.420426
0.3	1	-0.053029	-0.051169	-0.692734	-1.013897
	2	+0.055193	+0.055728	+0.703892	+1.045209
0.49	1	-0.003365	-0.003215	+0.027529	+0.021353
	2	+0.003542	+0.003588	-0.029822	-0.024105
0.499	1	-0.000341	-0.000326	+0.002510	+0.001978
	2	+0.000359	+0.000364	-0.002771	-0.002279
0.4999	1	-0.000034	-0.000033	+0.000249	+0.000197
	2	+0.000036	+0.000036	-0.000276	-0.000227

It follows from equations (6.37) and (6.38) that as ν goes to 0.5^- the trace of $\mathbf{P}$ is given by:

$$trace\,\mathbf{P} = p_1 + p_2 \tag{6.39}$$

In order to show that the trace of the membrane strains goes to zero pointwise recall from Chapter 3 that the stress strain weak relation is given by:

$$\mathbf{H}^n\mathbf{p} - \mathbf{A}^n\mathbf{n} = 0 \tag{6.40}$$

To simplify notations and without loss of generality, ξ and η in the assumed strain field, equation (6.37), may be replaced by $\bar{\xi}$ and $\bar{\eta}$, given by:

$$\bar{\xi} = \xi - \xi_0 \quad ; \quad \bar{\eta} = \eta - \eta_0$$

where, ξ_0 and η_0 are shifts introduced in order to make $\mathbf{H}^n$ block diagonal. In order to obtain this result the following requirements must be met:

$$\int_A \bar{\xi}\, dA = 0$$

and

$$\int_A \bar{\eta}\, dA = 0$$

The resulting ξ_0 and η_0 are given by:

$$\xi_0 = \frac{J_1}{3J_0}$$

and

$$\eta_0 = \frac{J_2}{3J_0}$$

The $\mathbf{H}^n$ matrix is now of the following form:

$$\mathbf{H}^n = \begin{bmatrix} \mathbf{D}^n A & 0 \\ 0 & \hat{\mathbf{H}} \end{bmatrix} \tag{6.41}$$

where $\mathbf{D}^n$ is given by equation (2.23), A is the element area, and $\hat{\mathbf{H}}$ is the "material" properties for the linear part of the membrane strains. Based on results in equations (6.38), $\hat{\mathbf{H}}$ satisfies pointwise the incompressibility constraint. Hence, it remains only to consider the constant part, given by $\mathbf{D}^n A$.

Combining equations (6.40) and (6.41) yields:

$$p_1 = \frac{1}{\alpha A}\left\{(\lambda + 2\mu)\bar{n}_1 - \lambda \bar{n}_2\right\} \tag{6.42a}$$

and

$$p_2 = \frac{1}{\alpha A}\left\{(\lambda + 2\mu)\bar{n}_2 - \lambda \bar{n}_1\right\} \tag{6.42b}$$

where $\bar{\mathbf{n}} = \mathbf{A}^n \mathbf{n}$.

Substituting equations (6.42) into equation (6.39) yields:

$$trace\,\mathbf{P} = \frac{2\mu(\bar{n}_1 + \bar{n}_2)}{\alpha A} \tag{6.43}$$

As ν goes to 0.5^-, α goes to infinity while μ is bounded; hence the desired result is obtained. ▪

6.6.3 Plate bending elements: Hellinger-Reissner formulation

The rotation field given by equation (6.3) and the enhanced transverse displacement field, together with the assumed moment resultant and shear resultant fields presented in equations (6.19) and (6.22), respectively, form the independent fields for the Hellinger-Reissner based elements. As in the case of the membrane elements, the two elements differ only by the incompatible shape displacements used to reduce the assumed resultant fields. The element associated with the incompatible shape functions given by equations (6.30) is CRB1, and the element associated with the incompatible shape functions given by equations (6.31) is CRB2. In both elements the incompatible shape functions given by equations (6.32) are used for the incompatible transverse displacement.

The coupled structure of the assumed resultant field can easily be seen from the structure of the constraint equations. Unfortunately, due to symmetry conditions, the coupling involves only the terms associated with the constant part of the transverse shear resultants in the direction in which the Jacobian is constant. Consequently, in the worst case, these elements have two constraints per element. It follows that these elements will, in the worst case, lock whenever the S1 element locks. Note, however, that for a nonconstant Jacobian element in both directions, there are no constraints. Also, if the element is such that the Jacobian is constant only in one direction, then there is one constraint per element. Consequently, in both of these cases, shear locking will not occur.

6.6.4 Plate bending elements: Hu-Washizu formulation

The rotation field given by equation (6.3) and the enhanced transverse displacement field; together with the assumed moment and shear resultant fields presented in equations (6.19) and (6.22), respectively; the assumed curvature field, either equation (6.26a) or equation (6.26b); and the assumed shear strain field, given by either equation (6.27a) or equation (6.27b); form the independent fields for the Hu-Washizu based elements. The four elements proposed differ by the incompatible shape functions used to reduce the

assumed stress resultant and strain fields, and by the assumed strain fields. The elements associated with the incompatible shape functions given by equations (6.30) are CRB3 (strain fields given by equations (6.26a) and (6.27a)) and CRB5 (strain fields given by equations (6.26b) and (6.27b)); the elements associated with the incompatible shape functions given by equations (6.31) are CRB4 (strain fields given by equations (6.26a) and (6.27a)) and CRB6 (strain fields given by equations (6.26b) and (6.27b)). In all four elements the incompatible shape functions given by equations (6.32) are used for the incompatible transverse displacement.

The coupled structure of the assumed moment field to the assumed shear resultant field, as well as the coupled structure of the assumed curvature to the assumed shear strain field is obvious from the structure of the constraint equations introduced in Chapter 5. As in the case of the Hellinger-Reissner-based elements, the rank of the coupling is dependent upon the symmetry of the element, and once again the worst case scenario is the constant Jacobian element. In this case, there seem to be four constraints, two in the shear resultant field and two in the shear strain field, to be enforced in order to avoid shear locking at the thin plate limit. However, as was pointed out in Chapter 4, it is sufficient to constrain only the shear strain parameters. The constraint on the shear resultant parameters will follow. Consequently, as for the CRB1 and CRB2 elements, the Hu-Washizu based elements will lock, in the worst case, whenever the S1 element locks. Note, however, that for a nonconstant Jacobian element in both directions, there are no constraints. Also, if the element is such that the Jacobian is constant only in one direction, then there is one constraint per element. Consequently, in both of these cases, shear locking will not occur.

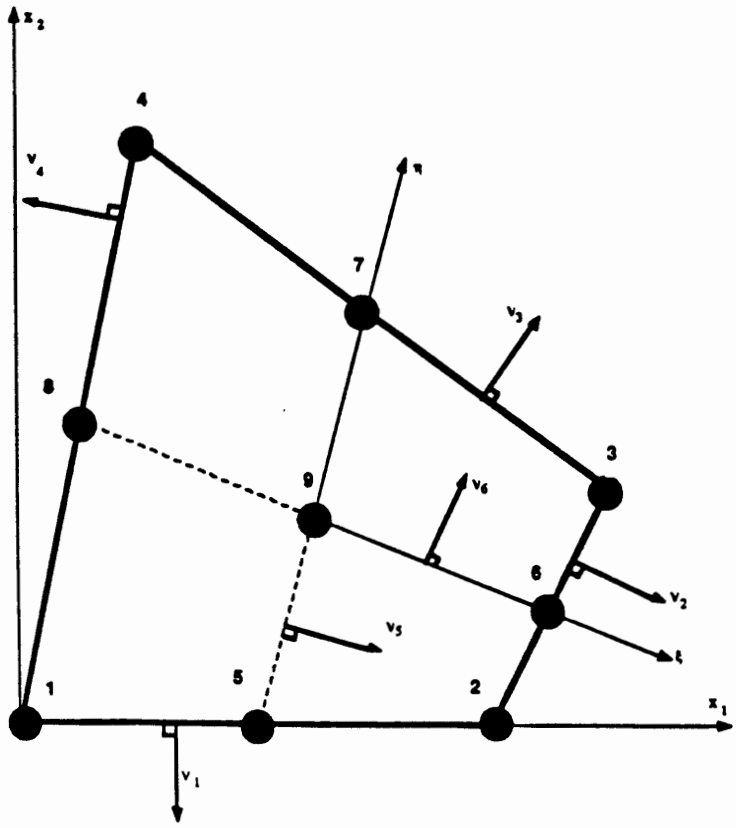

Figure 6.1: Location of the additional five "nodes" (numbers 5-9) and the normals to the paths used in the integration scheme to provide enhanced interpolation for the transverse displacement.

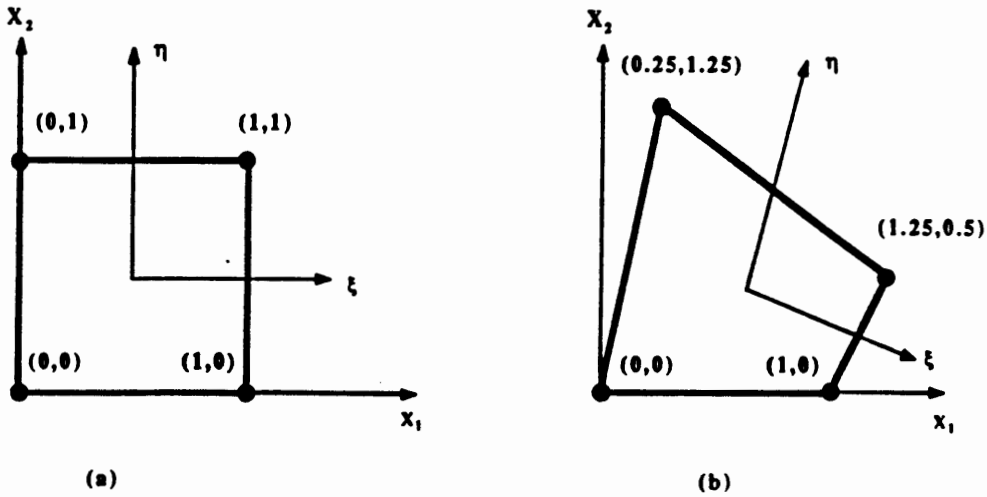

Figure 6.2: (a) Square element; (b) Element distorted from a parallelogram shape.

CHAPTER 7: NUMERICAL EXAMPLES

7.1 Introduction

The performance of the plane stress/strain (PSS) and plate bending (CRB) elements proposed in Chapter 6 is evaluated with several discriminating problems selected from the literature. The purpose of these evaluations is to test the proposed formulation sensitivity to the specific choice of the incompatible shape functions as well as the overall performance of the proposed elements.

First tackled are the constant strain patch tests in Section 7.2. Following these are the beam problems suggested by MacNeal & Harder [1985] in Section 7.3, the membrane problem suggested by Cook [1987] in Section 7.4, the thick walled cylinder also suggested by MacNeal & Harder [1985] in Section 7.5, a finite width strip with a hole in Section 7.6, bending of circular and square plates in Sections 7.7 and 7.8, respectively, and bending of a highly skewed rhombic plate in Section 7.9.

Convergence of the results obtained by the four-node elements presented in Chapter 6 are compared with other well-known four-node plane stress/strain and plate bending elements. A listing of these elements, and the abbreviations used to identify them is given in Tables 7.1.

Table 7.1a Reference Elements

Element	Description
2X2	Isoparametric plane stress/strain.
P-S	Pian & Sumihara [1984], plane stress/strain.
QBI	Belytschko & Bachrach [1986], plane stress/strain.
S1	Hughes *et. al.* [1978], plate bending.
T1	Hughes & Tezduyar[1981], plate bending.

Table 7.1b Proposed Plane Stress/Strain Elements			
Element	Formulation	Incompatible shape function equations	Strain transformation equations
PSS1	Hellinger-Reissner	(6.30)	-
PSS2	Hellinger-Reissner	(6.31)	-
PSS3	Hu-Washizu	(6.30)	(6.16)
PSS4	Hu-Washizu	(6.31)	(6.16)
PSS5	Hu-Washizu	(6.30)	(6.23)
PSS6	Hu-Washizu	(6.31)	(6.23)

Table 7.1c Proposed Plate Bending Elements			
Element	Formulation	Incompatible shape function equations	Strain transformation equations
CRB1	Hellinger-Reissner	(6.30)	-
CRB2	Hellinger-Reissner	(6.31)	-
CRB3	Hu-Washizu	(6.30)	(6.16) and (6.21)
CRB4	Hu-Washizu	(6.31)	(6.16) and (6.21)
CRB5	Hu-Washizu	(6.30)	(6.23) and (6.24)
CRB6	Hu-Washizu	(6.31)	(6.23) and (6.24)

Three types of boundary conditions are used for the plate bending examples:

SS1 - Simply Supported, $w = M_n = M_{nt} = 0$.

SS2 - Simply Supported, $w = M_n = \theta_t = 0$.

CL - Clamped, $w = \theta_n = \theta_t = 0$.

Two types of boundary conditions are used for the in-plane examples:

Fixed - $U_\alpha = 0$.

Free - $N^a_\alpha = 0$.

In all the examples given in this dissertation, identical results are obtained for elements formulated via the Hellinger-Reissner variational principle and the corresponding (i.e., same incompatible shape functions) elements formulated via the Hu-Washizu variational principle. Identical results are also obtained for the two approaches taken to transform the assumed strain field from the element's natural space into the physical space.

Convergence of the energy norm is the natural convergence test for the finite element method (Strang & Fix [1973]). It is common practice in the literature, however, to

examine convergence of the finite element solution by analyzing the displacement at some characteristic points. In this dissertation, convergence is examined in terms of both the energy norm and displacement at characteristic points (energy norm reported is twice the internal strain energy). All tables and figures show the displacement/energy norm as a function of the number of elements (denoted nel) used in the corresponding mesh.

7.2 Patch test

A rectangular domain is modeled by a single element shown in Figure 7.1a and the skewed mesh shown in Figure 7.1b. The mesh is subjected to constant states of tension, bending, shear and in-plane twist. The elements presented in this dissertation pass all tests with the exception of the constant out-of-plane shear, when the skewed mesh is used. The failure of the plate bending elements to pass the constant shear patch test is discussed in Section 6.2.2. Constant shear strain is modeled exactly, however, when all rotational degrees-of-freedom are fixed (this is the common test for constant shear in the finite element literature).

7.3 Beam problems

These problems were suggested by MacNeal & Harder [1985] as standard problems to evaluate the performance of different elements. Plane elements are used to model extension and in-plane shear, and plate bending elements are used to model out-of-plane shear and twist. The meshes used contain only one row of six elements for both the straight beams, shown in Figure 7.2, and the curved beam, shown in Figure 7.3. Geometrical and material properties used are summarized in Table 7.2. Results are normalized with respect to solutions obtained by beam theory which are summarized in Table 7.3.

Table 7.2 Material and Geometrical Properties for Beam Problems						
	E	ν	thickness	length/ inner radius	width/ outer radius	arc
straight beam	1.0E+7	0.3	0.1	6.0	0.2	-
curved beam	1.0E+7	0.25	0.1	4.12	4.32	90°

Table 7.3 Theoretical Solutions for Beam Problems		
Tip load direction	Displacement in the direction of the load	
	Straight beam	Curved beam
Extension	3.0E-5	-
In-plane-shear	0.1081	0.08734
Out-of-plane shear	0.4321	0.5022
Twist	0.03208	-

7.3.1 Extension

The straight beam meshes shown in Figure 7.2 are used for this problem. The exact solution is obtained for all (plane) elements. This example is equivalent to the patch test for plane elements.

7.3.2 In-plane shear

Both the straight beam meshes shown in Figure 7.2, and curved beam mesh shown in Figure 7.3 are used. The results are normalized with respect to the solution obtained by the beam theory, given in table 7.3, and are summarized in Table 7.4.

Table 7.4 In-plane shear			
mesh	PSS/P-S	2X2	QBI
straight (a)	0.9929	0.0933	0.9929
straight (b)	0.2208	0.0278	0.0777
straight (c)	0.7963	0.0348	0.0890
curved	0.9782	0.0740	0.2324

Results obtained for all proposed elements are identical to the results obtained by the Pian & Sumihara [1984] element. The 2X2 element locks for all meshes. However, if two rows of elements are used, the 2X2 element yields reasonable results. All elements exhibit

locking when trapezoid-shape elements are used (straight mesh (b)). This is in accordance with the theorem put forth by MacNeal [1987] regarding the locking of tapered four-node membrane elements. The QBI element appears to be much more sensitive to mesh distortion than the PSS or P-S elements.

7.3.3 Out-of-plane shear

Both the straight beams, Figure 7.2, and curved beam, Figure 7.3, meshes are used. The results are normalized with respect to the solution obtained by the beam theory, given in Table 7.3, and are summarized in Table 7.5.

Table 7.5 Out-of-plane shear

mesh	CRB1,3,5	CRB2,4,6	S1	T1
straight (a)	0.9825	0.9877	0.9801	0.9801
straight (b)	0.9706	0.9684	0.9963	0.9634
straight (c)	0.9843	0.9889	0.9912	0.9780
curved	0.9308	0.9248	29.535	0.9290

The proposed elements exhibit a slight sensitivity to the incompatible shape functions used, less than 0.5% for all meshes. The results for the CRB and T1 elements are comparable. The S1 element exhibits unstable behavior in the curved beam problem.

7.3.4 Twist of a beam

The straight beam meshes shown in Figure 7.2 are used. The results are normalized with the theoretical beam solution given in Table 7.3, and are summarized in Table 7.6.

Table 7.6 Twist of a straight beam

mesh	CRB1,3,5	CRB2,4,6	S1	T1
straight (a)	0.9429	0.9373	377.36	0.9445
straight (b)	0.9882	0.9622	108.83	0.8844
straight (c)	0.9478	0.9412	138.16	0.8490

The S1 element shows instability in this problem. The proposed elements show slightly superior results over the T1 element for distorted meshes (a and b). As in the

example of out-of-plane shear, the proposed elements show only slight sensitivity, a maximum of 2.6% for mesh b, to the type of incompatible shape functions used.

7.3.5 Beam bending: Sensitivity to mesh distortion

In this standard test, a beam is modeled by two elements. The beam is fixed at one end and subjected to a bending moment on the other, as shown in Figure 7.4. The material properties used are: E = 1.0 and ν = 0.4999. A state of plane strain is assumed. The edge separating the two elements is gradually rotated, as shown in the Figure, to skew the mesh. Results, normalized with the exact beam theory solution (w = 562.575), are reported in Table 7.7, and shown in Figure 7.5. Results for the 2X2 element are not reported since it exhibits severe locking.

Table 7.7 Beam bending; sensitivity to mesh distortion

Δ	PSS/P-S	QBI
0.00	1.0000	1.0000
0.25	0.9583	0.7891
0.50	0.8540	0.5103
1.00	0.7041	0.2773
2.00	0.6643	0.1944
4.99	0.7217	0.1885

All proposed elements yield identical results to the Pian & Sumihara [1984] element. The QBI element exhibits rapid deterioration as Δ is increased.

7.4 Cook's Membrane Problem

The problem consists of a trapezoidal plate clamped on one end and loaded by a uniformly distributed in-plane bending load on the other end, as shown in Figure 7.6. This problem has a considerable amount of shear deformation. It was suggested by Cook [1987] as an excellent problem to test membrane elements using skewed meshes. No analytical solution is available for this problem. The best known solution is given by Cook as: V_C = 0.29 (vertical displacement), σ_A = 0.236 (maximum principal stress) and σ_B = -0.201

(minimum principal stress). The material properties used are: E = 1.0, ν = 1.0/3.0, thickness = 1.0; plane stress assumption was used. The results normalized with respect to these best known answers are summarized in Tables 7.8 (V_C), 7.9 (σ_A) and 7.10 (σ_B), and shown in Figures 7.7, 7.8 and 7.9, respectively.

Table 7.8 V_C - Vertical displacement at point C

nel	PSS/P-S	2X2	QBI
1	0.6997	0.2497	0.2880
4	0.8841	0.4956	0.5782
16	0.9633	0.7657	0.8322
64	0.9912	0.9238	0.9506
256	0.9993	0.9804	0.9883

Table 7.9 σ_A - Maximum principal stress at point A

nel	PSS/P-S	2X2	QBI
1	0.8208	0.5074	0.4381
4	0.7858	0.4566	0.5246
16	0.9495	0.7667	0.7920
64	0.9935	0.9428	0.9623
256	1.0143	0.9967	1.0030

Table 7.10 σ_B - Minimum principal stress at point B

nel	PSS/P-S	2X2	QBI
1	0.7919	0.2388	0.5143
4	0.7709	0.3813	0.5587
16	0.9235	0.7142	0.7970
64	0.9882	0.9161	0.9482
256	1.0075	0.9930	1.000

The results presented for one element are obtained by interpolating the nodal values; for the finer meshes the nodal values are reported. The results obtained for all plane elements proposed in this dissertation yield identical results to the Pian & Sumihara [1984] element. Excellent results are obtained even for very coarse meshes; about 70% of the vertical displacement and 80% of the stresses are obtained using only one element. The 2X2 and QBI elements yield poor results for coarse meshes; less than 50% and 60% of the

vertical displacement and stresses are obtained by the 2X2 and QBI elements, respectively, when a four-element mesh is used.

7.5 Thick-Walled Cylinder

This problem was suggested by MacNeal & Harder [1985] as an excellent problem to test the effect of nearly incompressible material. The mesh used is shown in Figure 7.10. The material properties are: E = 1.0 and ν varies from 0.0 to 0.4999. The exact radial solution is given by:

$$u = \frac{(1+\nu)p R_1^2}{E(R_2^2 - R_1^2)}\left[\frac{R_2^2}{r} + (1-2\nu)r\right] \tag{7.1}$$

where p is the internal pressure; R_1 is the inner radius; R_2 is the outer radius; and r is the radius where the radial displacement, u, is to be computed.

Results at $r = R_1$, normalized with respect to the exact solution, are summarized in Table 7.11.

Table 7.11 Thick-Walled Cylinder

ν	PSS/P-S	2X2	QBI
0.	0.9987	0.9964	0.9985
0.3	0.9954	0.9908	0.9952
0.49	0.9913	0.8490	0.9911
0.499	0.9910	0.3606	0.9909
0.4999	0.9910	0.0534	0.9908

Once again all proposed plane elements yield identical results with the Pian & Sumihara [1984] element. Almost no deterioration with ν is observed, only 0.77% difference between the two extreme values of ν. The QBI element yields almost identical results. The 2X2 element exhibits the well known locking at the nearly incompressible limit.

7.6 Finite Strip With a Hole

This problem is introduced in order to test the accuracy of the stress distribution inside the proposed plane elements. A finite width strip with a hole, of width b, is subjected to uniform tensile stress in the axial direction, as shown in Figure 7.11. The axial stress along the critical section, line A-B, is investigated.

First, the relatively simple case of plane stress with free upper and lower edges is investigated in Section 7.6.1. Then, the more challenging case of plane strain, at the nearly incompressible limit, with the upper and lower edges fixed in the vertical direction, is tackled in Section 7.6.2.

7.6.1 Finite strip with a hole: Plane stress

The material properties used are E = 1.0 and ν = 0.3. First, convergence in the energy norm is examined. No analytical solution for the energy is known. Therefore, a converged finite element solution of 19.37 obtained for the Pian & Sumihara [1984] element using 3072 elements is used as the reference solution. Results normalized with respect to this reference solution are summarized in Table 7.12 and shown in Figure 7.12. The axial stress distribution along the critical section for the meshes containing 48 and 192 elements is presented in Figure 7.13. The results are compared with the analytical solution given by Savin [1961].

Table 7.12 Strip With a Hole - Plane Stress
Convergence in the energy norm

nel	PSS/P-S	2X2	QBI
3	0.9582	0.9515	0.9587
12	0.9763	0.9716	0.9747
48	0.9897	0.9876	0.9886
192	0.9964	0.9959	0.9964
768	0.9990	0.9990	0.9990
3072	1.0000	1.0000	1.0000

Almost identical results are obtained for the proposed elements and the Pian & Sumihara element (about 5.0E-3 difference in energy norm for the three-element mesh). A very small sensitivity to the incompatible shape functions used is observed (about 2.0E-3 difference in the energy norm for the three-element mesh).

Excellent results are obtained for both the energy norm, 95.82% of the reference solution with only three elements, and stress distribution inside the elements. The 2X2 and QBI elements yield comparable results for this problem.

7.6.2 Finite strip with a hole: Plane strain

The material properties used are E = 1.0 and ν = 0.4999. First, convergence in the energy norm is examined. No analytical solution for the energy is available. Therefore, a converged finite element solution of 2.389 obtained for the Pian & Sumihara [1984] element using 12288 elements is used as the reference solution. Results normalized with respect to this reference solution are summarized in Table 7.13 and shown in Figure 7.14. The axial stress distribution along the critical section for the meshes containing 48 and 192 elements is presented in Figure 7.15. No analytical solution for the stress distribution is available. Therefore, the smoothed stresses obtained for the 768-element mesh are used as a reference.

Table 7.13 Strip With a Hole - Plane Strain
Convergence in the energy norm

nel	PSS1,3,5	PSS2,4,6	P-S	2X2	QBI
3	0.6974	0.6844	0.7082	0.0061	0.5919
12	0.8363	0.8326	0.8401	0.0084	0.8108
48	0.9368	0.9360	0.9372	0.0167	0.9330
192	0.9812	0.9812	0.9812	0.0477	0.9807
768	0.9967	0.9967	0.9967	0.1754	0.9958
3072	0.9992	0.9992	0.9992	0.3968	0.9992

The results obtained show the Pian & Sumihara element to exhibit a marginal superiority over the proposed elements for the coarse meshes, only 0.8% for a twelve-element mesh. The formulation shows a small sensitivity to the type of incompatible shape

functions used, only 1.3% and 0.04% for three- and twelve-element meshes, respectively.

Excellent results are obtained; with only three elements in the mesh, 69% and 68% of the reference solution is obtained for the PSS1,3,5 and PSS2,4,6, respectively. Excellent results are also obtained for the stress distribution inside the elements.

7.7 Circular Plates

A circular plate is modeled using 3, 12, 48 and 192 elements. Due to symmetry, only one quadrant is discretized. A typical mesh used is shown in Figure 7.16. While the three-element mesh results are retained, it should be noted that significant errors result in approximating the domain. SS1 and CL boundary conditions are used. The material properties and geometrical data used are summarized in Table 7.14.

Table 7.14 Material and Geometrical Data for Circular plates

	E	ν	h	R
Thin Plate	10920	0.3	0.1	5.0
Thick Plate	1.365	0.3	2.0	5.0

With these properties the plate stiffness $D = \dfrac{E\,h^3}{12(1-\nu^2)} = 1.0$.

Two loading types are examined:

- Uniform transverse unit load, and
- Unit point load at the center of the plate.

The analytical solution for the case of uniform transverse unit load is given by:

Clamped boundary, center transverse displacement:

$$w(0) = \frac{q R^4}{64 D}\left[1 + \frac{8}{3\alpha(1-\nu)}\left(\frac{h}{R}\right)^2\right] \tag{7.2}$$

Clamped boundary, external work:

$$E_{CL} = \frac{q^2 R^6 \varnothing}{384 D}\left[1 + \frac{4}{\alpha(1-\nu)}\left(\frac{h}{R}\right)^2\right] \tag{7.3}$$

Simply supported, center transverse displacement:

$$w(0) = \frac{qR^4}{64D}\left[\frac{5+\nu}{1+\nu} + \frac{8}{3\alpha(1-\nu)}\left(\frac{h}{R}\right)^2\right] \tag{7.4}$$

Simply supported, external work:

$$E_{SS} = \frac{q^2R^6\varnothing}{384D}\left[\frac{7+\nu}{1+\nu} + \frac{4}{\alpha(1-\nu)}\left(\frac{h}{R}\right)^2\right] \tag{7.5}$$

where, for all examples considered in this section, $\varnothing$ is the sector analyzed, and is equal to $\frac{\pi}{2}$; and $\alpha = \frac{5}{6}$ is the correction factor that was introduced in Section 2.4.

It should be noted again that the above energy expressions represent the total work performed by the external transverse loads, and consequently are twice the actual strain energy.

In theories that account for shear deformations, the analytical solution for the transverse displacement under a point load is infinite. Consequently, the external work is also infinite. The finite element method, however, being a weak approximation, yields a finite transverse displacement under the load. The sensitivity of the finite element solution depends heavily on the plate thickness. For thin plates, the finite element solution converges to the thin plate solution in the initial phase of mesh refinement. However, when very fine meshes are used in the vicinity of the point load, the singularity will be evident. When thick plates are considered, the singularity is evident even for coarse meshes. In the case of thick plates, some elements exhibit unstable behavior. These examples are included in order to test the proposed elements' sensitivity to singularity in the solution.

7.7.1 Simply supported thin plate: Uniform transverse load

The analytical solutions are: w(0) = 39.83156 and E_{SS} = 359.08748. The results obtained, normalized with respect to these solutions, are summarized in Table 7.15, and are shown in Figures 7.17 and 7.18 for the convergence of the center displacement and

energy norm, respectively.

Table 7.15 Simply Supported (SS1) Circular Plate
Uniform Load, h = 0.1

nel	CRB1,3,5		CRB2,4,6		S1		T1	
	disp.	energy	disp.	energy	disp.	energy	disp.	energy
3	1.1075	1.0913	1.1866	1.1964	0.7588	0.5846	0.9141	0.7589
12	1.0314	1.0324	1.0617	1.0842	0.9305	0.8760	0.9801	0.9336
48	1.0083	1.0089	1.0174	1.0242	0.9826	0.9675	0.9950	0.9830
192	1.0021	1.0023	1.0045	1.0063	0.9957	0.9918	0.9988	0.9957

Monotonic convergence in both the energy norm and center transverse displacement is obtained for all elements. The elements proposed in this dissertation show some sensitivity to the type of incompatible shape functions used for coarse meshes, from 10.5% difference in the energy norm for the three-element mesh to only 1.5% difference for the 48-element mesh. Convergence is from above for all elements proposed in this dissertation in both the energy norm and the center displacement. The S1 and T1 elements, on the other hand, converge from below in both criteria. Results for all elements are comparable, with a slight advantage to the CRB1,3,5 elements.

7.7.2 Simply supported thick plate: Uniform transverse load

The analytical solutions are: w(0) = 46.95656 and E_{SS} = 429.03701. The results obtained, normalized with respect to these solutions, are summarized in Table 7.16 and are shown in Figures 7.19 and 7.20 for the convergence of the center displacement and energy norm, respectively.

Table 7.16 Simply Supported (SS1) Circular Plate
Uniform Load, h = 2.0

nel	CRB1,3,5		CRB2,4,6		S1		T1	
	disp.	energy	disp.	energy	disp.	energy	disp.	energy
3	1.0855	1.0342	1.1552	1.1220	0.7877	0.6091	0.9255	0.7556
12	1.0244	1.0152	1.0533	1.0594	0.9385	0.8844	0.9816	0.9325
48	1.0064	1.0044	1.0143	1.0172	0.9847	0.9698	0.9954	0.9827
192	1.0016	1.0011	1.0036	1.0045	0.9962	0.9924	0.9989	0.9956

Monotonic convergence in both the energy norm and center transverse displacement is obtained for all elements. Again, the proposed elements show some sensitivity to the type of incompatible shape functions used for coarse meshes, from 8.8% difference in the energy norm for the three-element mesh to only 1.3% difference for the 48-element mesh. Convergence is from above for all elements proposed in this dissertation in both the energy norm and the center displacement. The S1 and T1 elements, on the other hand, converge from below in both criteria. Results for all elements are comparable, with a slight advantage to the CRB1,3,5 elements.

7.7.3 Clamped thin plate: Uniform transverse load

The analytical solutions are: w(0) = 9.78348 and E_{CL} = 64.09118. The results obtained, normalized with respect to these solutions, are summarized in Table 7.17 and are shown in Figures 7.21 and 7.22 for the convergence of the center displacement and energy norm, respectively.

Table 7.17 Clamped Circular Plate
Uniform Load, h = 0.1

nel	CRB1,3,5		CRB2,4,6		S1		T1	
	disp.	energy	disp.	energy	disp.	energy	disp.	energy
3	1.1813	1.1567	1.5918	1.7975	0.7341	0.5257	0.9274	0.8003
12	1.0530	1.0742	1.1912	1.3643	0.9128	0.8566	0.9865	0.9508
48	1.0146	1.0279	1.0526	1.1064	0.9784	0.9623	0.9969	0.9877
192	1.0037	1.0057	1.0136	1.0277	0.9947	0.9905	0.9993	0.9965

Monotonic convergence in both the energy norm and center transverse displacement is obtained for all elements. The proposed elements show great sensitivity to the type of incompatible shape functions used. 64% difference in the energy norm is observed for the three-element mesh. However, for the 192-element mesh, only 2.4% difference is observed in the energy norm. Again, convergence is from above for all elements proposed in this dissertation in both the energy norm and the center displacement. The S1 and T1 elements, on the other hand, converge from below in both criteria. The T1 element appears

to yield the best results, but the CRB1,3,5 elements yield comparable results.

7.7.4 Clamped thick plate: Uniform transverse load

The analytical solutions are: w(0) = 16.90848 and E_{CL} = 134.04070. The results obtained, normalized with respect to these solutions, are summarized in Table 7.18 and are shown in Figures 7.23 and 7.24 for the convergence of the center displacement and energy norm, respectively.

Table 7.18 Clamped Circular Plate
Uniform Load, h = 2.0

nel	CRB1,3,5		CRB2,4,6		S1		T1	
	disp.	energy	disp.	energy	disp.	energy	disp.	energy
3	1.0725	0.9372	1.2954	1.2441	0.8192	0.6348	0.9275	0.7681
12	1.0239	0.9979	1.1066	1.1394	0.9427	0.8937	0.9858	0.9384
48	1.0065	1.0007	1.0289	1.0413	0.9859	0.9724	0.9967	0.9843
192	1.0017	1.0003	1.0074	1.0108	0.9965	0.9930	0.9992	0.9960

Monotonic convergence in both criteria is obtained by S1, T1 and CRB2,4,6 elements. The CRB1,3,5 elements converge monotonically only in the center displacements. As in the case of the thin plate a great sensitivity to the incompatible function used is shown. The best results are shown by the CRB1,3,5 elements; unfortunately, however, they exhibit non-monotonic convergence in the energy norm. For this reason, the T1 appears to yield the best results, with the S1 and CRB2,4,6 elements yielding comparable results.

7.7.5 Simply supported plates: Unit concentrated load at the center

The results for simply supported (SS1) plates under unit concentrated load at the center of the plate are summarized in Tables 7.19 and shown in Figures 7.25 (thin plate) and 7.26 (thick plate). The results obtained for the thin plate are normalized with the solution given by the thin plate solution, w(0) = 1.26253 (Timoshenko & Woinowsky-Krieger [1959]). The results obtained for the thick plate are normalized with $\frac{P R^2}{16 \pi D}$. As

noted above, the displacement at the center for the thick plate is infinite, due to shear deformations.

Table 7.19a Circular Plate - Point Load, Simply Supported (SS1), h = 0.1				
nel	CRB1,3,5	CRB2,4,6	S1	T1
3	1.0725	1.2213	0.9883	0.9837
12	1.0234	1.0679	0.9725	0.9970
48	1.0096	1.0261	0.9943	1.0000
192	1.0045	1.0107	1.0007	1.0013

Table 7.19b Circular Plate - Point Load, Simply Supported (SS1), h = 2.0				
nel	CRB1,3,5	CRB2,4,6	S1	T1
3	3.8051	4.3236	3.8978	3.7070
12	3.9092	4.1173	4.3675	3.8938
48	4.1125	4.1821	4.9250	4.1204
192	4.3506	4.3719	5.4466	4.3598

All elements exhibit monotonic convergence for the thin plate limit. In the thick plate case only the CRB2,4,6 elements do not exhibit monotonic convergence. If the three-element mesh results are ignored, the CRB2,4,6 elements, too, exhibit monotonic convergence. As was pointed out in the beginning of this section, the three-element mesh is a rather poor approximation of the domain. Consequently, all elements exhibit monotonic convergence for the thick plate as well as for the thin plate.

The proposed elements exhibit sensitivity to the incompatible shape functions used. This sensitivity, however, diminishes under mesh refinement, from about 15% for the three-element mesh to only about 0.5% for the 192-element mesh.

7.7.6 Clamped plates: Unit concentrated load at the center

The results for thin and thick plates are summarized in Tables 7.20a and 7.20b, respectively, and shown in Figures 7.27 (thin plate) and 7.28 (thick plate). The results for the thin plate case are normalized with the thin plate solution, w(0) = 0.4973592

(Timoshenko & Woinowsky-Krieger [1959]). The results for the thick plate are normalized with $\frac{P R^2}{16 \pi D}$.

Table 7.20a Circular Plate - Point Load, Clamped, h = 0.1				
nel	CRB1,3,5	CRB2,4,6	S1	T1
3	1.0479	1.3759	0.8452	0.8089
12	1.0217	1.1202	0.9315	0.9534
48	1.0157	1.0585	0.9860	0.9905
192	1.0093	1.0256	1.0022	1.0010

Table 7.20b Circular Plate - Point Load, Clamped, h = 2.0				
nel	CRB1,3,5	CRB2,4,6	S1	T1
3	2.1361	2.6792	2.3496	1.9342
12	2.3394	2.5571	2.9134	2.2919
48	2.5668	2.6387	3.4677	2.5609
192	2.8104	2.8263	3.9883	2.8135

Identical behavior to that observed for the simply supported plate under point load is repeated for the clamped plate.

Next the thick plate case is used to demonstrate the stability of the proposed elements. The transverse displacement along the radius, normalized with $\frac{P R^2}{16 \pi D}$, for a mesh of 48 elements, is reported in Table 7.21 and shown in Figure 7.29. The analytical solution can be found in Lukasiewicz [1979]. The S1 shows the well known instability (Hughes [1987]); the T1 and all CRB elements, on the other hand, show excellent results.

7.8 Square Plates

A square plate is modeled using meshes of uniform square elements. Due to symmetry, only one quadrant is discretized. A typical mesh is shown in Figure 7.30. The material properties and geometrical data are summarized in Table 7.22. Using these properties, the plate bending stiffness D = 1.0.

Table 7.21 Thick clamped circular plate, transverse displacement along the radius					
r/R	CRB1,3,5	CRB2,4,6	S1	T1	EXACT
0.000	2.5668	2.6387	3.4677	2.5609	∞
0.125	1.6499	1.6839	0.8499	1.6338	1.5659
0.250	1.2703	1.2924	1.8104	1.2603	1.1951
0.375	0.9426	0.9589	0.4793	0.9343	0.8895
0.500	0.6575	0.6836	0.9985	0.6500	0.6189
0.625	0.4152	0.4273	0.1176	0.4104	0.3883
0.750	0.2202	0.2292	0.4170	0.2167	0.2033
0.875	0.0794	0.0844	-0.0298	0.0776	0.0714
1.000	0.0000	0.0000	0.0000	0.0000	0.0000

Table 7.22 Material Properties and Geometrical Data				
	E	ν	h	L
Thin Plate	10.92E+6	0.3	0.01	10.0
Thick Plate	1.365	0.3	2.0	10.0

Only the case of uniform transverse loading is examined. The boundary conditions examined are: SS1, SS2, and CL.

The "exact" energy reported is computed from:

$$E = \int_{\Omega} q(x_1,x_2)\, w(x_1,x_2)\, d\Omega \tag{7.6}$$

using a Fourier series solution and, thus, is twice the actual strain energy.

7.8.1 Thin simply supported (SS1) plate

The exact solution is $w = 40.623$ (Timoshenko & Woinowsky-Krieger [1959]) and $E = 425.6276$. Results, normalized with the exact solution, are summarized in Table 7.23 and shown in Figures 7.31 (center displacement) and 7.32 (energy).

Monotonic convergence is obtained for all elements. The T1 element yields the best results. All other elements, however, yield comparable results.

With the exception of the one-element mesh, only mild sensitivity to the incompatible shape function used is observed. A difference of only 2.4% and 3.4% is observed in the center transverse displacement and energy norm, respectively, for the four-element mesh.

Table 7.23 Square Plate - SS1 - h = 0.01								
nel	CRB1,3,5		CRB2,4,6		S1		T1	
	disp.	energy	disp.	energy	disp.	energy	disp.	energy
1	1.3663	1.3585	1.0987	1.1897	1.4794	0.8825	0.7850	0.4683
4	1.1012	1.0901	1.0764	1.0565	1.0645	0.9456	0.9770	0.8552
16	1.0328	1.0233	1.0174	1.0199	1.0162	0.9863	0.9949	0.9628
64	1.0062	1.0062	1.0046	1.0059	1.0041	0.9966	0.9988	0.9907
256	1.0022	1.0022	1.0021	1.0025	1.0012	0.9994	0.9997	0.9977

7.8.2 Thin simply supported (SS2) plate

The exact solution is $w = 40.623$ and $E = 425.6276$ (thick plate theory, series solution). Results, normalized with the exact solution, are summarized in Table 7.24 and shown in Figures 7.33 (center displacement) and 7.34 (energy).

Table 7.24 Square Plate - SS2 - h = 0.01								
nel	CRB1,3,5		CRB2,4,6		S1		T1	
	disp.	energy	disp.	energy	disp.	energy	disp.	energy
1	1.3665	1.3585	1.1611	1.1544	0.7850	0.4683	0.7850	0.4683
4	1.0881	1.0789	1.0515	1.0425	0.9770	0.8552	0.9770	0.8552
16	1.0212	1.0190	1.0129	1.0106	0.9949	0.9628	0.9949	0.9628
64	1.0060	1.0056	1.0039	1.0034	0.9988	0.9907	0.9988	0.9907
256	1.0021	1.0020	1.0022	1.0024	0.9997	0.9977	0.9997	0.9977

Monotonic convergence is obtained for all elements. T1 and S1 elements yield identical results. The CRB2,4,6 elements obtain the smallest error in the energy norm. All other elements, however, yield comparable results.

As observed for the SS1 boundary condition, with the exception of the one-element mesh, only mild sensitivity to the incompatible shape function used is observed.

7.8.3 Thin clamped plate

The exact thin plate solution is $w = 12.6$ (Timoshenko & Woinowsky-Krieger [1959]). No analytical solution is available for the energy. Consequently, a converged finite element solution obtained using 4096 elements is used, $E = 97.3$. Results, normalized with these values, are summarized in Table 7.25 and shown in Figures 7.35 (center

displacement) and 7.36 (energy).

Table 7.25 Clamped - h = 0.01

nel	CRB1,3,5		CRB2,4,6		S1		T1	
	disp.	energy	disp.	energy	disp.	energy	disp.	energy
1	0.0001	0.0001	0.0001	0.0001	0.0000	0.0000	0.0000	0.0000
4	0.9774	0.7912	0.9174	0.7427	0.9613	0.7781	0.9613	0.7781
16	0.9976	0.9475	0.9824	0.9333	0.9926	0.9421	0.9926	0.9421
64	1.0059	0.9922	1.0025	0.9894	1.0013	0.9852	1.0013	0.9852
256	1.0072	1.0021	1.0109	1.0095	1.0035	0.9962	1.0035	0.9962
1024	1.0052	1.0007	1.0076	1.0051	1.0041	0.9989	1.0041	0.9989
4096	1.0045	1.0000	1.0052	1.0013	1.0042	0.9996	1.0042	0.9996

The converged finite element solution of the transverse displacement is about 0.4% larger than the solution obtained by the thin plate theory. This result is expected since all the elements under discussion are based on a theory that accounts for shear deformation.

The S1 and T1 elements yield identical results. Both elements obtain monotonic convergence in both criteria. The CRB elements, on the other hand, do not converge monotonically. A small sensitivity to the incompatible shape functions is observed. Only about 1.5% difference is observed in both the energy norm and center transverse displacement for the 16-element mesh.

All elements exhibit locking for the one-element mesh. This result is expected since all rotational degrees-of-freedom are constrained, and consequently the rotations are zero pointwise in the element's domain. It follows from the shear strain transverse displacement relation (see Section 2.2) that the derivatives of the transverse displacement go to zero pointwise as the thickness is reduced to zero; consequently, the transverse displacement tends to zero as the plate thickness is reduced to zero.

7.8.4 Thick simply supported (SS1) plate

A converged finite element solution of $w = 55.45$ and $E = 600.9$, obtained using 4096 elements, is used as the reference solution. Results, normalized with this reference solution, are summarized in Table 7.26 and shown in Figures 7.37 (center displacement) and

7.38 (energy).

Table 7.26 Square Plate - SS1 - h = 2.0

nel	CRB1,3,5		CRB2,4,6		S1		T1	
	disp.	energy	disp.	energy	disp.	energy	disp.	energy
1	1.2998	1.1836	1.1859	1.0887	1.3414	0.7737	0.8026	0.4629
4	1.0833	1.0481	1.1548	1.1326	1.0197	0.8957	0.9462	0.8202
16	1.0168	1.0091	1.0517	1.0535	1.0036	0.9722	0.9788	0.9446
64	1.0036	1.0017	1.0138	1.0148	1.0008	0.9929	0.9936	0.9848
256	1.0008	1.0001	1.0035	1.0038	1.0002	0.9982	0.9983	0.9961

With the exception of the CRB2,4,6 elements, all elements obtain monotonic convergence in both the energy norm and center transverse displacements. If the results for the one-element mesh are ignored, the CRB2,4,6 elements, too, obtain monotonic convergence. All elements yield comparable results.

Only mild sensitivity to the incompatible shape functions used is observed.

7.8.5 Thick simply supported (SS2) plate

The analytical solution for the case of SS2 boundary conditions (series solution which includes shear deformation) is $w = 49.043$ and $E = 526.04$. Results, normalized with the analytical solution, are summarized in Table 7.27 and shown in Figures 7.39 (center displacement) and 7.40 (energy).

Table 7.27 Square Plate - SS2 - h = 2.0

nel	CRB1,3,5		CRB2,4,6		S1		T1	
	disp.	energy	disp.	energy	disp.	energy	disp.	energy
1	1.4559	1.2773	1.3448	1.1314	0.9495	0.5486	0.8687	0.5062
4	1.1267	1.0914	1.1743	1.1412	1.0035	0.8759	0.9899	0.8657
16	1.0315	1.0242	1.0466	1.0442	1.0003	0.9681	0.9979	0.9655
64	1.0078	1.0061	1.0117	1.0115	1.0000	0.9920	0.9995	0.9913
256	1.0020	1.0010	1.0091	1.0029	1.0000	0.9980	0.9999	0.9978
1024	1.0005	1.0004	1.0007	1.0007	1.0000	0.9995	1.0000	0.9995
4096	1.0001	1.0001	1.0002	1.0002	1.0000	0.9999	1.0000	0.9999

With the exception of the S1 element, all elements obtain monotonic convergence in both criteria. If the results for the one-element mesh are ignored, the S1 element, too,

obtains monotonic convergence. All elements yield comparable results. Only mild sensitivity to the incompatible shape functions used is observed. Results for the 4096-element mesh are reported in order to demonstrate that a converged solution is obtained when using this mesh. Consequently, solutions obtained for this mesh may be used as reference solutions when no analytical solution is available.

7.8.6 Thick clamped plate

A converged finite element solution of $w = 21.72$ and $E = 203.7$, obtained using 4096 elements, is used as the reference solution. Results, normalized with this reference solution, are summarized in Table 7.28 and shown in Figures 7.41 (center displacement) and 7.42 (energy).

Table 7.28 Square Plate - CL - h = 2.0

nel	CRB1,3,5		CRB2,4,6		S1		T1	
	disp.	energy	disp.	energy	disp.	energy	disp.	energy
1	0.9451	0.6298	1.4366	0.9573	0.6577	0.4383	0.4933	0.3287
4	1.1166	1.0121	1.4551	1.4287	1.0025	0.8658	0.9641	0.8375
16	1.0326	1.0087	1.1247	1.1369	1.0009	0.9660	0.9933	0.9586
64	1.0083	1.0026	1.0314	1.0357	1.0002	0.9916	0.9984	0.9898
256	1.0021	1.0009	1.0079	1.0092	1.0001	0.9981	0.9997	0.9976

The S1 and T1 elements obtain monotonic convergence in both the energy norm and center displacement criteria. The CRB elements obtain monotonic convergence only if the results obtained for the one-element mesh are ignored. The S1 element yields the best results. The T1 and CRB1,3,5 elements yield comparable results, with the CRB2,4,6 elements slightly more flexible.

A large sensitivity to the incompatible shape function is observed for the coarse meshes, more than 40% difference is observed in the energy norm for the four-element mesh. For the 256-element mesh, however, only 0.8% difference is observed.

7.8.7 Mesh distortion

To study the sensitivity to mesh distortion, a coarse mesh modeling a clamped square plate is used. Only four elements are used to model one quadrant of the plate. The plate is loaded by a uniform unit transverse load. The thin plate material properties are used. Two types of distortion are introduced. First, the center node of the mesh is moved along the main diagonal of the plate as shown in Figure 7.43. Results, normalized with respect to the thin plate solution $w = 12.6$ (Timoshenko & Woinowsky-Krieger [1959]), are summarized in Table 7.29, and shown in Figure 7.44.

Table 7.29 Mesh Distortion - Symmetric

Δ	CRB1,3,5	CRB2,4,6	S1	T1
-1.25	0.9992	1.7792	0.8773	0.8613
-1.00	1.0330	1.4123	0.9208	0.8790
-0.50	1.0171	1.0136	0.9600	0.9152
+0.00	0.9774	0.9174	0.9613	0.9613
+0.50	0.9089	0.8775	0.9248	1.0033
+1.00	0.7847	0.8935	0.8409	0.9998
+1.25	0.7030	0.8691	0.7735	0.9410

Next the center node is moved parallel to the edge as shown in Figure 7.45. Results, normalized with respect to the thin plate solution $w = 12.6$ (Timoshenko & Wionowsky-Krieger [1959]), are summarized in Table 7.30, and shown in Figure 7.46.

The difficulty of this mesh is that there are only eight degrees-of-freedom. The "optimal" number of constraints per element, according to the constraint count method (see Appendix 4.1), is two. Consequently, the ratio of degrees-of-freedom to constraints, for this mesh, is one. Thus, shear locking becomes an important issue as the symmetry of the mesh is lost.

Results show that all CRB elements do not lock. The S1 and T1, on the other hand, show severe locking. The T1 element locks much faster than the S1 element. This is in accordance with the remark made in Section 4.3, noting the S1 element behavior, in terms of shear locking, to be the best case scenario for the T1 element. Numerical results indicate that severe locking (of the S1 and T1 elements) occurs when the distortion, Δ,

Table 7.30 Mesh Distortion - Asymmetric				
Δ	CRB1,3,5	CRB2,4,6	S1	T1
0.00	0.9774	0.9174	0.9613	0.9613
0.02	0.9371	0.8817	0.9495	0.8917
0.04	0.8606	0.8136	0.9163	0.7316
0.06	0.7963	0.7560	0.8658	0.5629
0.08	0.7529	0.7170	0.8037	0.4256
0.10	0.7250	0.6919	0.7357	0.3241
0.15	0.6902	0.6611	0.5681	0.1773
0.20	0.6763	0.6498	0.4300	0.1086
0.30	0.6673	0.6457	0.2526	0.0516
0.50	0.6673	0.6602	0.1074	0.0193
0.80	0.6755	0.7065	0.0437	0.0077
1.00	0.6817	0.7534	0.0279	0.0049
1.50	0.6929	0.9392	0.0119	0.0022
2.00	0.6785	1.1534	0.0064	0.0013
2.49	0.6009	1.3373	0.0039	0.0009

becomes larger than about 30 times the plate thickness. Consequently, as the thickness is reduced to zero, the S1 and T1 elements become more and more sensitive to mesh distortion. The CRB elements, on the other hand, show the same type of behavior as indicated by Figure 7.46 (i.e., faster deterioration than the S1 element in the initial distortion phase, but deterioration stops at about 65% of the solution).

7.8.8 Shear and moment resultants

These examples were proposed by Hinton & Huang [1986] as a set of tests designed to test the stress resultants recovered by the finite element approximation. A square plate of side length $L = 10$ is modeled by a graded mesh shown in Figure 7.47. Due to symmetry only one quadrant is discretized. The stress distribution inside the elements is reported. Results are compared to the solutions given by Kant & Hinton [1983].

First, SS2 boundary conditions are considered. The distribution of M_{12} along the line $x_2 = 0$ is presented in Figures 7.48 and 7.49 for the CRB1,3,5 and CRB2,4,6 elements, respectively. The distribution of Q_2 along the line $x_2 = 0$ is reported in Figures 7.50 and 7.51 for the CRB1,3,5 and CRB2,4,6 elements, respectively. The distribution of Q_1 along

the line $x_2 = L/2$ for all CRB elements is presented in Figure 7.52.

The moment distribution inside the CRB1,3,5 elements has an opposing gradient to the exact moment gradient. This behavior results from the choice of the incompatible shape functions. These functions, in the CRB1,3,5 elements, do not satisfy the last criteria set in Box 5.3, which was introduced in order to avoid this pathology. On the other hand, in the CRB2,4,6 elements, in which the incompatible shape functions satisfy all criteria set in Box 5.3, the moment gradient has the same slope orientation as the exact solution.

The distribution of Q_2 along the line $x_2 = 0$ exhibits large oscillations whenever a big change in the element size occurs (only for distorted elements). For regular meshes, almost identical distributions are obtained for the CRB1,3,5 and CRB2,4,6 elements, as can be seen from the distribution of Q_1 in Figure 7.52.

Secondly, SS1 boundary conditions are imposed along the lines $x_1 = 0$ and $x_1 = L$. The distribution of Q_1 along the line $x_2 = L/2$ is shown in Figure 7.53, for both CRB1,3,5 and CRB2,4,6 elements. The M_{12} distribution along the line $x_2 = 0$ is shown in Figure 7.54 for the CRB1,3,5 elements and in Figure 7.55 for the CRB2,4,6 elements. The Q_2 distribution along the line $x_2 = 0$, for all CRB elements, is shown in Figure 7.56.

Both shear distributions reported are almost identical for both the CRB1,3,5 and CRB2,4,6 elements. The moment distribution in the CRB1,3,5 elements show the same pathology observed for the uniform SS2 boundary conditions. Excellent results are observed for the CRB2,4,6 elements.

7.9 Rhombic Plates

In this standard test, a highly skewed rhombic plate of side length $L = 100.0$ and an acute angle $\Theta = 30^o$ is modeled by a uniform mesh. A typical mesh is shown in Figure 7.57. The material properties used are: $E = 10E+6$ and $\nu = 0.3$. Two thicknesses are considered: $h = 1.0$ and $h = 0.1$. A comparison solution for the center displacement of

$w = 0.04455$ for $h = 1.0$ and $w = 44.55$ for $h = 0.1$ was obtained by Morley [1963]. No solution is available, however, for the energy. Consequently, converged finite element solutions of $E = 78.9$ ($h = 1.0$) and $E = 770317.0$ ($h = 0.1$) are used as reference solutions. Results for h = 1.0, normalized with the reference solution, are summarized in Table 7.31 and shown in Figures 7.58 (center displacement) and 7.59 (energy). The distribution of M_{11} and M_{22} along the short diagonal, for h = 1.0, is shown in Figures 7.60 (CRB1,3,5 elements) and 7.61 (CRB2,4,6 elements). Results, for h = 0.1, normalized with the reference solution, are summarized in Table 7.32 and shown in Figures 7.62 (center displacement) and 7.63 (energy).

Table 7.31 Rhombic Plate - Uniform load, SS1, h = 1.0, a = 100., $\Theta = 30^o$

nel	CRB1,3,5		CRB2,4,6		S1		T1	
	disp.	energy	disp.	energy	disp.	energy	disp.	energy
4	1.0910	1.2072	2.1844	1.9843	0.6581	0.4582	0.6239	0.4344
16	0.8823	0.8903	1.2229	1.1125	1.0121	0.8328	0.8795	0.7483
64	0.9363	0.9269	1.0598	1.0084	0.9962	0.9073	0.8752	0.8249
256	0.9856	0.9550	1.0473	1.0030	1.0061	0.9541	0.9400	0.9051
1024	1.0128	0.9742	1.0452	1.0001	1.0238	0.9794	0.9899	0.9526
4096	1.0295	0.9872	1.0434	1.0000	1.0341	0.9901	1.0166	0.9760

In the case of h = 1.0, monotonic convergence is obtained only by the CRB2,4,6 and T1 elements. The converged center displacement is about 4% higher than the solution predicted by the thin plate theory (Morley [1963]). These results are in agreement with the observation made by Babuska and Scopolla [1989]. The T1 element exhibits relatively slow convergence, with 4096 elements only 97.6% of the converged energy is obtained. The proposed elements show great sensitivity to the incompatible shape functions used, 78% and 22% difference in the energy norm are observed for the four- and 16-element meshes, respectively.

As observed for the square plate, the moment slope orientation in the CRB1,3,5 elements is opposite to the slope orientation of the exact solution. The slope orientation in the CRB2,4,6 elements, on the other hand, is of the same orientation as the slope of the exact solution. It must be noted that the corner element exhibits a pathological behavior

(for both CRB1,3,5 and CRB2,4,6 elements). Excellent behavior, however, is observed in all other elements. Also note that good moments are recovered at the center of the corner element.

Table 7.32 Rhombic Plate - Uniform load, SS1, h = 0.1, a = 100., $\Theta = 30^o$

nel	CRB1,3,5		CRB2,4,6		S1		T1	
	disp.	energy	disp.	energy	disp.	energy	disp.	energy
4	1.0839	1.2357	2.1822	2.0513	0.6558	0.4741	0.6219	0.4496
16	0.8563	0.8831	1.2259	1.1219	1.0084	0.8614	0.8769	0.7739
64	0.8813	0.9143	0.9622	0.9246	0.9599	0.9149	0.9411	0.8286
256	0.9299	0.9465	0.9327	0.9349	0.9128	0.9153	0.8411	0.8587
1024	0.9621	0.9690	0.9714	0.9755	0.9414	0.9478	0.8862	0.9025
4096	0.9802	0.9830	1.0007	1.0000	0.9740	0.9770	0.9330	0.9430

For the case of h = 0.1, only the T1 element exhibits monotonic convergence. However, with 4096 elements only 94.3% of the reference energy is obtained. The proposed elements' sensitivity to the incompatible shape functions increases with the reduction in thickness. A difference of 82% and 24% is observed for the four- and 16-element meshes, respectively.

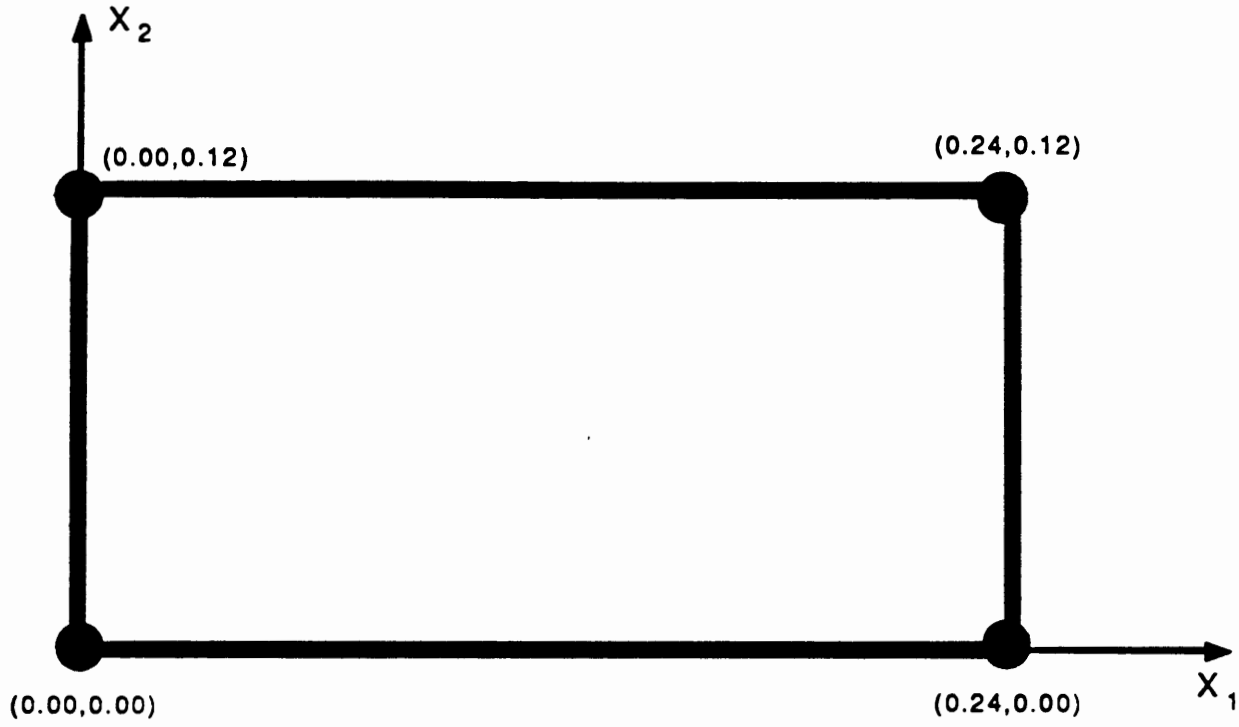

Figure 7.1a: Patch test, one-element mesh.

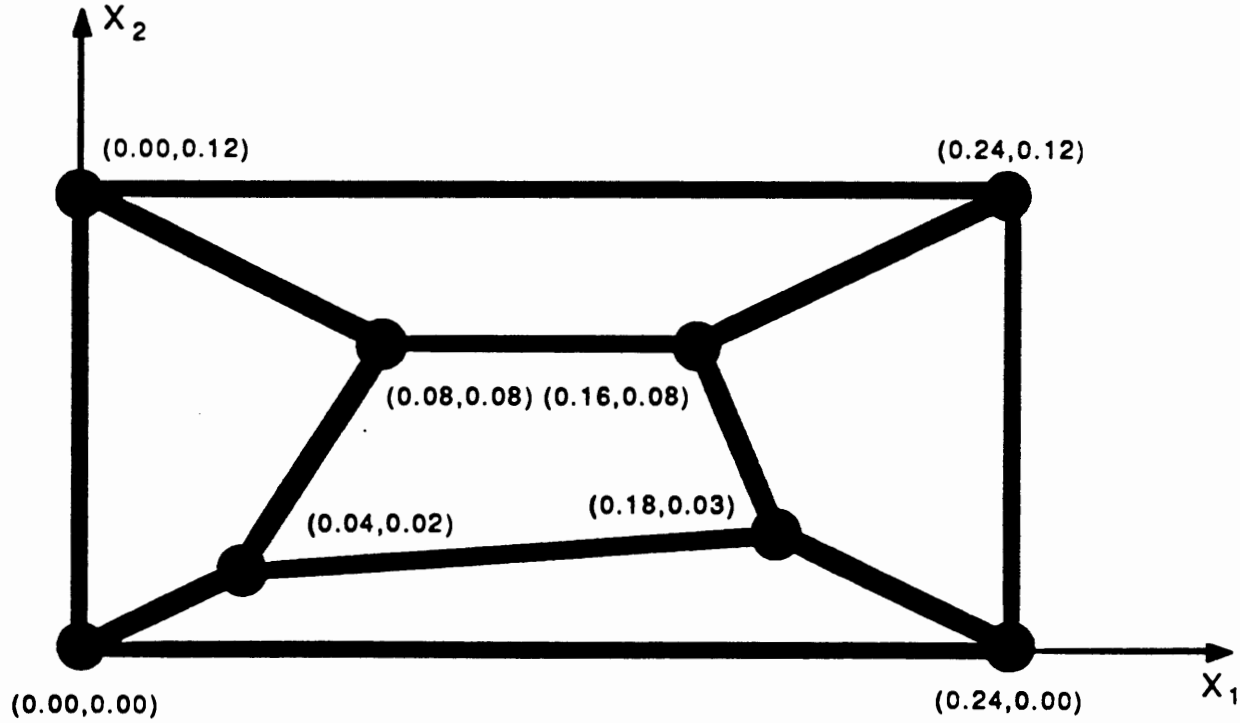

Figure 7.1b: Patch test, skewed mesh.

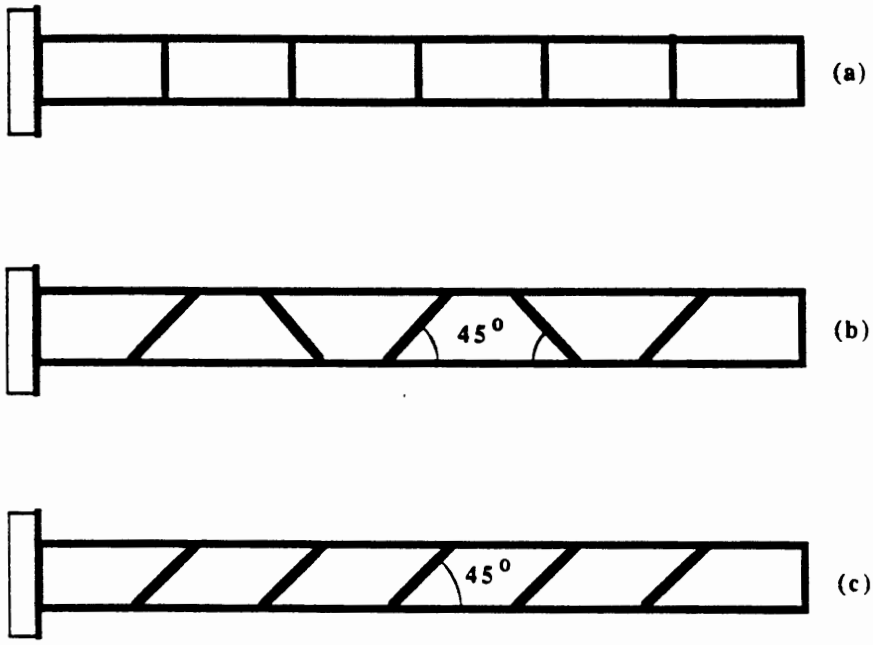

Figure 7.2: Straight cantilever beam. (a) Regular shape elements; (b) Trapezoid shape elements; (c) Parallelogram shape elements.

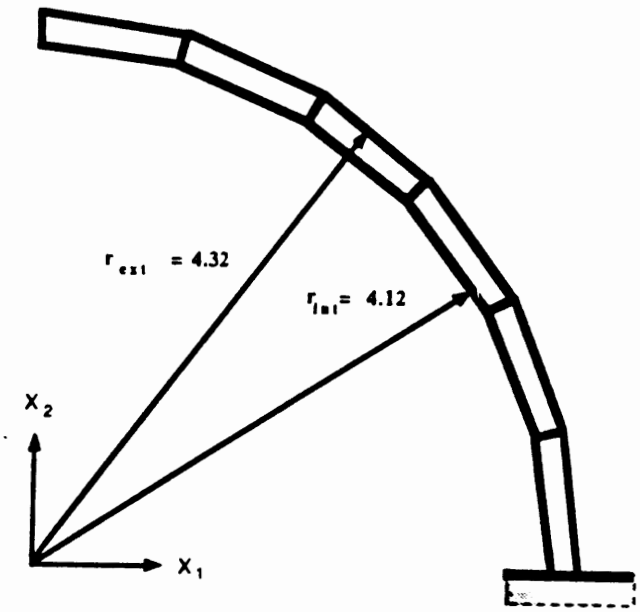

Figure 7.3: Curved beam mesh.

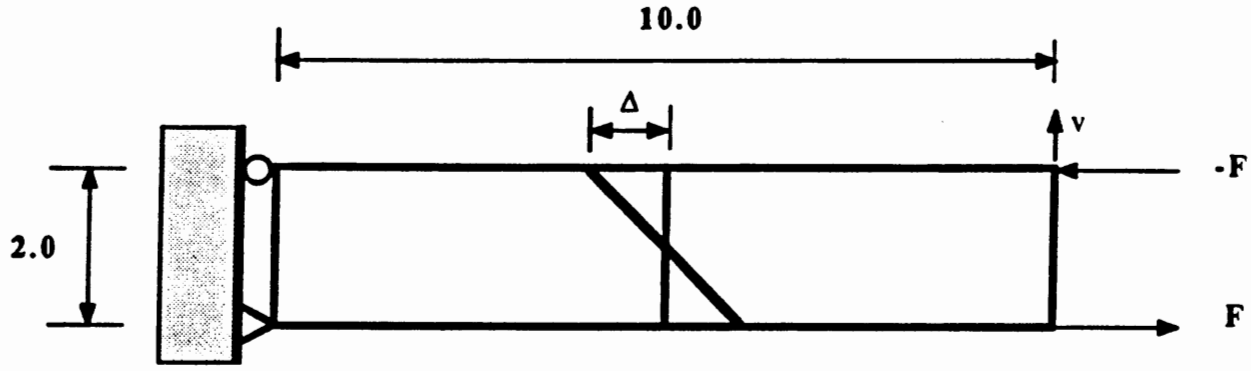

Figure 7.4: Beam bending problem, sensitivity to mesh distortion.

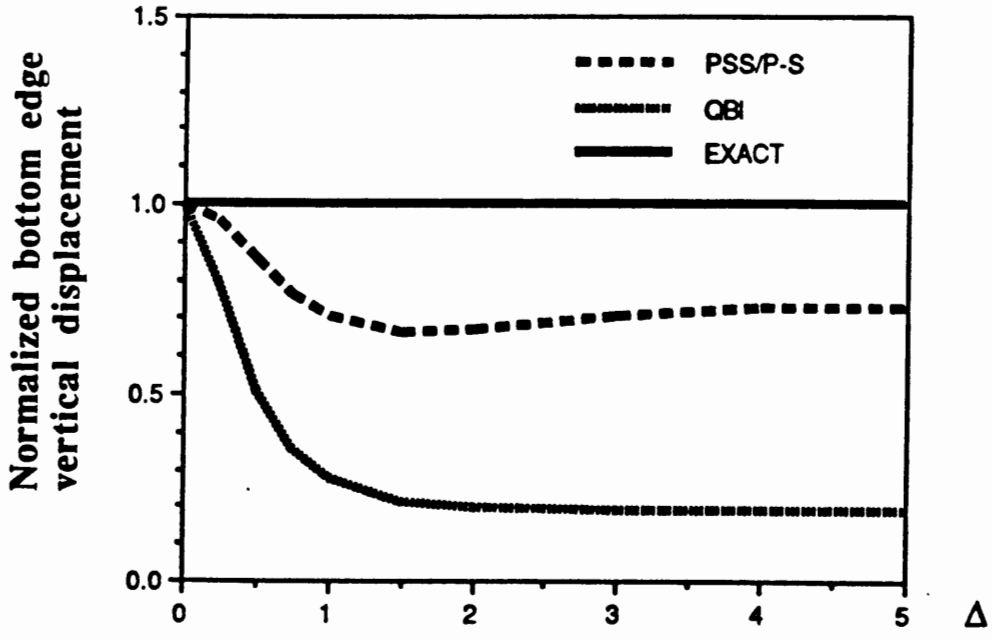

Figure 7.5: Beam bending; sensitivity to mesh distortion.

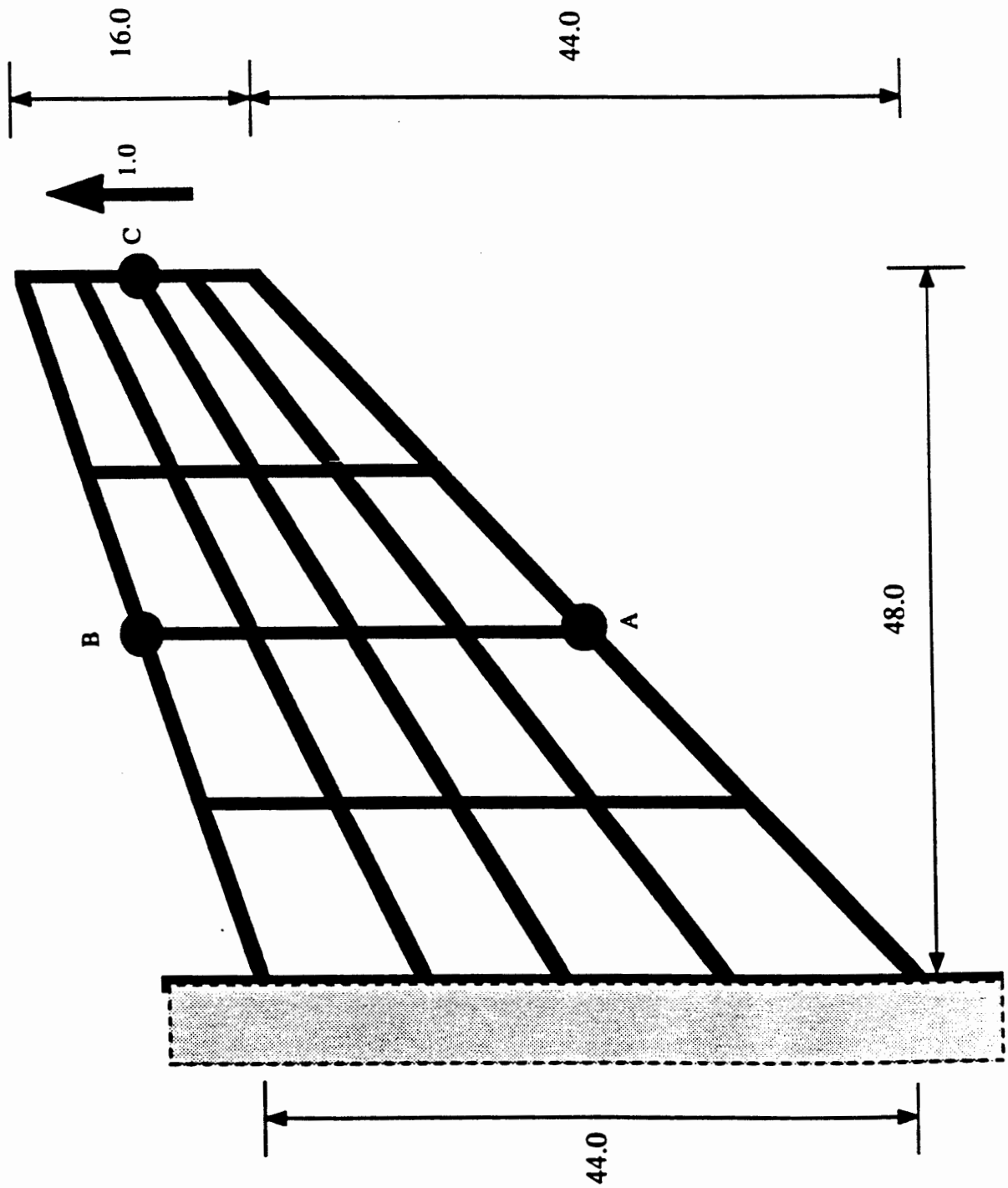

Figure 7.6: Cook's membrane problem.

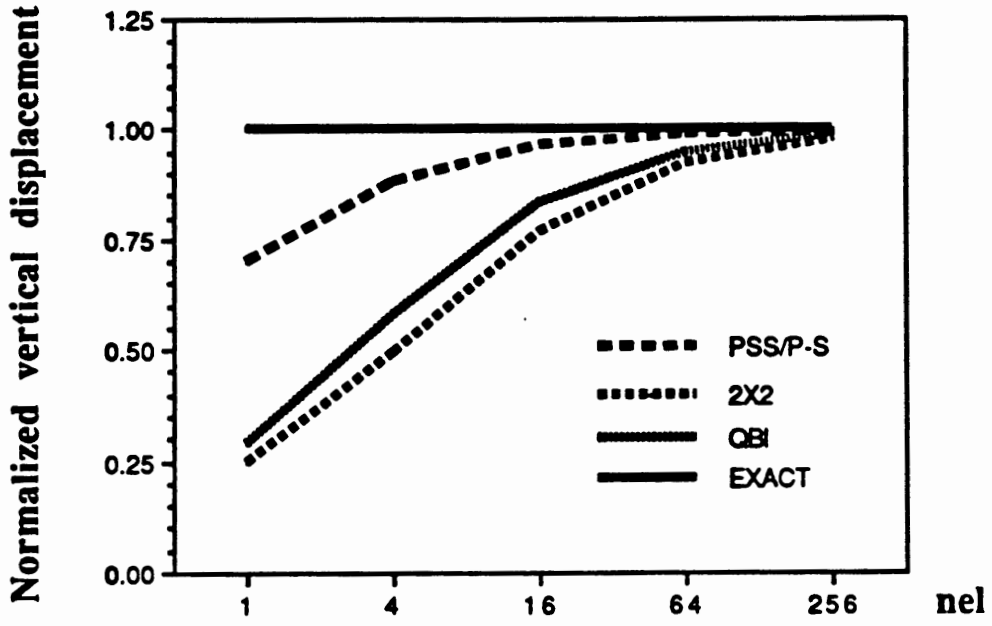

Figure 7.7: Cook's membrane problem; vertical displacement at point C.

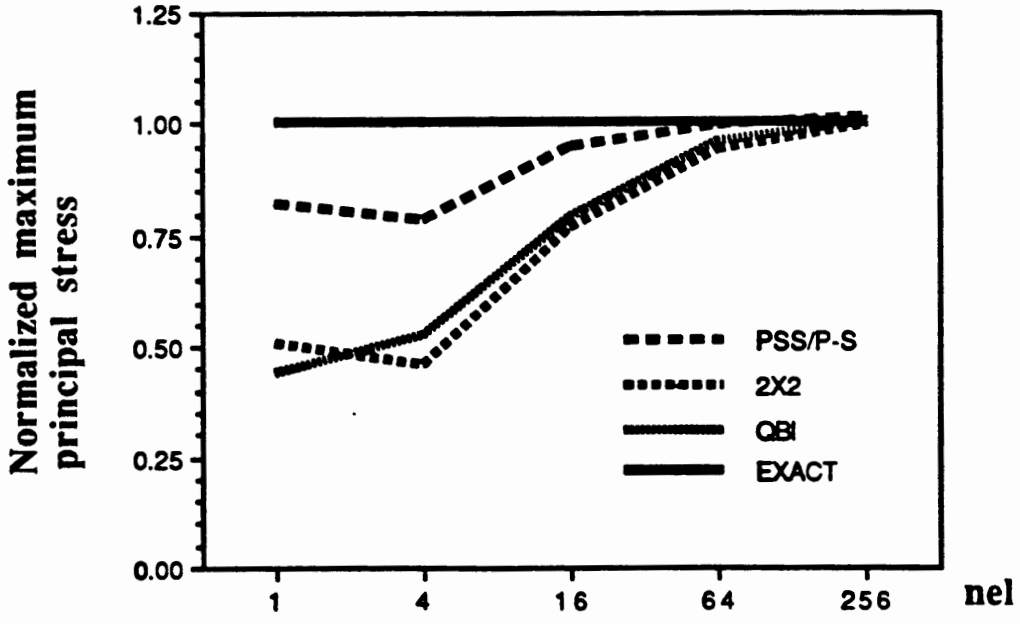

Figure 7.8: Cook's membrane problem; maximum principal stress at point A.

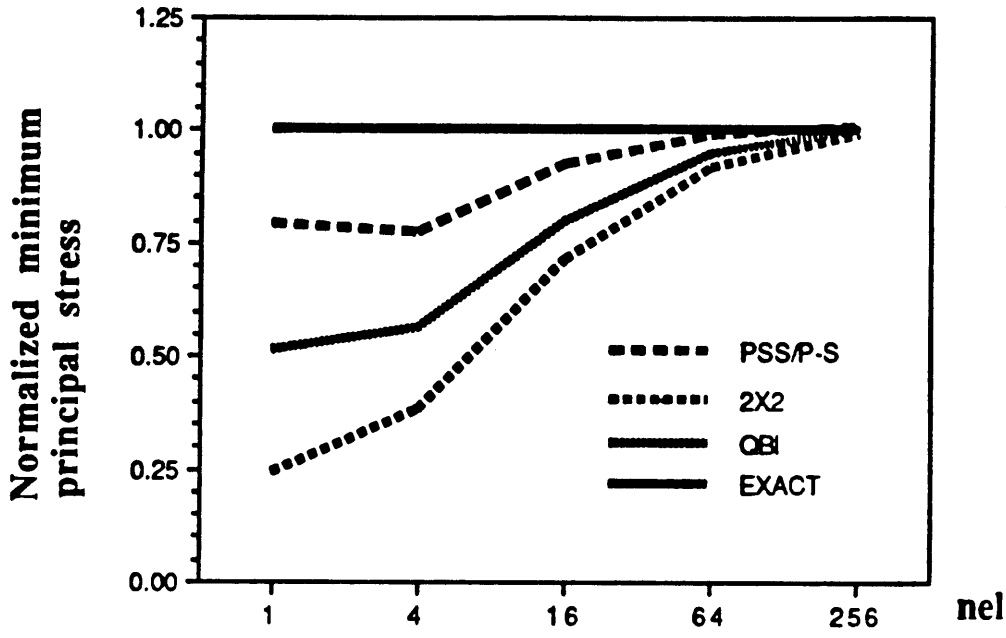

Figure 7.9: Cook's membrane problem; principal minimum stress at point B.

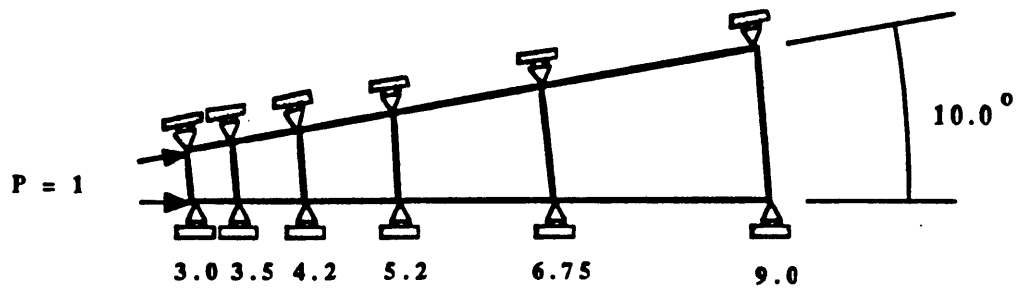

Figure 7.10: Thick-walled cylinder problem.

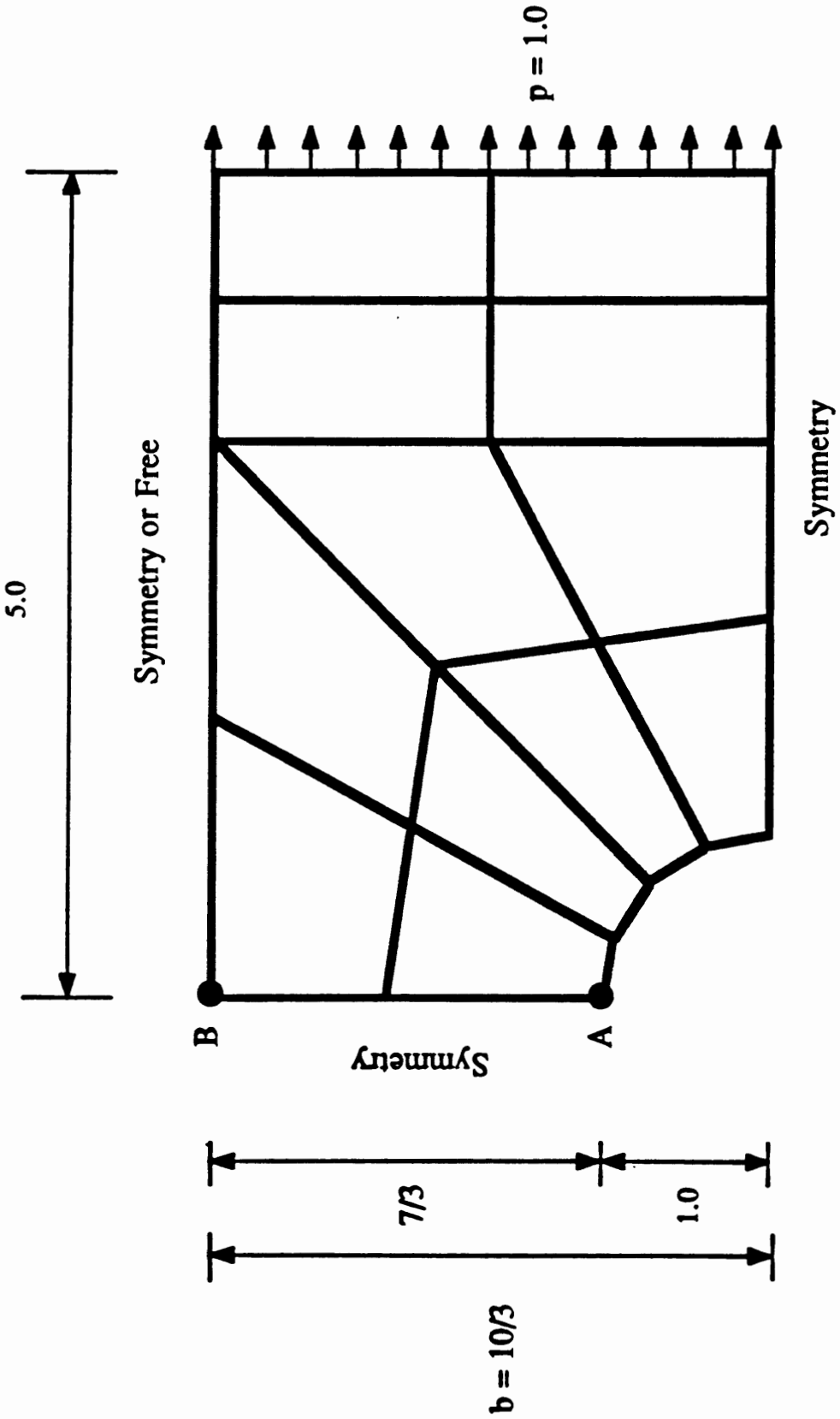

Figure 7.11: Strip with a hole problem.

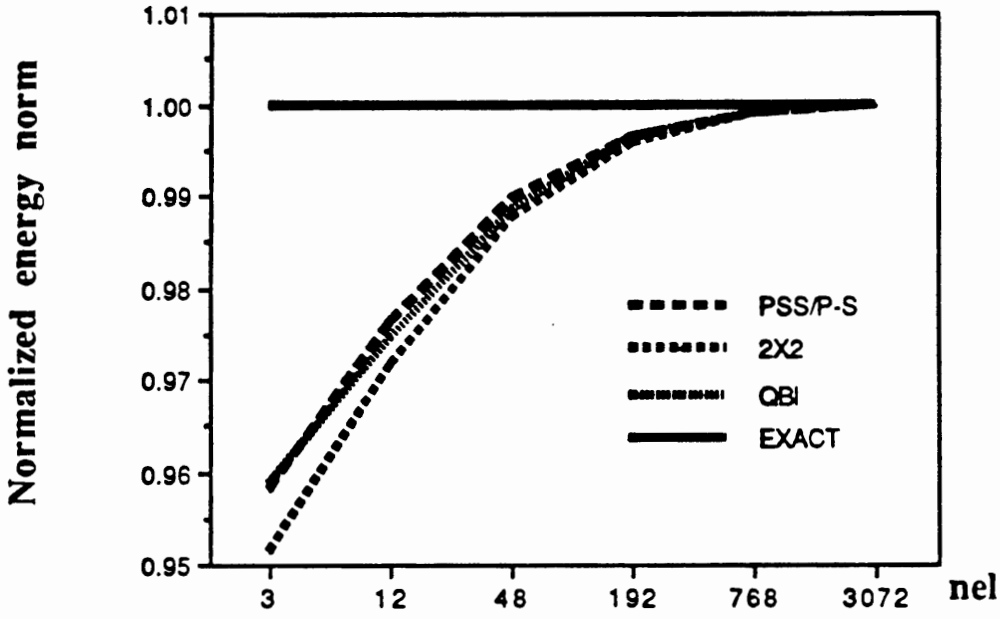

Figure 7.12: Strip with a hole; plane stress; convergence in the energy norm.

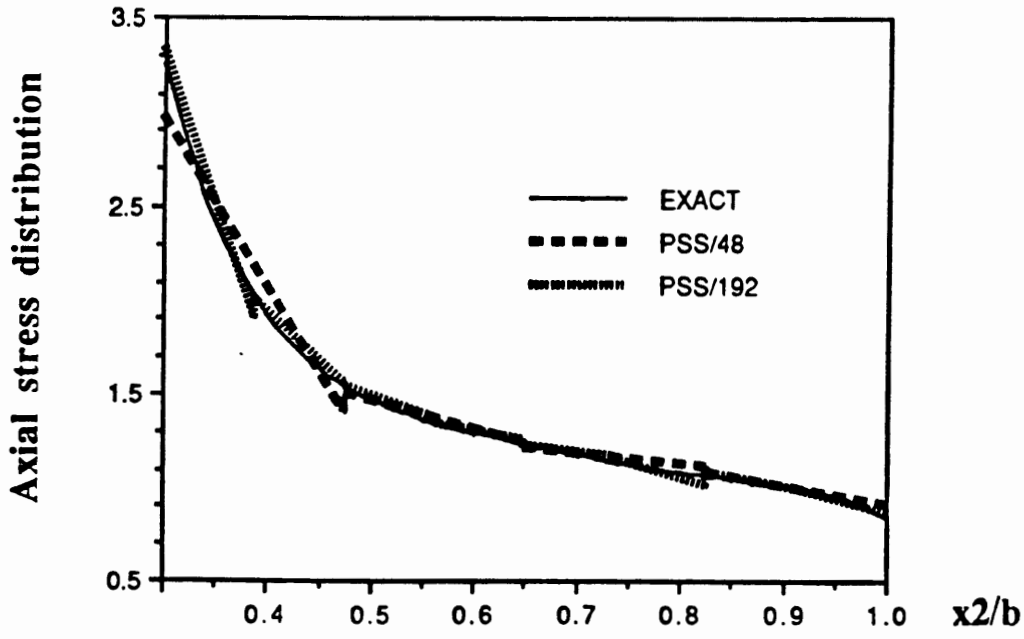

Figure 7.13: Strip with a hole; plane stress; axial stress distribution along the line A-B.

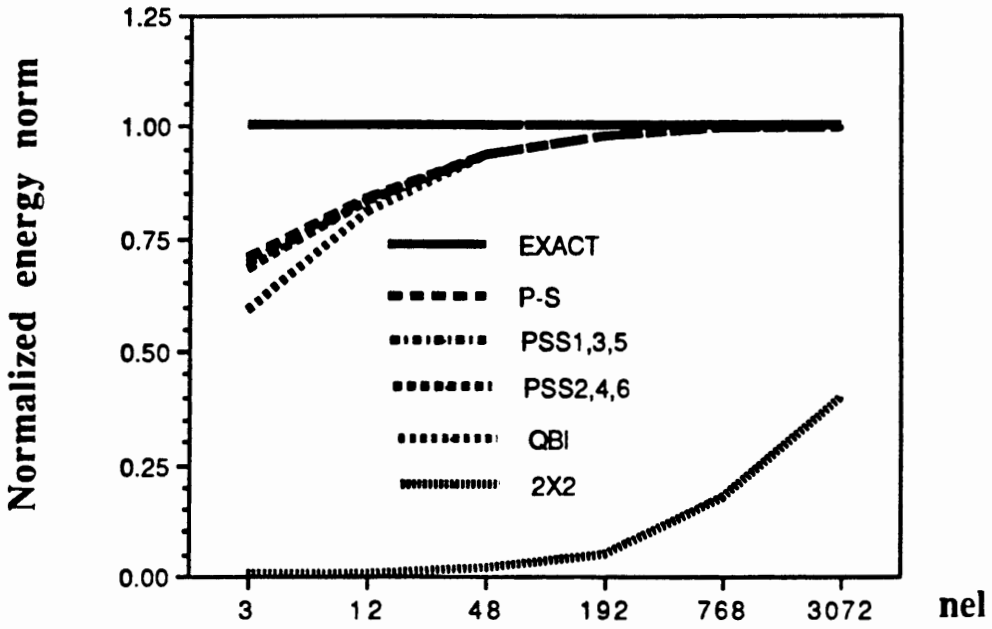

Figure 7.14: Strip with a hole; plane strain; convergence in the energy norm.

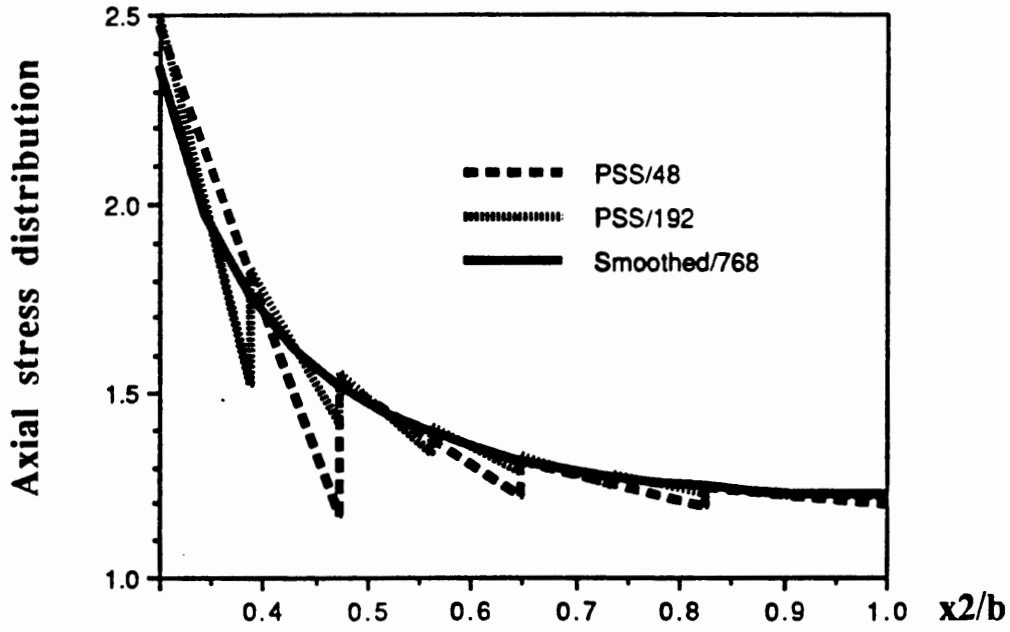

Figure 7.15: Strip with a hole; plane strain; axial stress distribution along the line A-B.

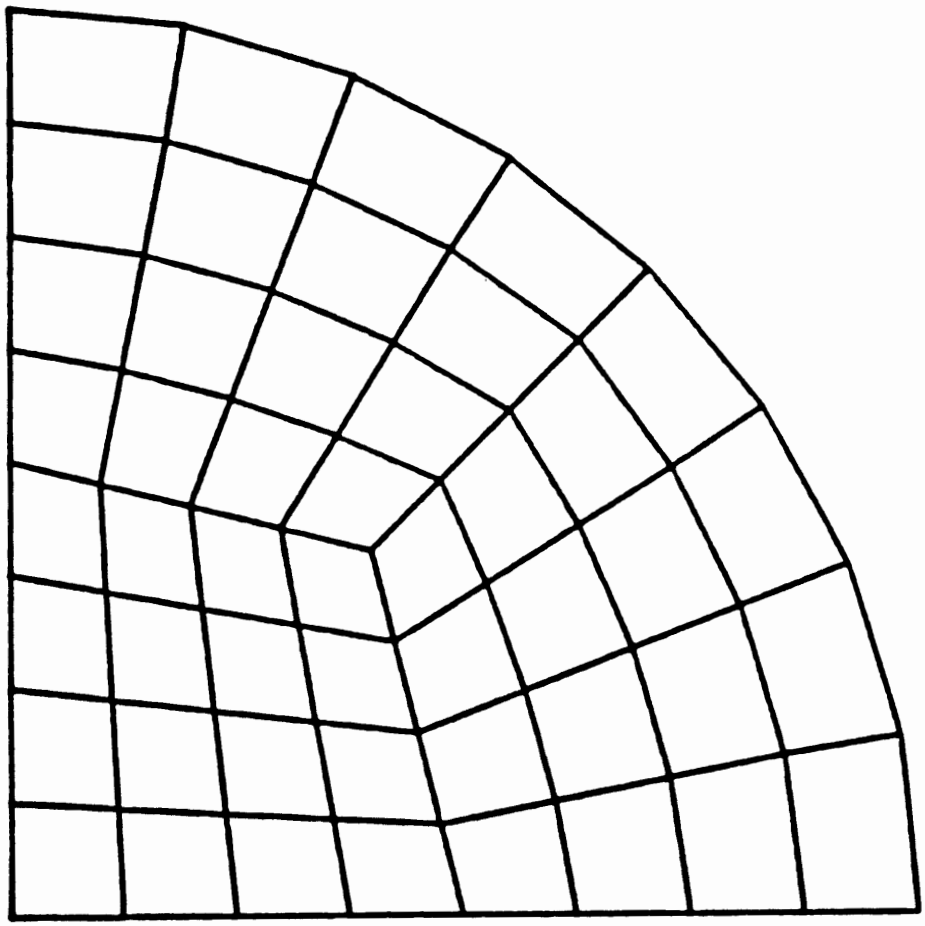

Figure 7.16: Circular plate. Due to symmetry only one quadrant is discretized.

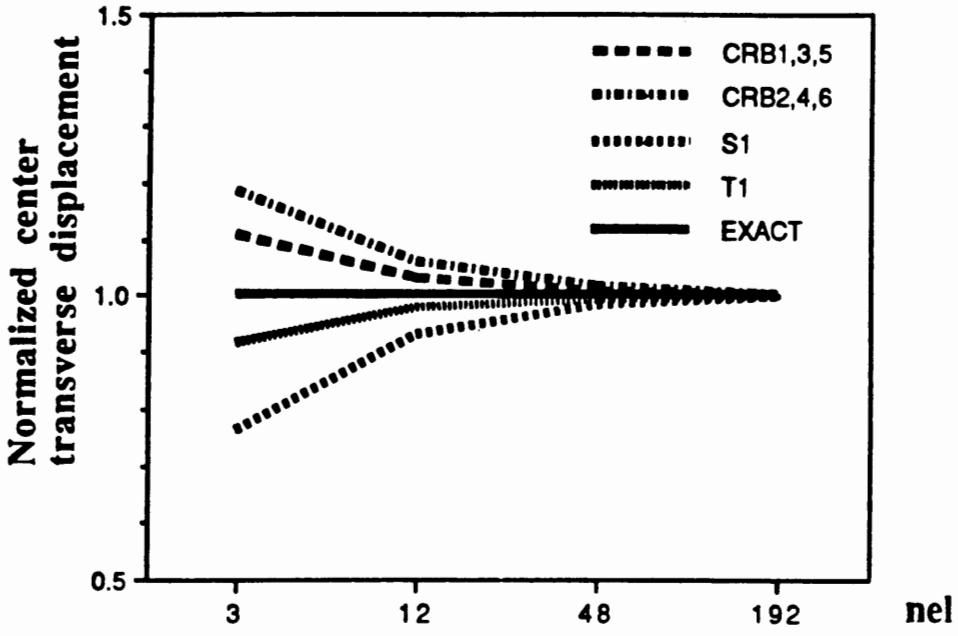

Figure 7.17: Simply supported (SS1) thin circular plate; uniform load; convergence of center transverse displacement.

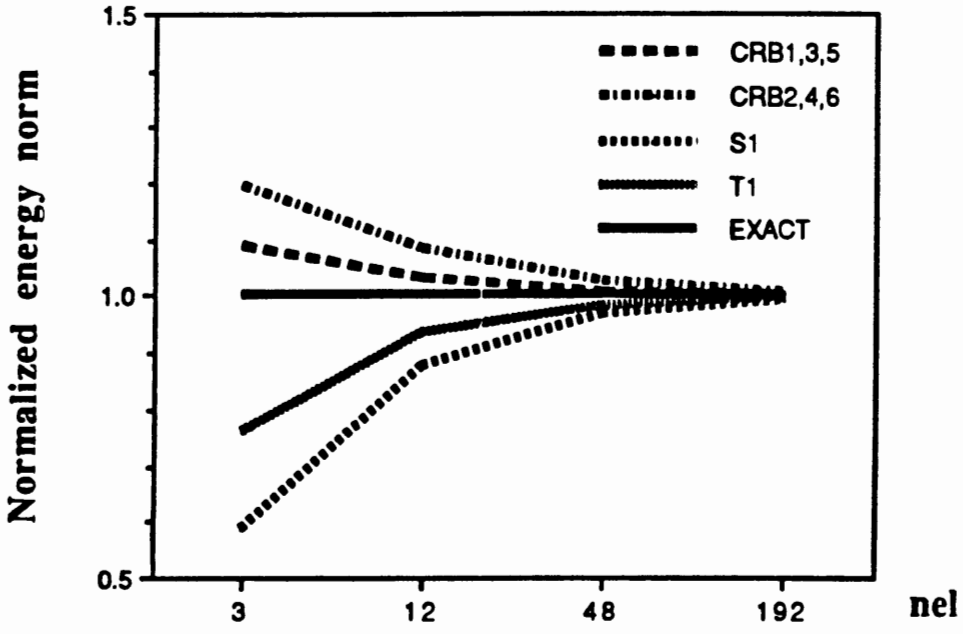

Figure 7.18: Simply supported (SS1) thin circular plate; uniform load; convergence in the energy norm.

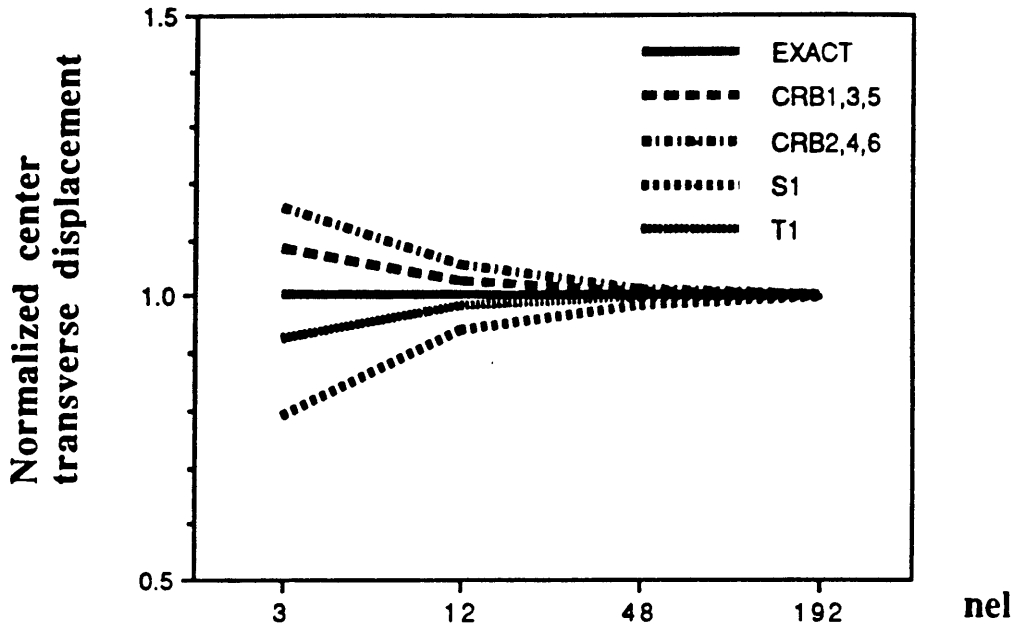

Figure 7.19: Simply supported (SS1) thick circular plate; uniform load; convergence of the center transverse displacement.

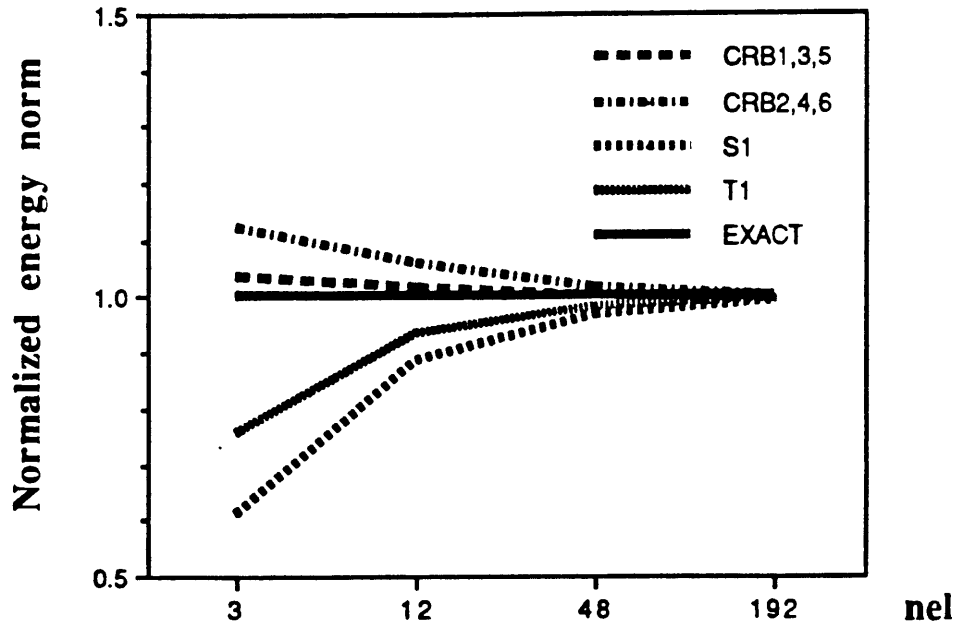

Figure 7.20: Simply supported (SS1) thick circular plate; uniform load; convergence in the energy norm.

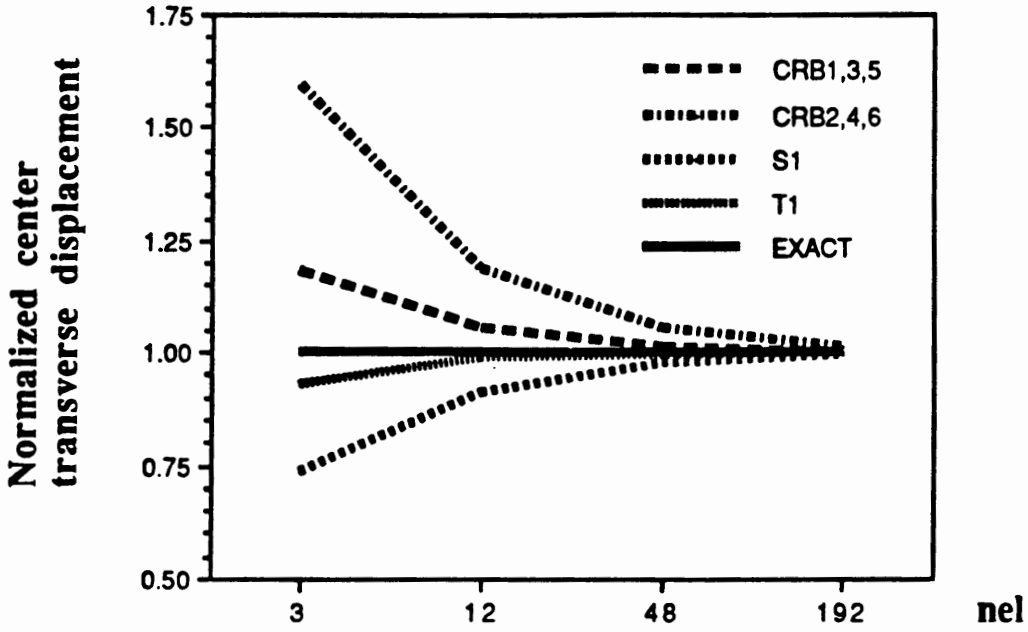

Figure 7.21: Clamped thin circular plate; uniform load; convergence of the center transverse displacement.

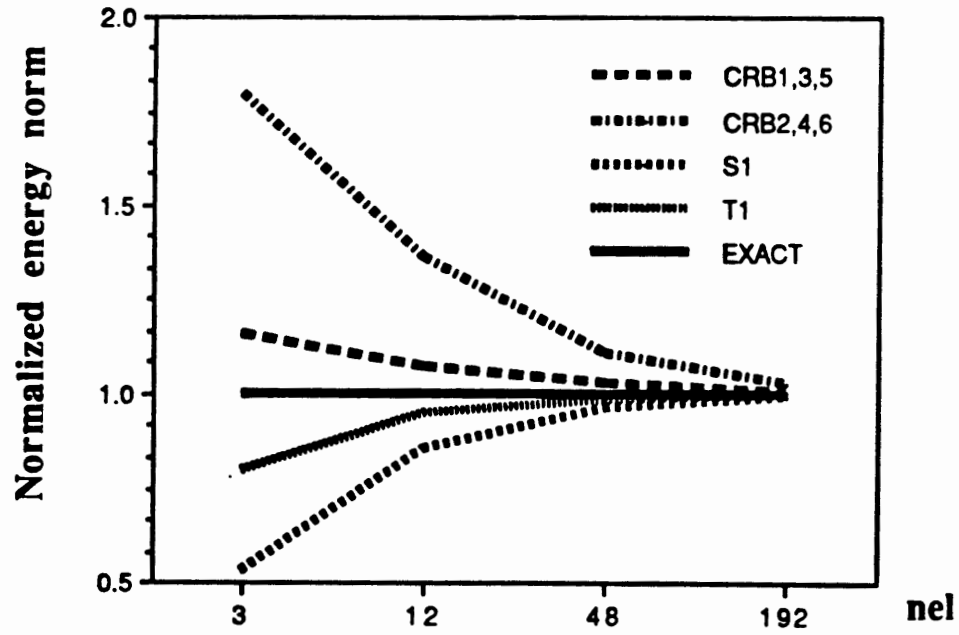

Figure 7.22: Clamped thin circular plate; uniform load; convergence in the energy norm.

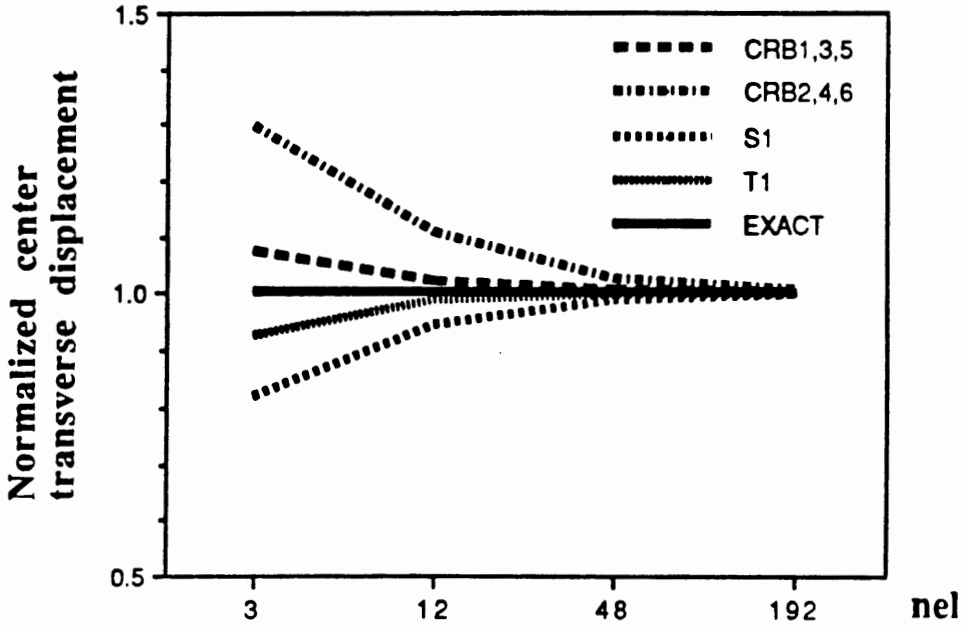

Figure 7.23: Clamped thick circular plate; uniform load; convergence of the center transverse displacement.

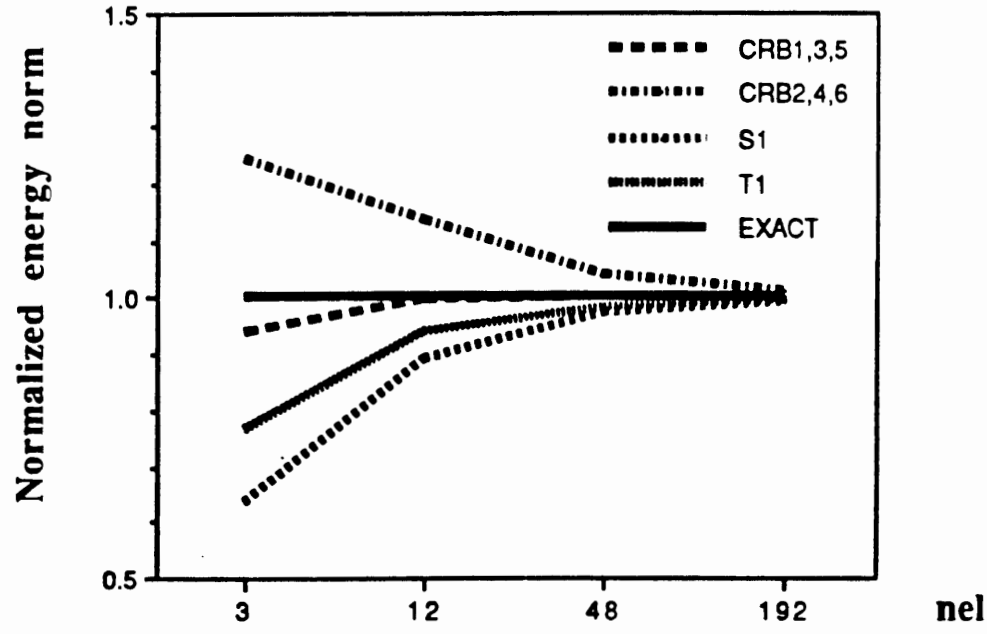

Figure 7.24: Clamped thick circular plate; uniform load; convergence in the energy norm.

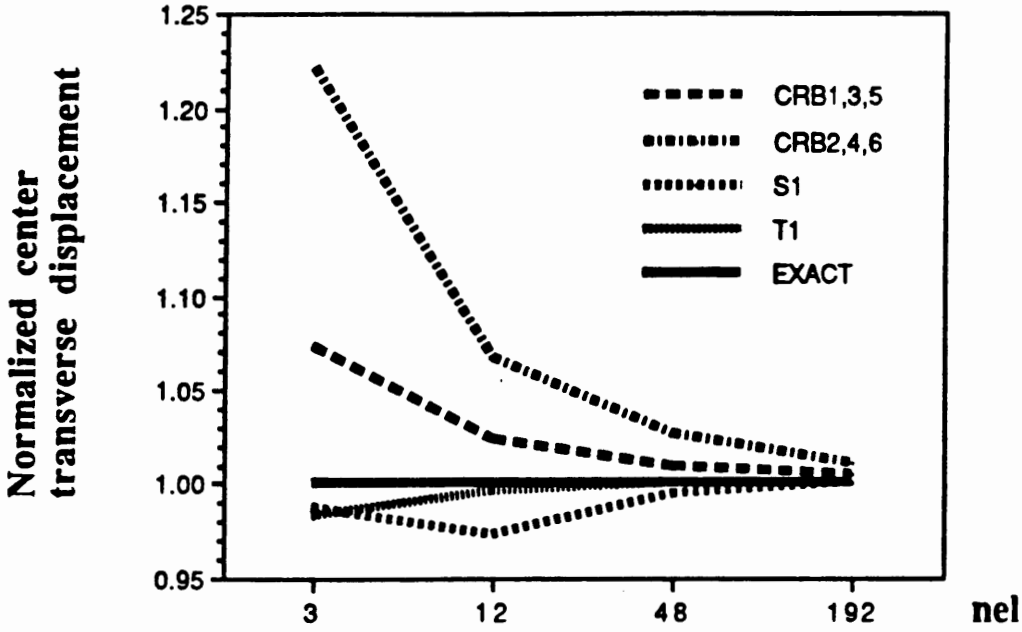

Figure 7.25: Simply supported (SS1) thin circular plate; concentrated unit load at the center; normalized center transverse displacement.

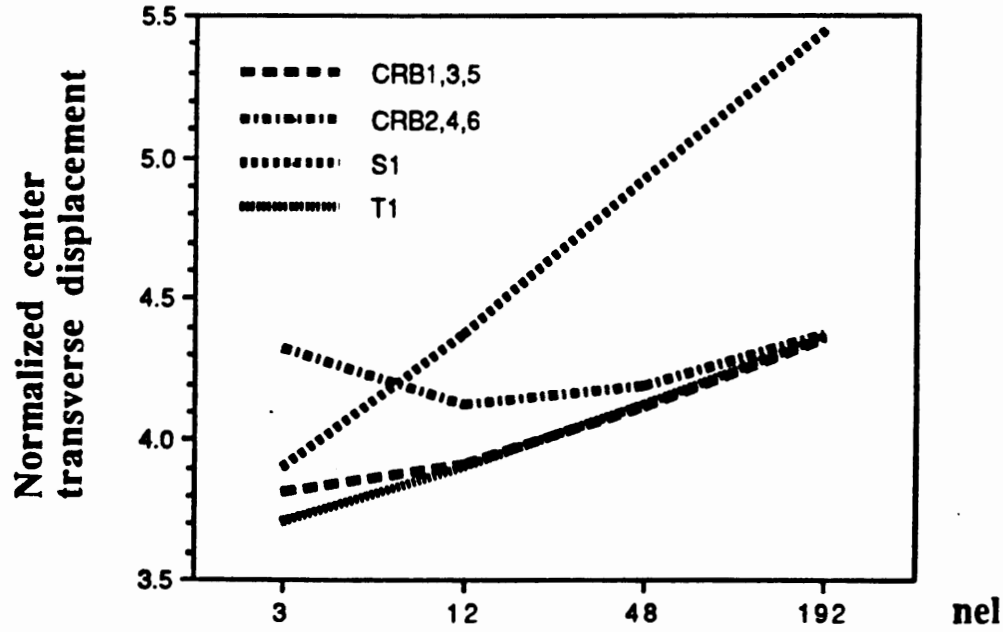

Figure 7.26: Simply supported (SS1) thick plate; concentrated unit load at the center; normalized center transverse displacement.

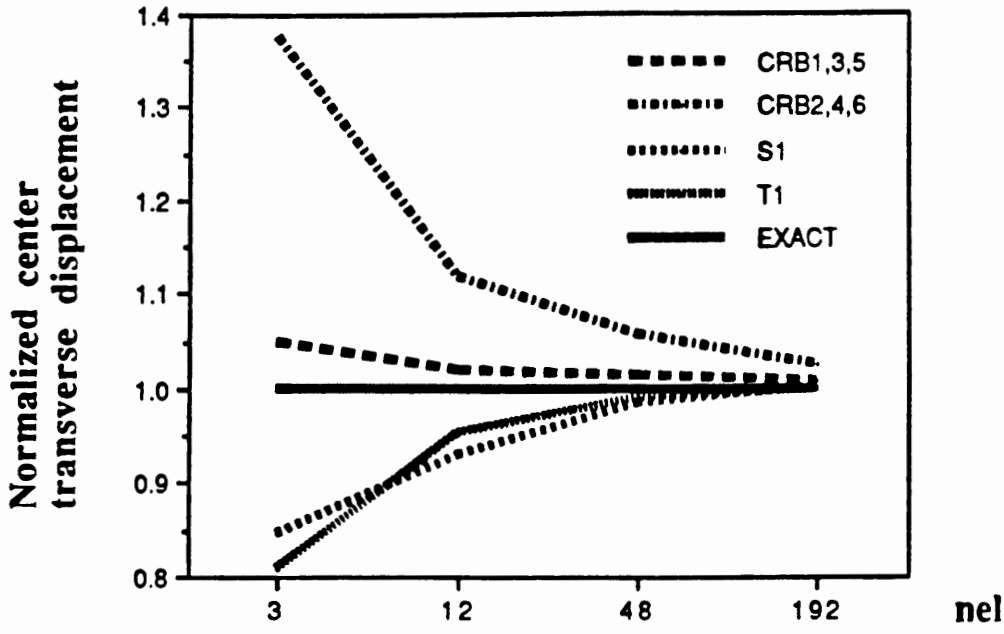

Figure 7.27: Clamped thin plate; concentrated unit load at the center; normalized center transverse displacement.

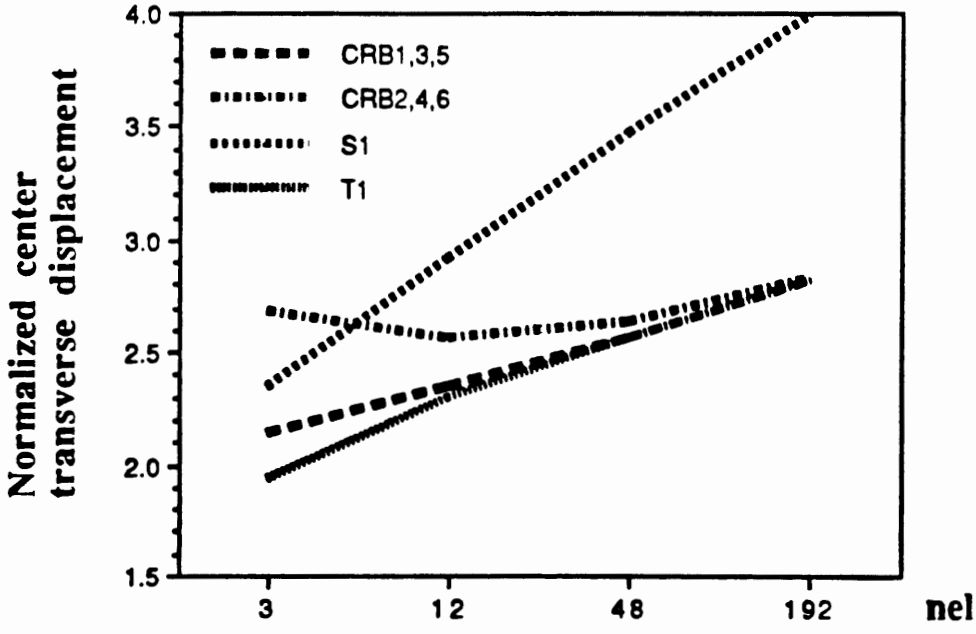

Figure 7.28: Clamped thick plate; concentrated unit point load at the center; normalized center transverse displacement.

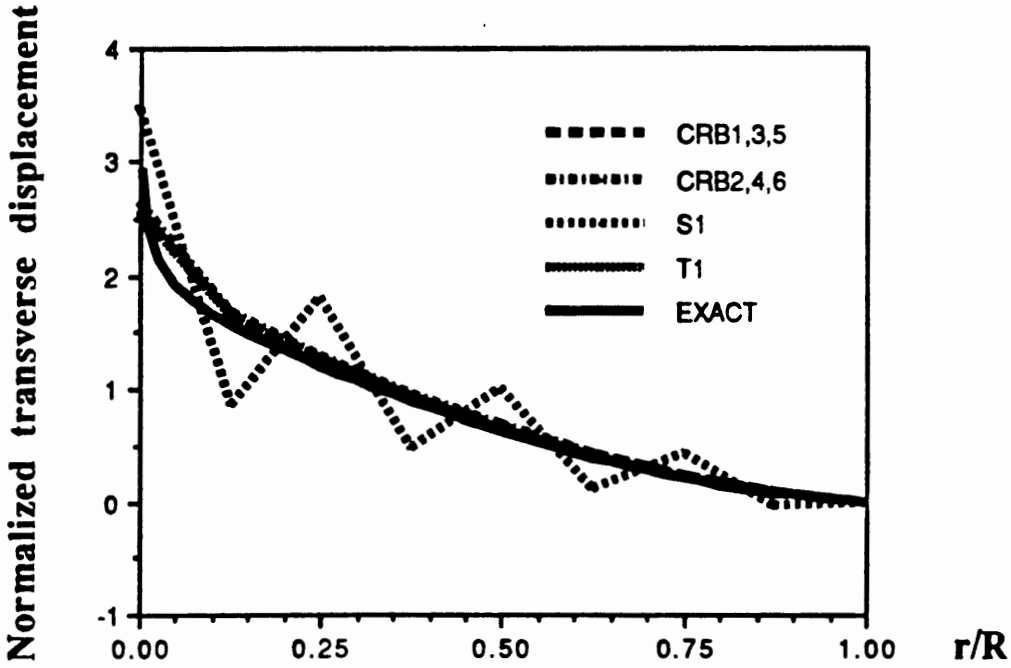

Figure 7.29: Clamped thick plate; concentated unit load at the center; normalized transverse displacement along the radius.

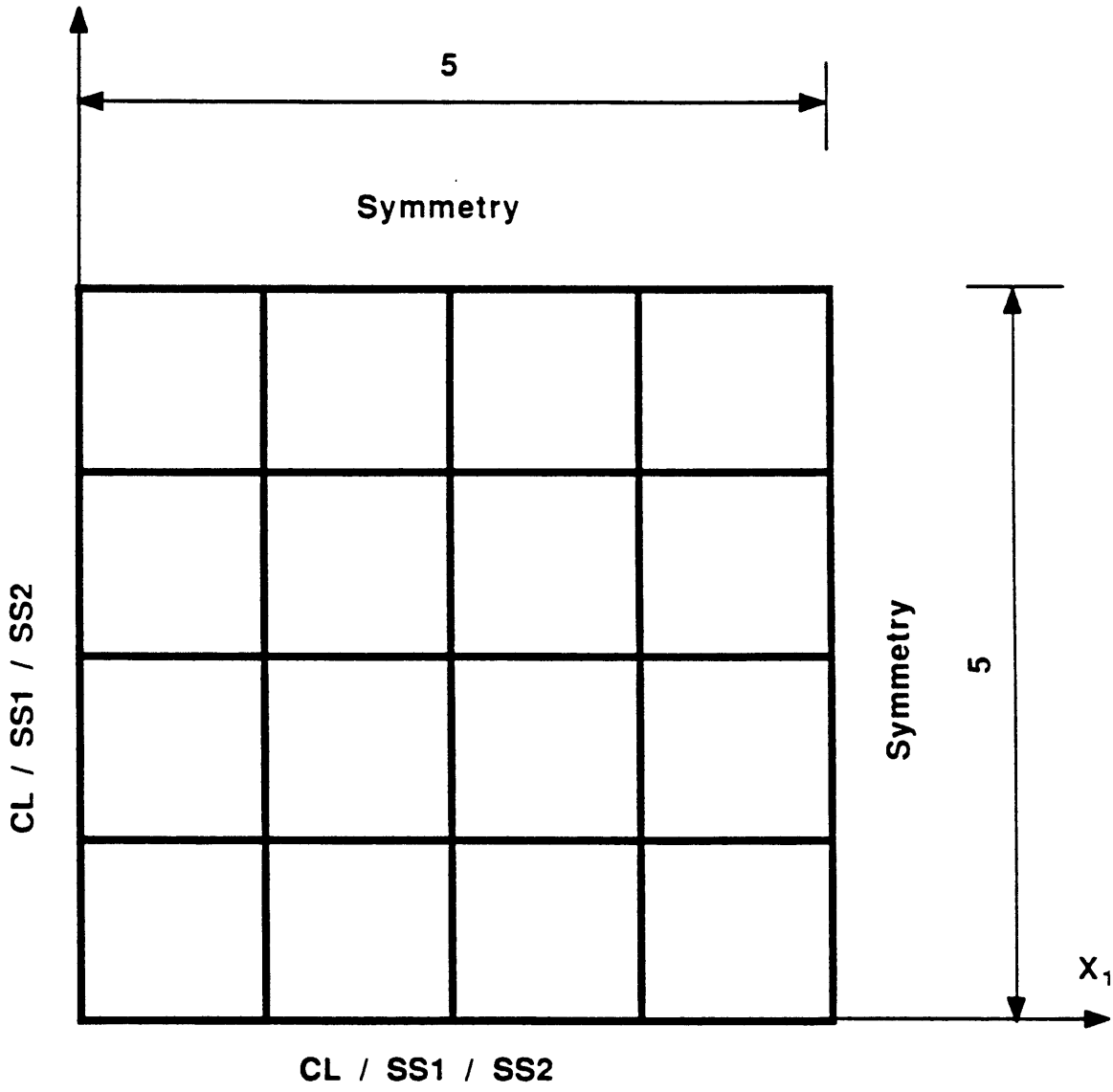

Figure 7.30: Square plate. Due to symmetry, only one quadrant is discretized.

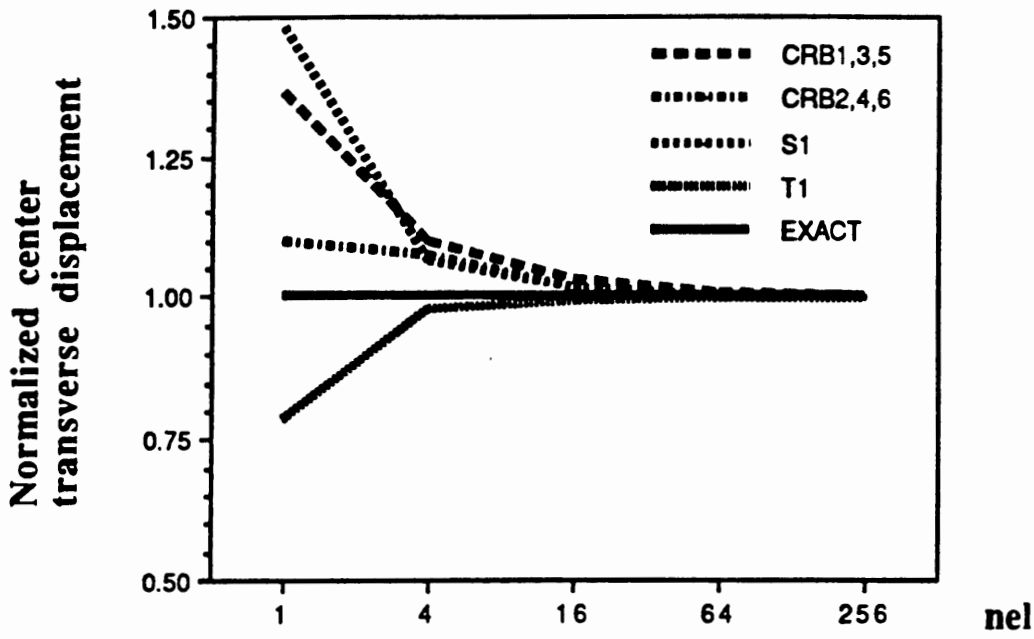

Figure 7.31: Simply supported (SS1) thin square plate; uniform load; convergence of the center transverse displacement.

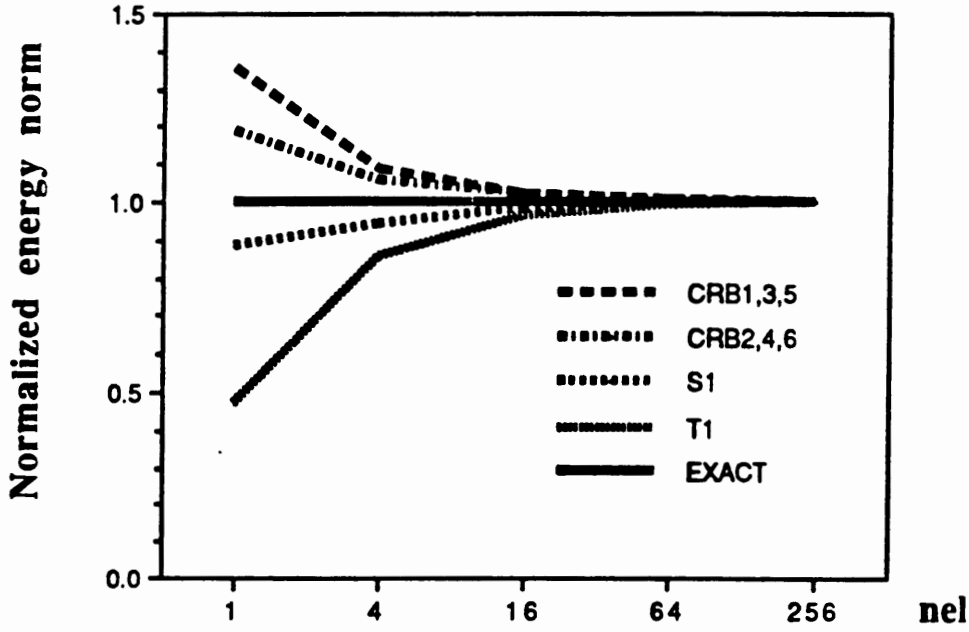

Figure 7.32: Simply supported (SS1) thin square plate; uniform load; convergence in the energy norm.

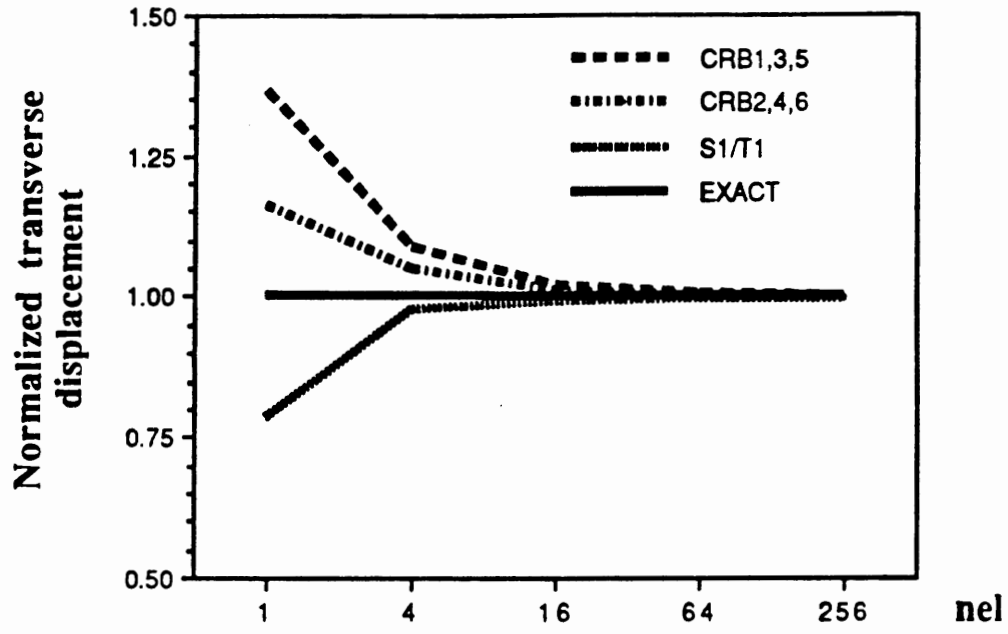

Figure 7.33: Simply supported (SS2) thin square plate; uniform load; convergence of the center transverse displacement.

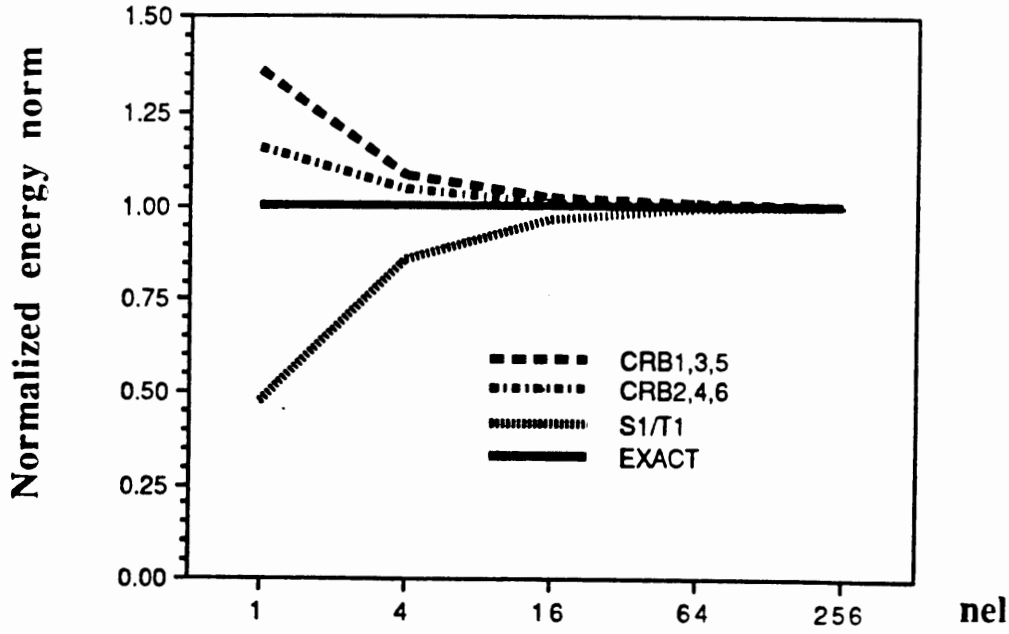

Figure 7.34: Simply supported (SS2) thin square plate; uniform load; convergence in the energy norm.

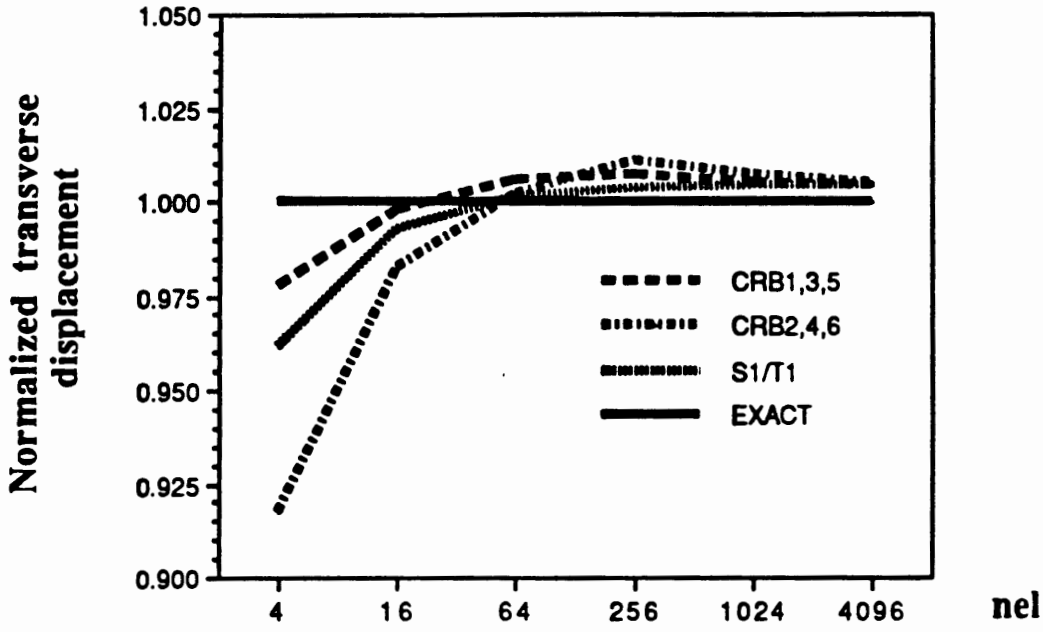

Figure 7.35: Clamped thin square plate; uniform load; convergence of the center transverse displacement.

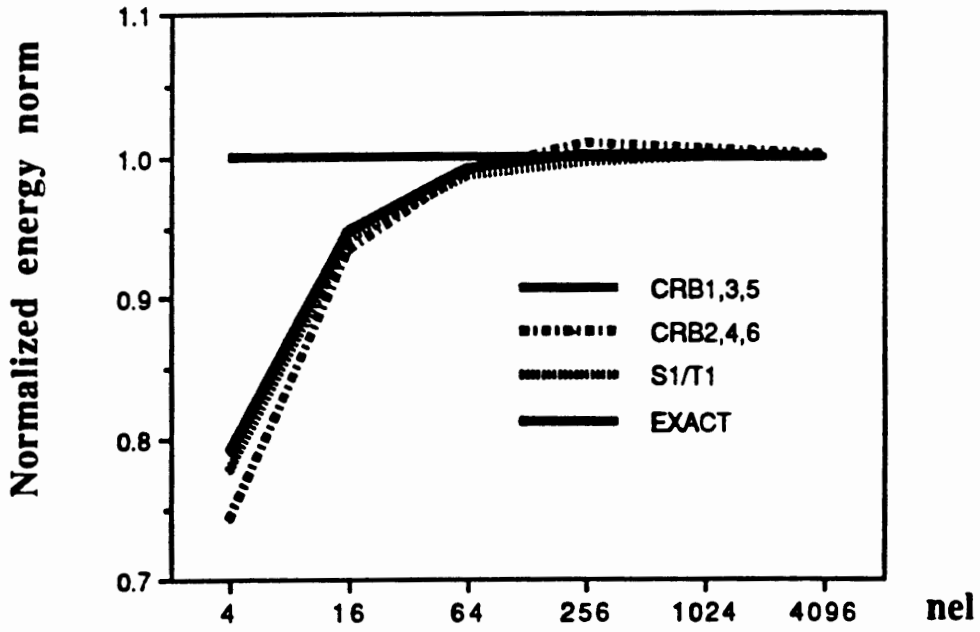

Figure 7.36: Clamped thin square plate; uniform load; convergence in the energy norm.

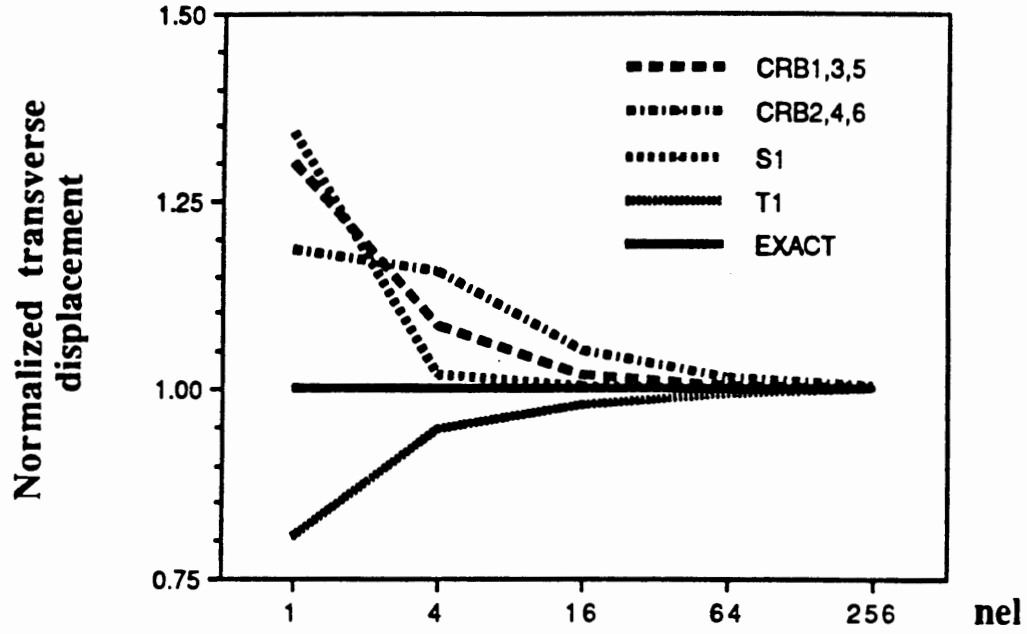

Figure 7.37: Simply supported (SS1) thick square plate; uniform load; convergence of the center transverse displacement.

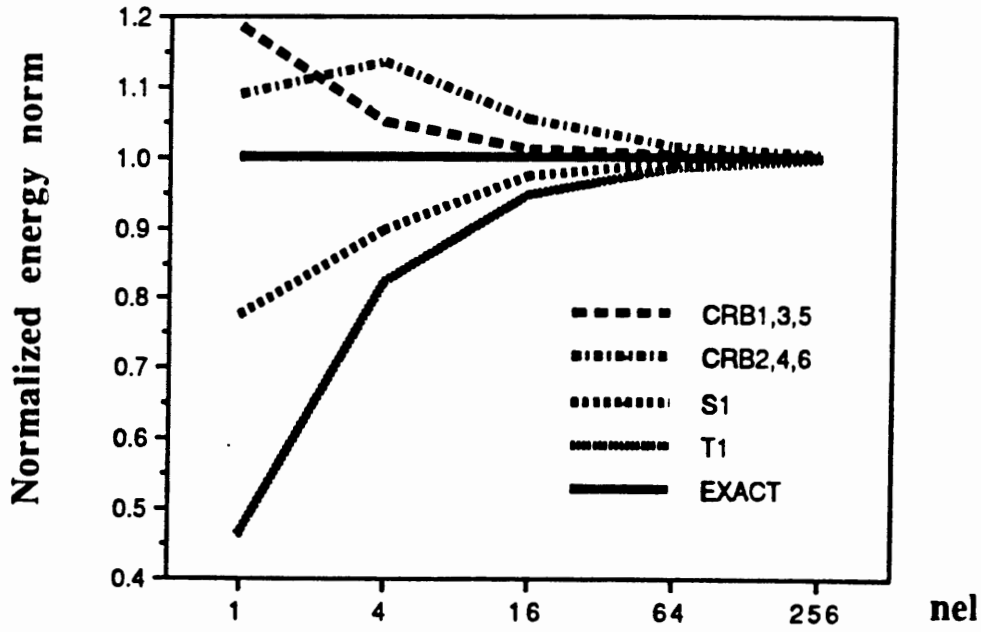

Figure 7.38: Simply supported (SS1) thick square plate; uniform load; convergence in the energy norm.

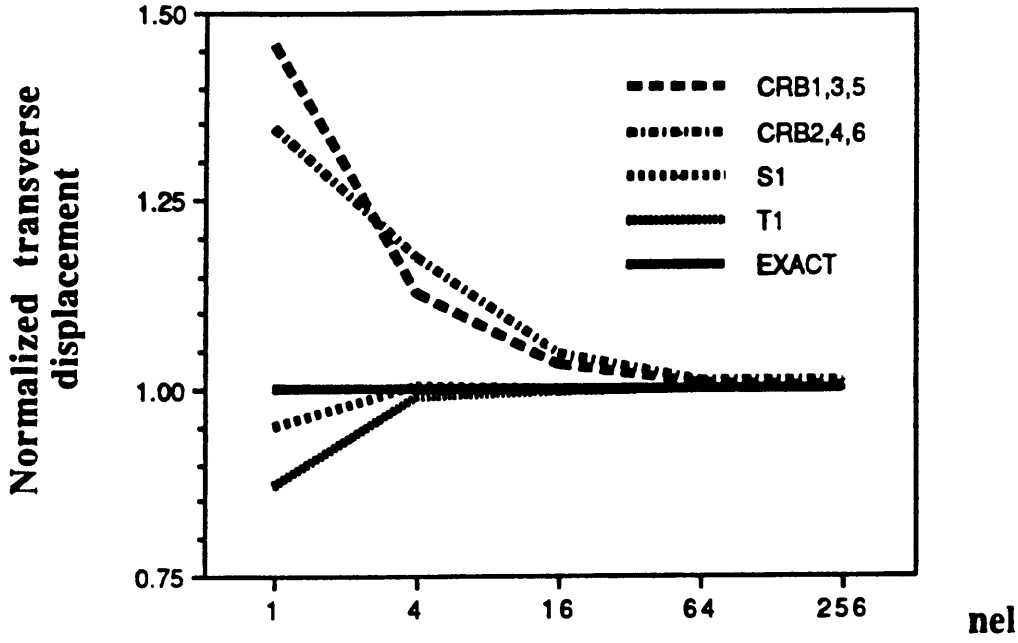

Figure 7.39: Simply supported (SS2) thick square plate; uniform load; convergence of the center transverse displacement.

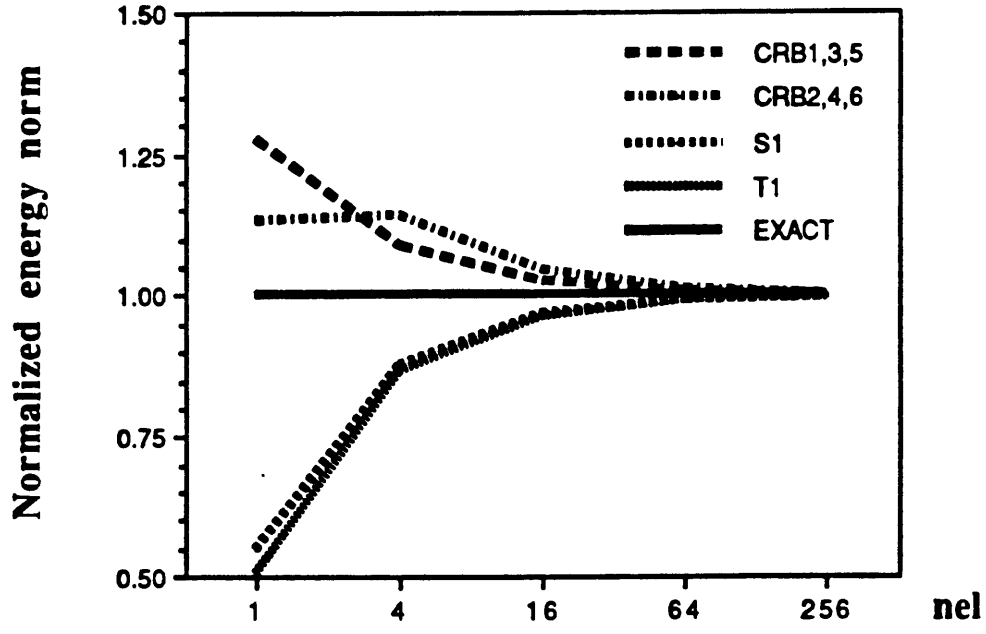

Figure 7.40: Simply supported (SS2) thick square plate; uniform load; convergence in the energy norm.

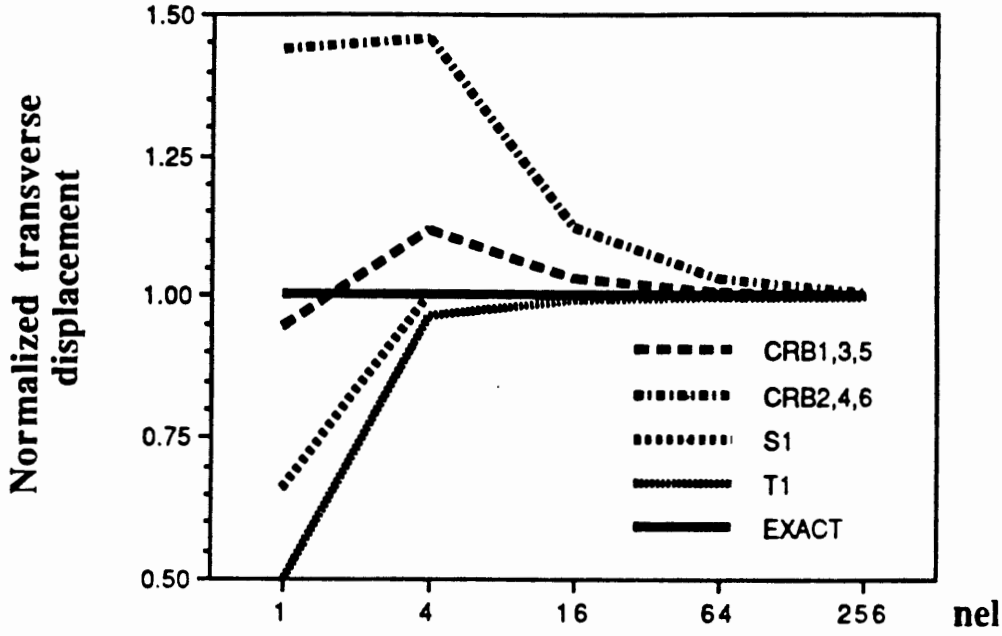

Figure 7.41: Clamped thick square plate; uniform load; convergence of the center transverse displacement.

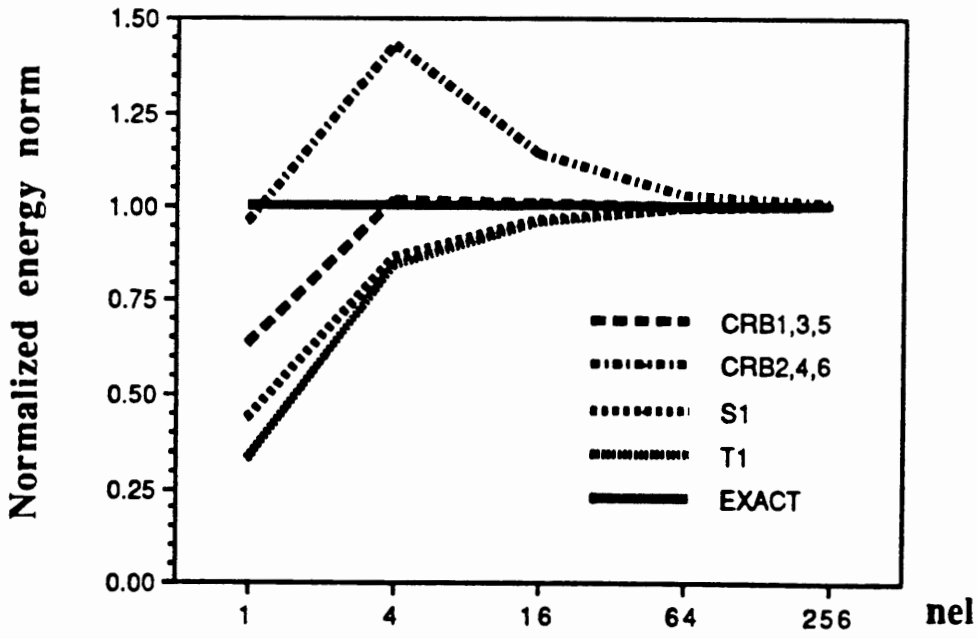

Figure 7.42: Clamped thick square plate; uniform load; convergence in the energy norm.

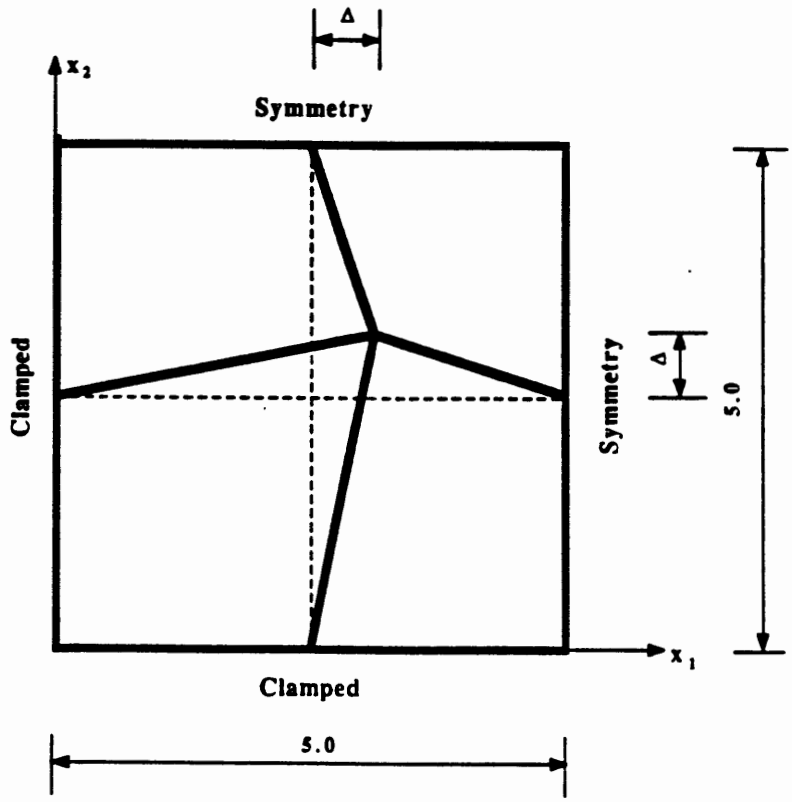

Figure 7.43: Mesh distortion; symmetric.

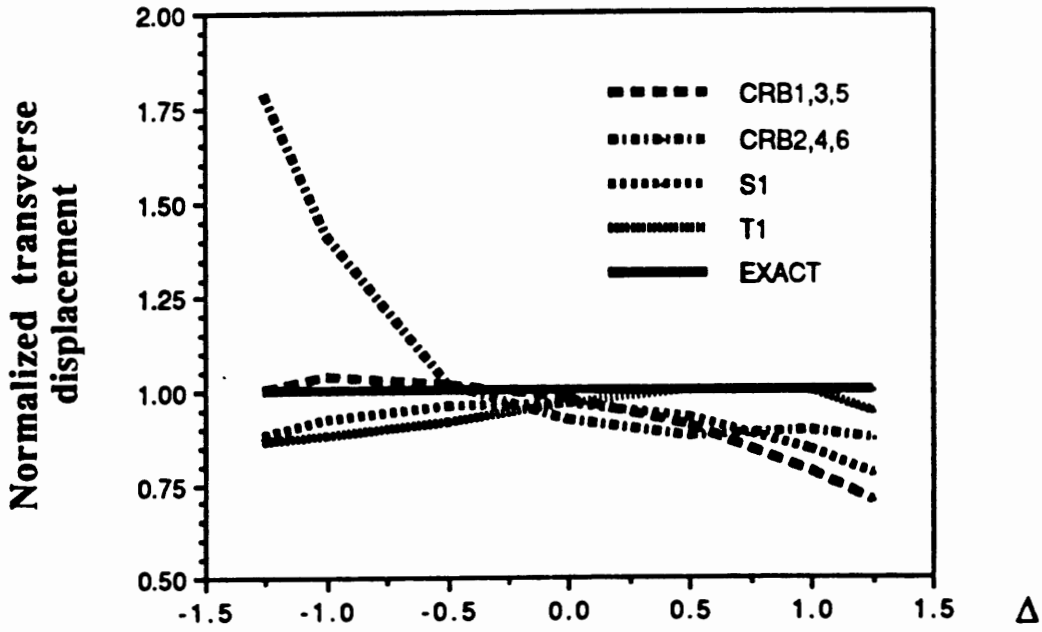

Figure 7.44: Sensitivity to mesh distortion; symmetric distortion; normalized center transverse displacement.

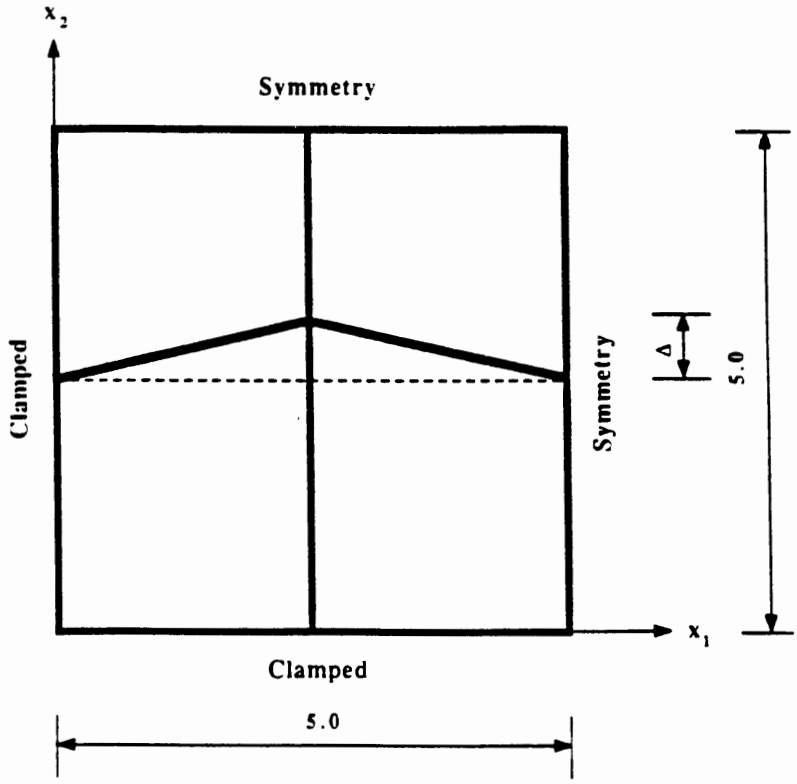

Figure 7.45: Mesh distortion; asymmetric.

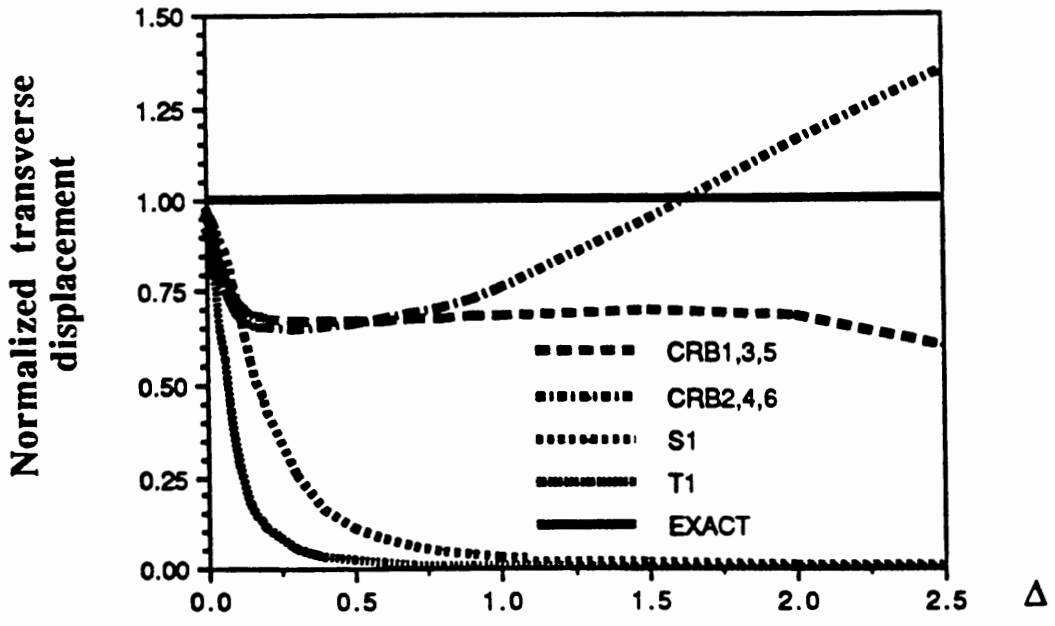

Figure 7.46: Sensitivity to mesh distortion; asymmetric distortion; normalized center transverse displacement.

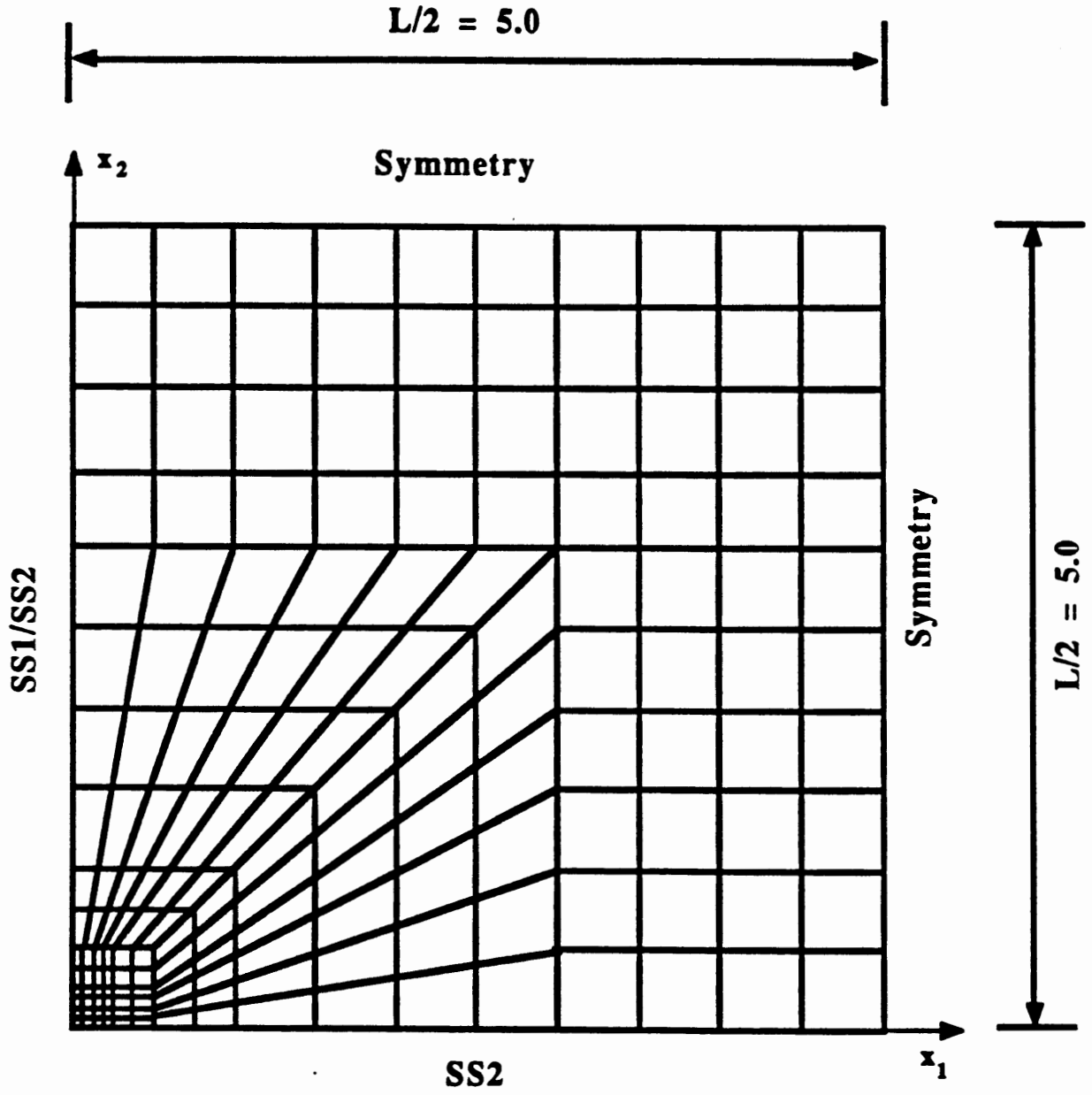

Figure 7.47: Square plate; graded mesh.

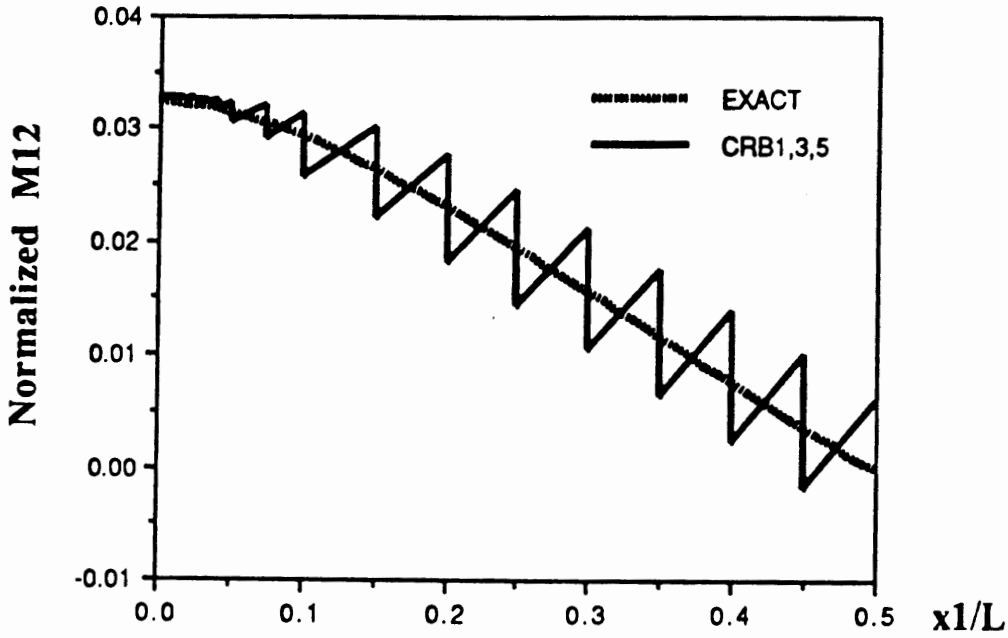

Figure 7.48: Variation of M12 along the line x2 = 0 for the uniformly loaded square plate with SS2 boundary conditions; CRB1,3,5 elements.

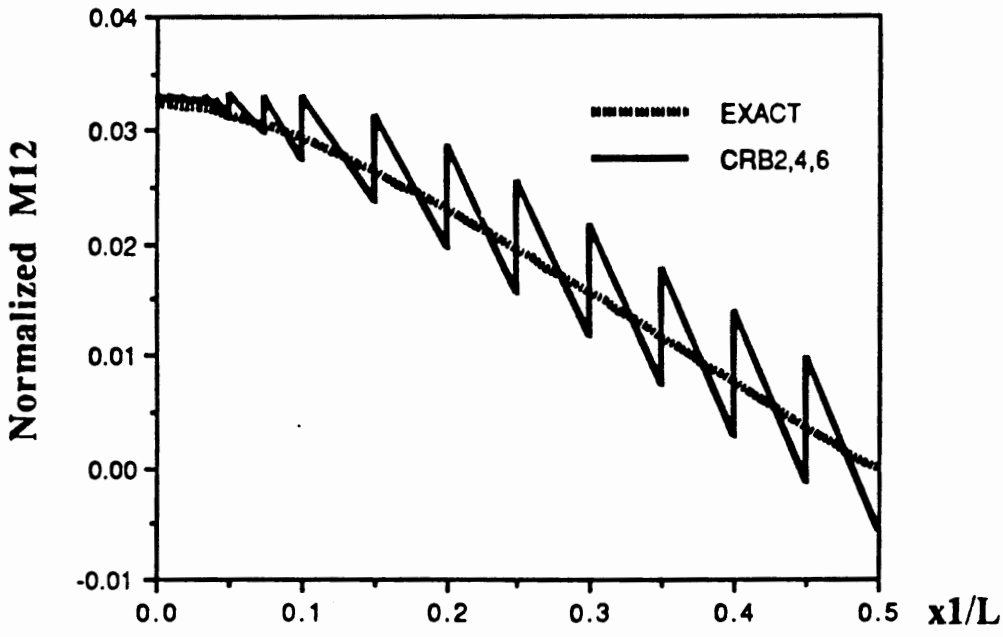

Figure 7.49: Variation of M12 along the line X2 = 0 for the uniformly loaded square plate with SS2 boundary conditions; CRB2,4,6 elements.

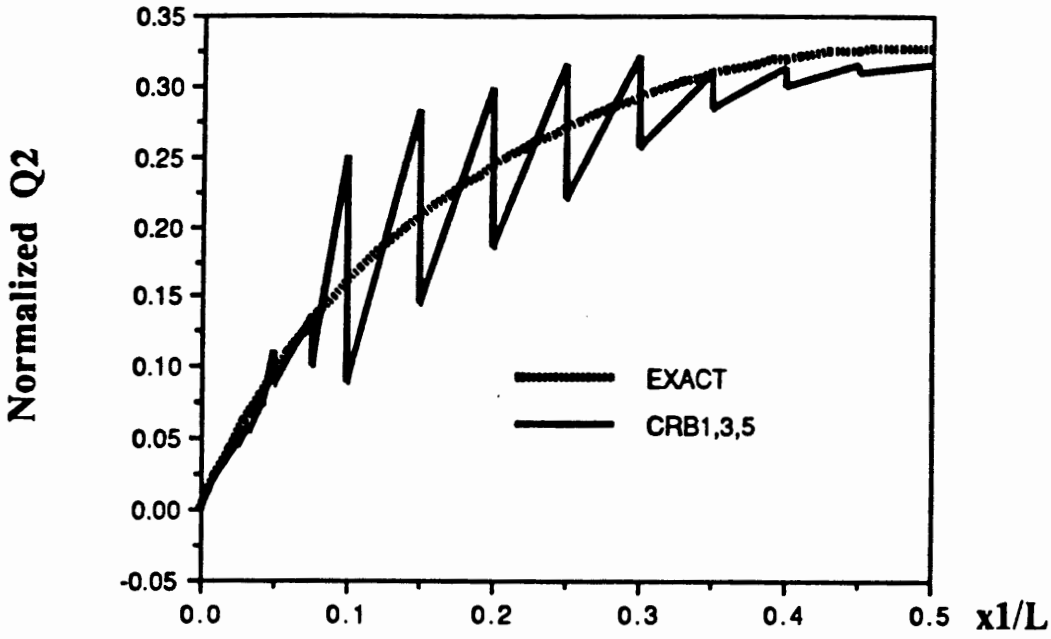

Figure 7.50: Variation of Q2 along the line x2 = 0 for the uniformly loaded square plate with SS2 boundary conditions; CRB1,3,5 elements.

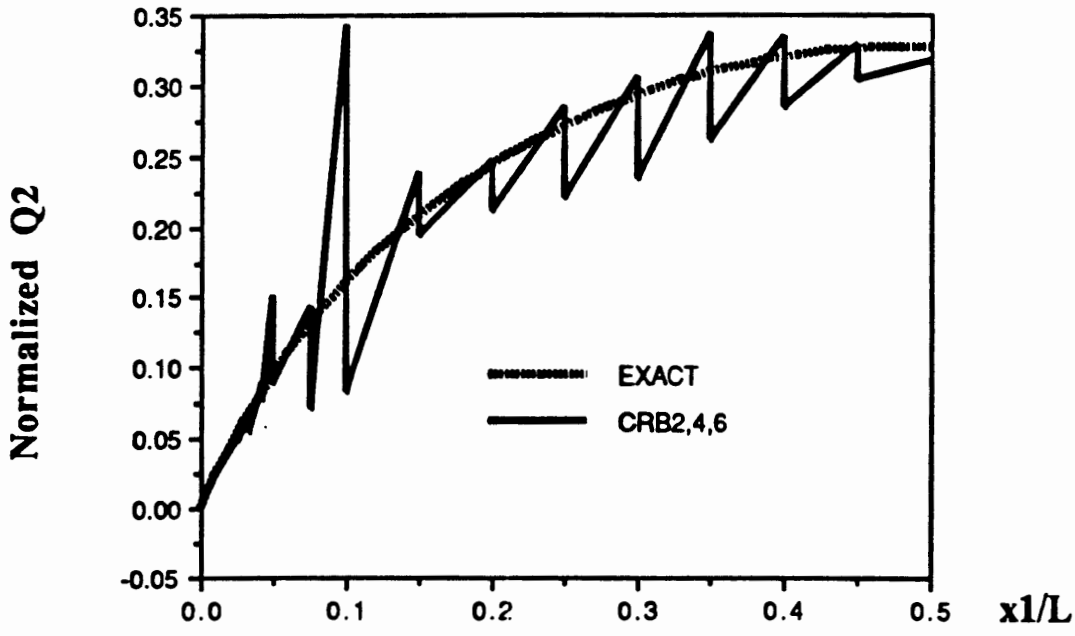

Figure 7.51: Variation of Q2 along the line x2 = 0 for the uniformly loaded square plate with SS2 boundary conditions; CRB2,4,6 elements.

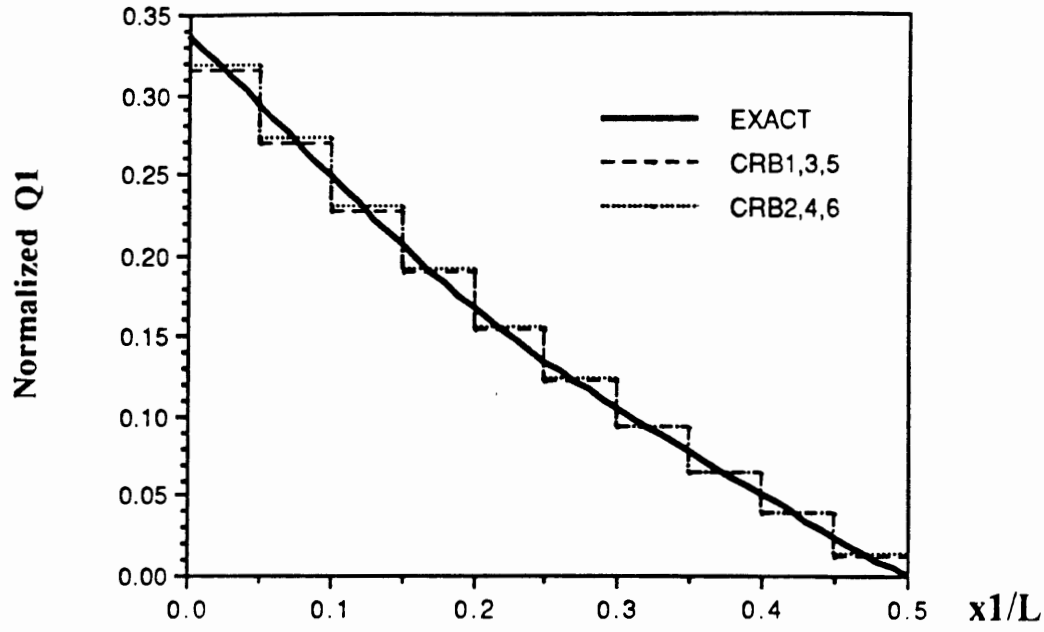

Figure 7.52: Variation of Q1 along the line x2 = L/2 for the uniformly loaded square plate with SS2 boundary conditions.

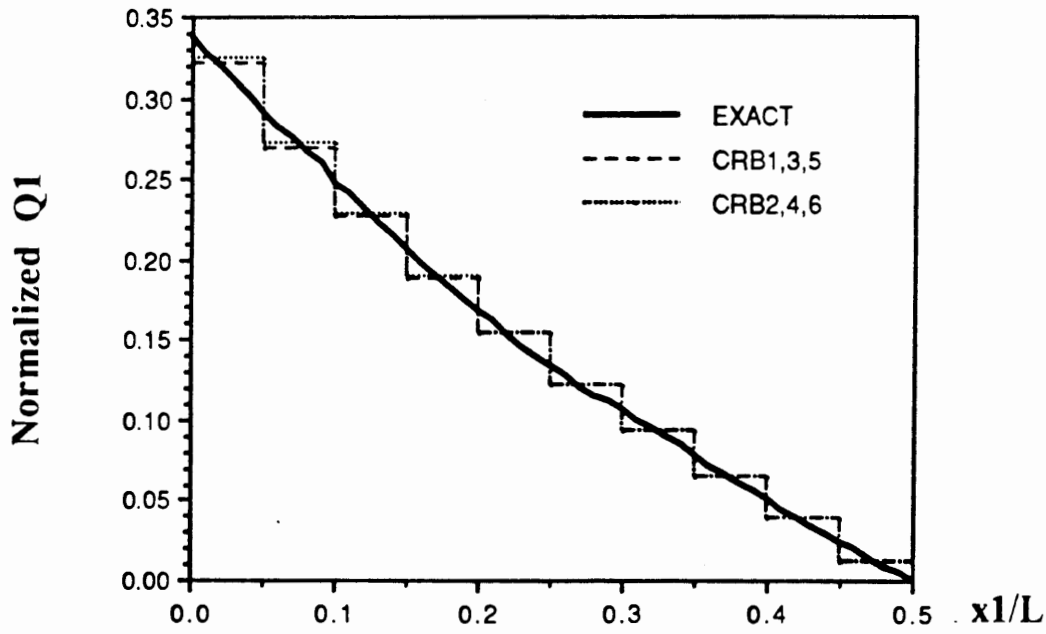

Figure 7.53: Variation of Q1 along the line x2 = L/2 for the uniformly loaded square plate with SS1/SS2 boundary conditions.

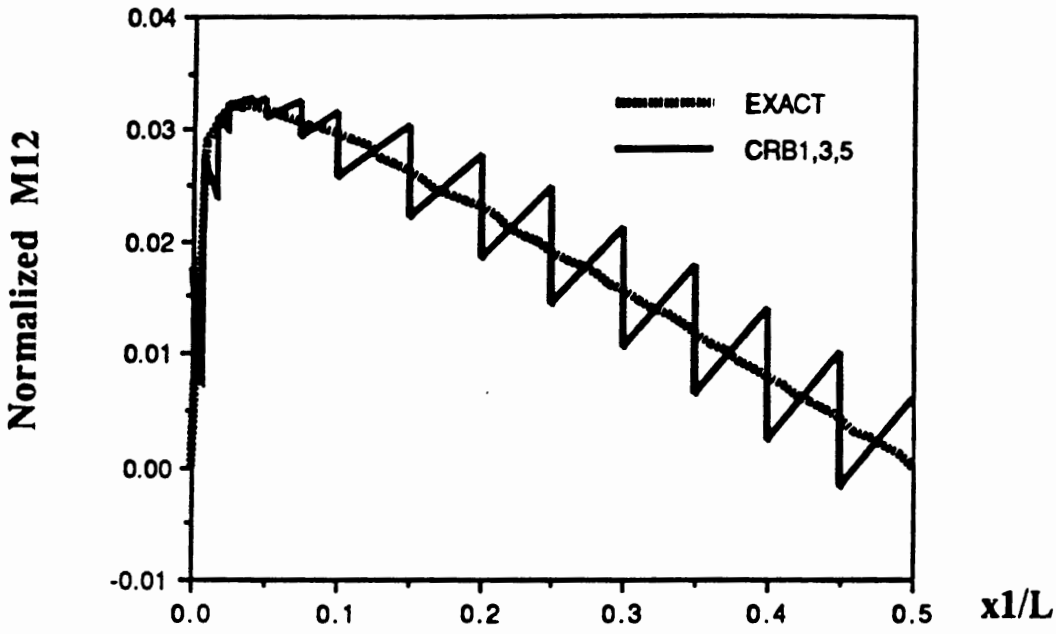

Figure 7.54: Variation of M12 along the line x2 = 0 for the uniformly loaded square plate with SS1/SS2 boundary conditions; CRB1,3,5 elements.

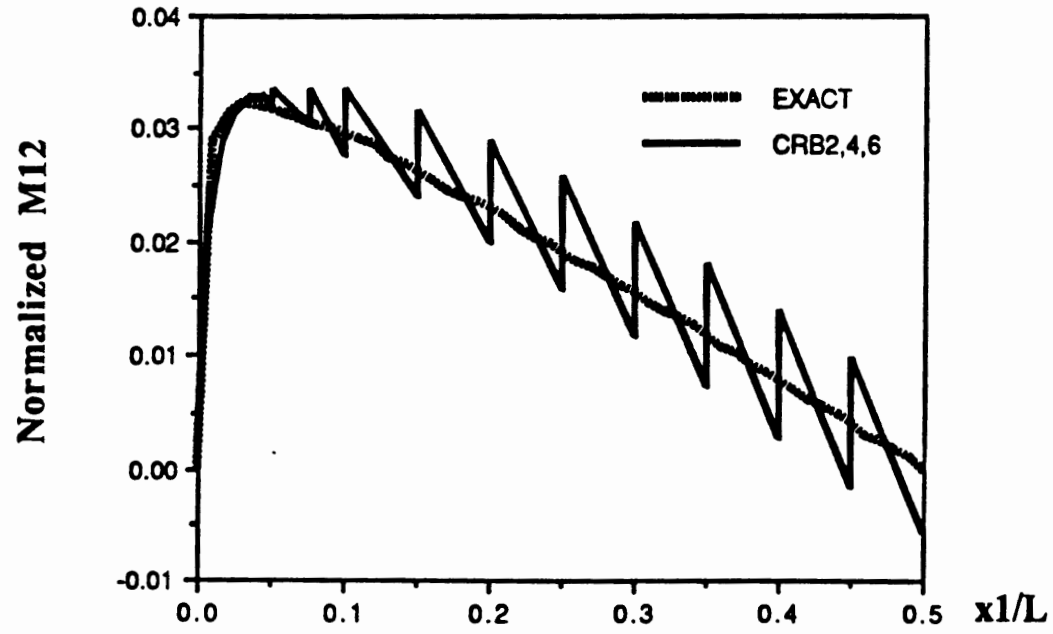

Figure 7.55: Variation of M12 along the line x2 = 0 for the uniformly loaded square plate with SS1/SS2 boundary conditions; CRB2,4,6 elements.

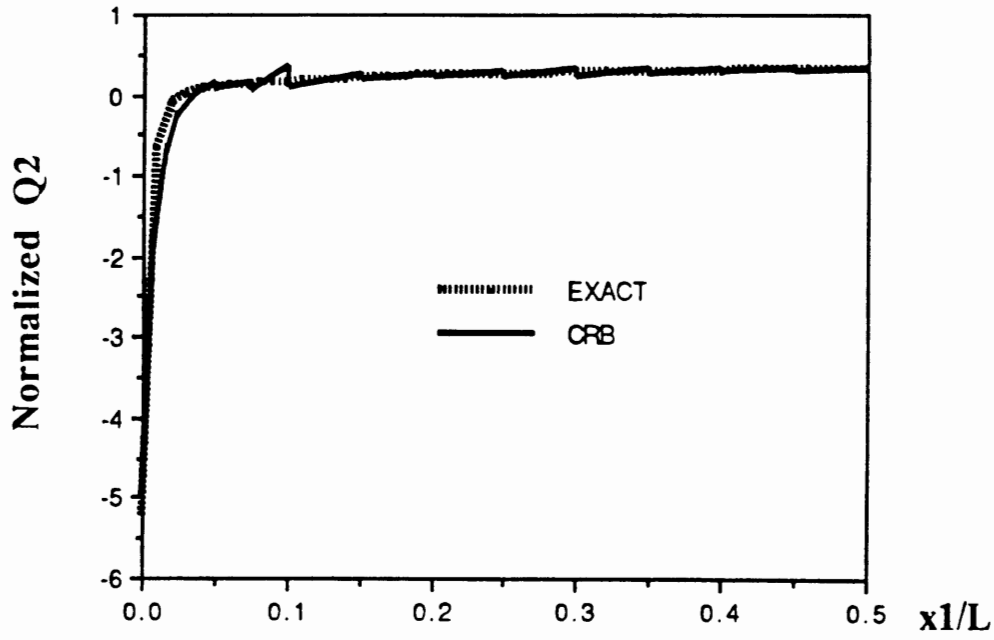

Figure 7.56: Variation of Q2 along the line x2 = 0 for the uniformly loaded square plate with SS1/SS2 boundary conditions; all CRB elements.

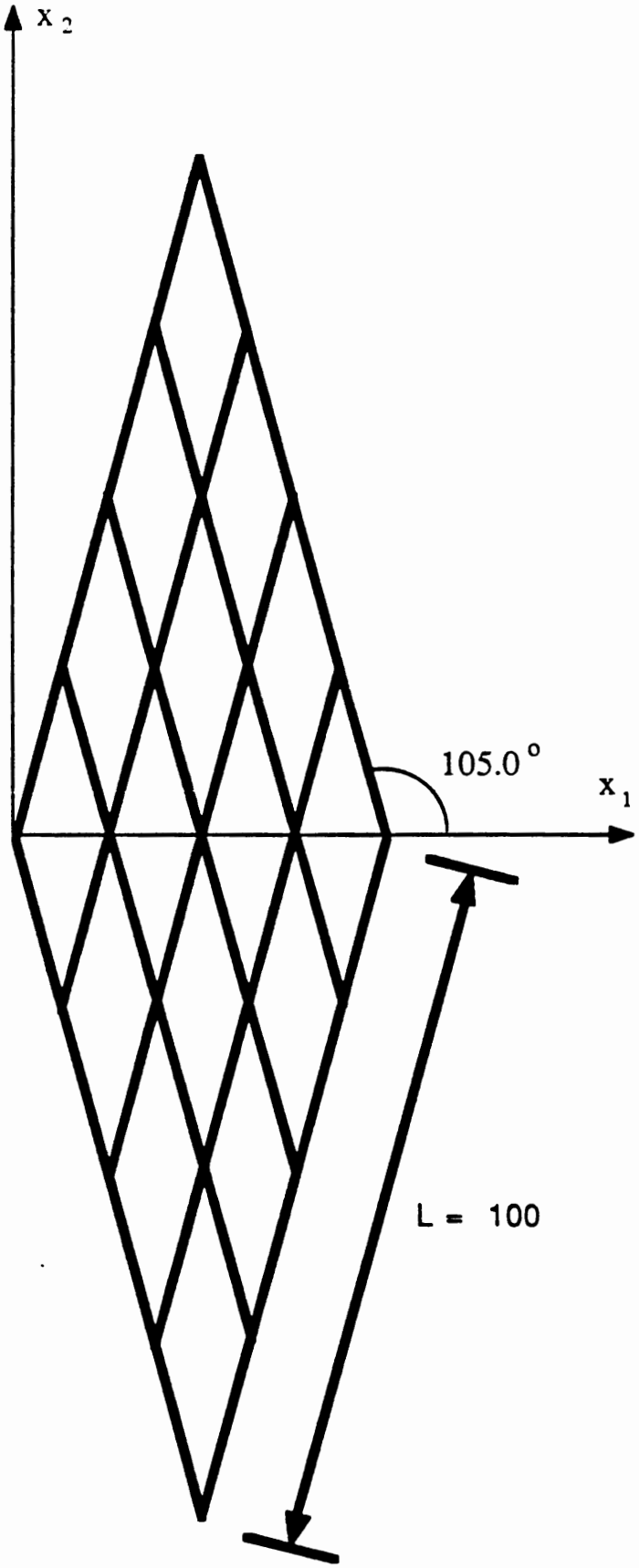

Figure 7.57: Rhombic plate mesh.

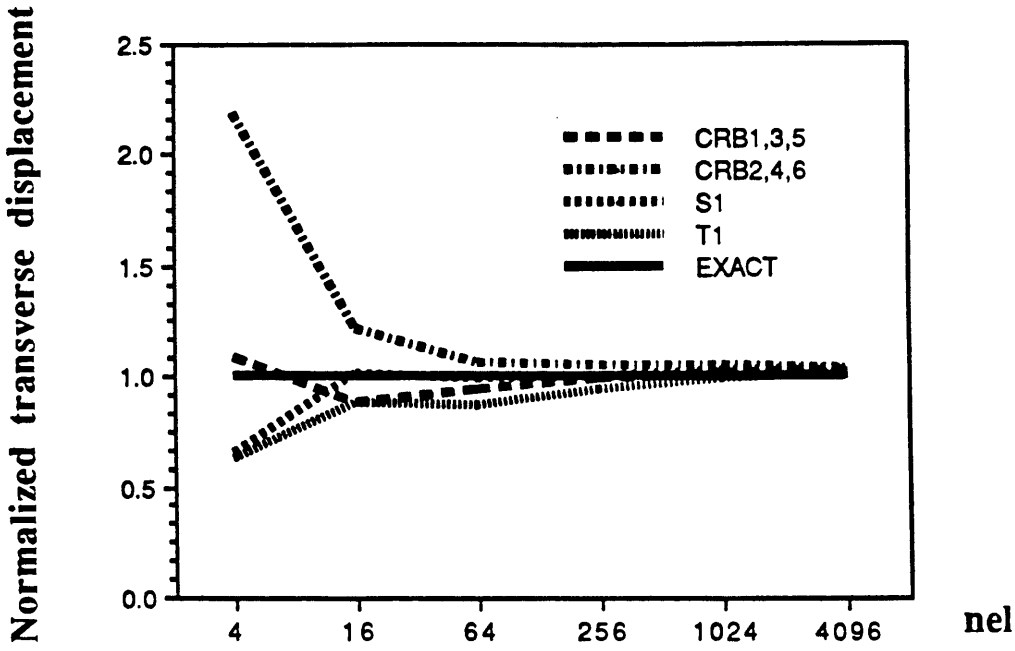

Figure 7.58: Rhombic plate; h = 1.0; convergence of the center displacement.

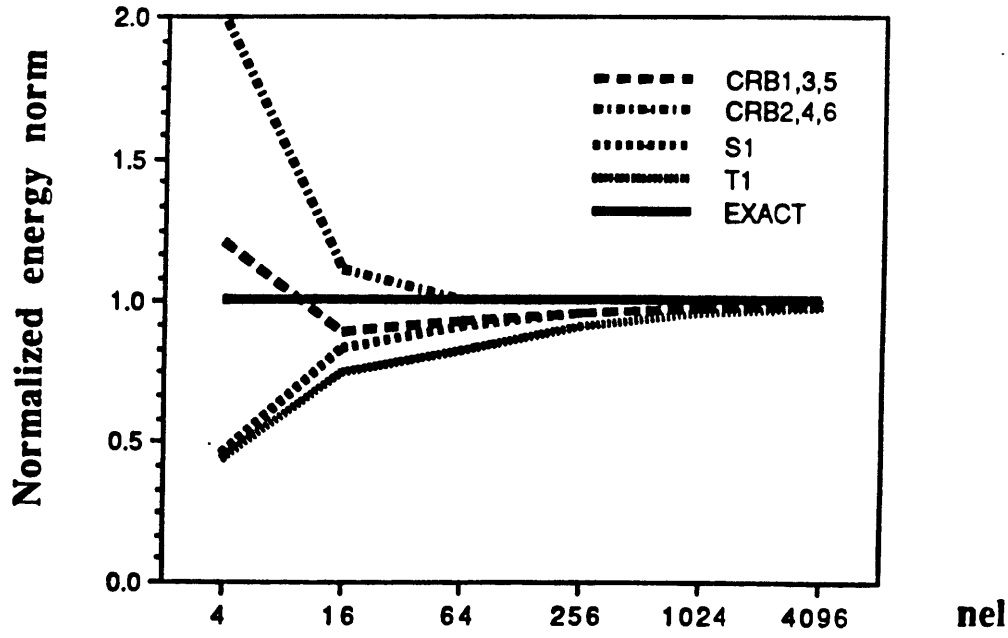

Figure 7.59: Rhombic plate; h = 1.0; convergence in the energy norm.

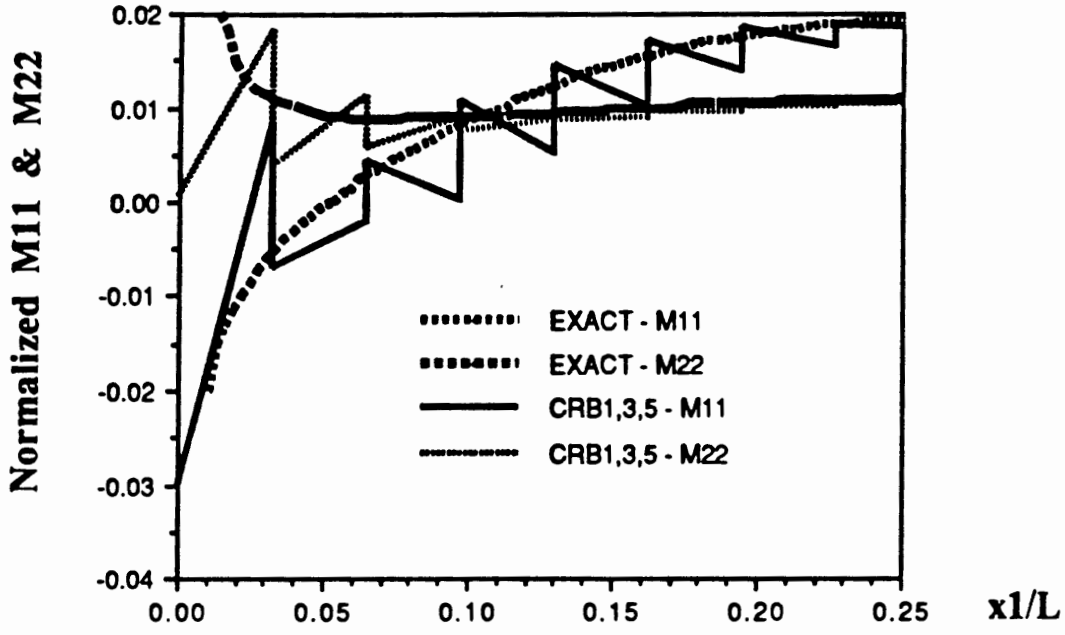

Figure 7.60: Rhombic plate; h = 1.0; variation of M11 & M22 along the line x2 = 0; CRB1,3,5 elements.

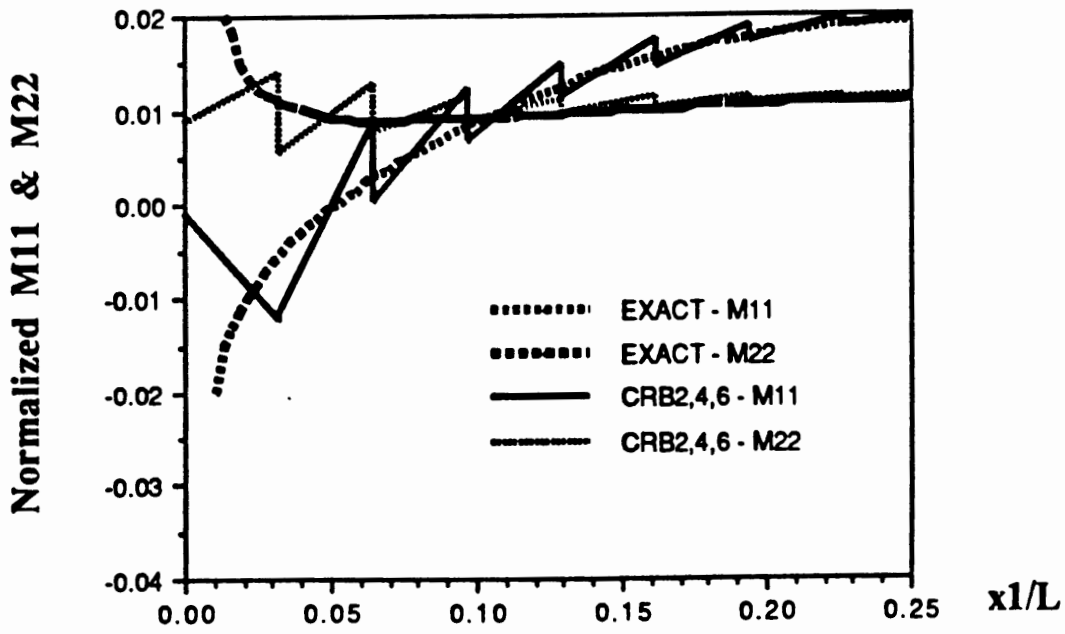

Figure 7.61: Rhombic plate; h = 1.0; variation of M11 & M22 along the line x2 =0; CRB2,4,6 elements.

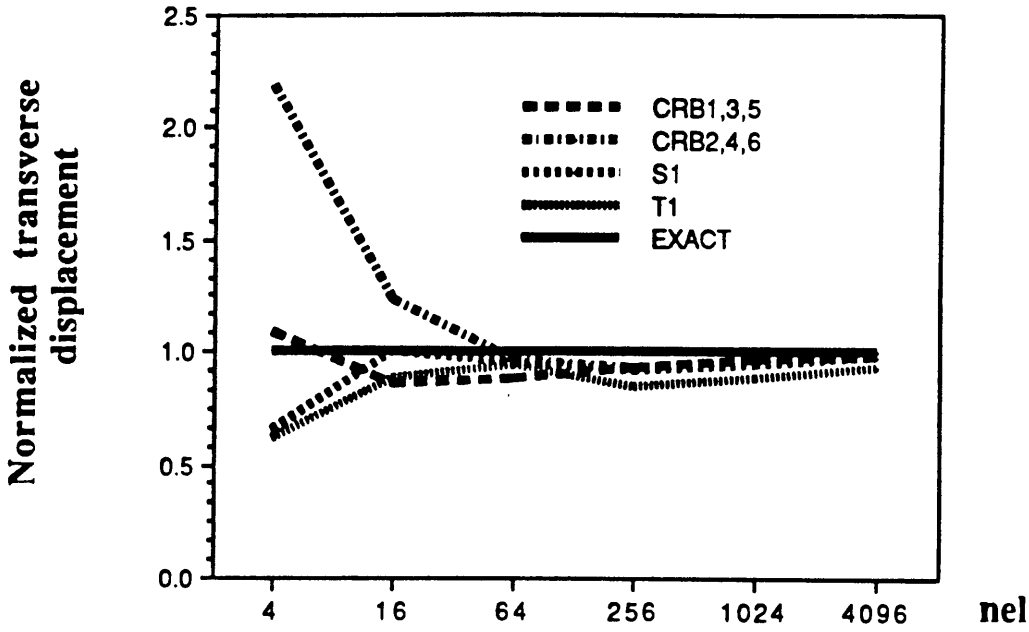

Figure 7.62: Rhombic plate; h = 0.1; convergence of the center transverse displacement.

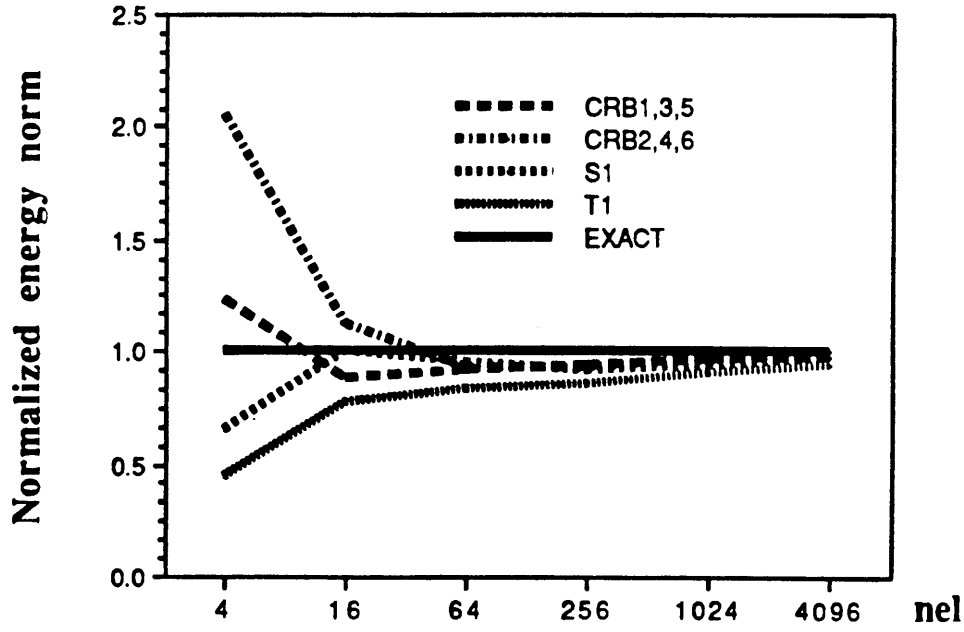

Figure 7.63: Rhombic plate; h = 0.1; convergence in the energy norm.

CHAPTER 8: CONCLUSION AND FUTURE WORK

8.1 Conclusion

A unified approach to mixed finite element methods has been presented in this dissertation. The proposed method has been used to formulate plane stress/strain and plate bending elements. It was proved that plane strain elements formulated by this method do not lock at the nearly incompressible limit. It was also proved that plate bending elements formulated by this method do not lock in shear when applied to model thin plates. Furthermore, the elements derived via this method possess all the properties presented in Chapter 1 as the objective for this dissertation.

The plane stress/strain elements presented show no sensitivity to the type of incompatible shape functions used. The plate bending elements, on the other hand, appear to be sensitive to these functions for coarse meshes. Both classes of elements yield identical results for both approaches taken to transform the assumed strain field from the element natural space into the physical space. Furthermore, the elements formulated via the Hellinger-Reissner variational principle yield identical results to their corresponding elements formulated via the Hu-Washizu variational principle.

The main contributions of this dissertation are:

- Uniform treatment of all fields (displacement, strain and stress) in the context of the Hu-Washizu and Hellinger-Reissner variational principles.
- A proof that by introducing coupling between the assumed shear and moment resultant fields, shear locking is avoided at the element level in plate bending elements formulated via the Hellinger-Reissner variational principle.
- A proof that by introducing coupling between the assumed shear strain and curvature fields as well as between the assumed shear and moment resultant fields, shear locking at the thin plate limit is avoided at the element level in plate

bending elements formulated via the Hu-Washizu variational principle.

- The introduction of a general method to generate the assumed stress and strain fields used in the variational principles. When applied to formulate plate bending elements, the desired couplings are obtained.
- A proof that in the case of plane strain, the trace of the strain field produced by the proposed method goes to zero pointwise as Poisson's ratio, ν, goes to 0.5^{-}. Thus, locking is avoided at the nearly incompressible limit.
- It is shown that shear locking in plate bending elements and locking at the nearly incompressible limit in plane strain elements can be avoided, in the context of mixed formulations, without resorting to the constraint count method.
- Variationally consistent recovery of all stresses.
- It is shown that in the case of linear isotropic elastic materials, elements that yield identical results can be derived via the Hellinger-Reissner and Hu-Washizu variational principles. Thus, an equivalence is established between elements formulated via the two principles.
- Establishing an equivalence between the two approaches taken to transform the strain field from the element natural space into the physical space.
- A simple and efficient method to enhance the assumed transverse displacement field so that four-node plate bending elements pass the constant curvature patch test.

8.2 Suggested Future Work

In this dissertation a general method that may be applied to all types of solid mechanics problems has been presented. This method, however, in the context of this dissertation, was applied only to small deformation analysis of linear isotropic elastic materials. A number of issues remain to be addressed:

- An extension of the method proposed by Wu, Huang & Pian [1987] to generate the incompatible shape functions so that a unique constant will be defined.
- A study of possible modifications to the proposed method, the initially assumed independent fields, and incompatible shape functions, so that the coupling between the shear and moment resultant fields and the coupling between the curvature and shear strain fields will not be rank deficient for parallelogram-shaped elements.
- A reformulation of the enhancement of the transverse displacement, introduced in four-node plate bending elements, as a modification to the assumed shear strain field in order to model the SS1 boundary condition pointwise.
- A study of the equivalence of the two approaches taken to transform the assumed strain field from the element natural space into the physical space.
- An extension of the notion of coupled stress resultant fields and coupled strain fields to the analysis of shells and beams.
- An application of the method to generate higher order elements.
- An application of the method to model non-isotropic materials.
- An extension of the proposed method to the non-linear regime (non-elastic large deformations/rotations undergoing large strains).

REFERENCES

Babuska, I. & T. Scapolla, [1989], "Benchmark Computation and Performance Evaluation for a Rhombic Plate Bending Problem," *International Journal for Computer-Aided Engineering and Software*, Vol. 27, pp. 155-179.

Bathe, K.J. & F. Brezzi, [1985], "On the Convergence of a Four-Node Plate Bending Element Based on Mindlin-Reissner Plate Theory and a Mixed Interpolation," *Proceedings of Conference on Mathematics of Finite Elements and Applications V*, Academic Press, (J.R. Whiteman, ed.), Vol. 99, pp. 491-503.

Bathe, K.J. & F. Brezzi, [1987], "A Simplified Analysis of Two Plate Bending Elements - The MITC4 and MITC9 Elements," *Proceedings, Conference NUMETA 87*, University College of Swansea, Wales.

Bathe, K.J. & E.N. Dvorkin, [1985], "A Four Node Plate Bending Element Based on Mindlin/Reissner Plate Theory and Mixed Interpolation," *International Journal for Numerical Methods in Engineering*, Vol. 18, pp. 1077-1089.

Belytschko, T. & W.E. Bachrach, [1986], "Efficient Implementation of Quadrilaterals With High Coarse-Mesh Accuracy," *Computer Methods in Applied Mechanics and Engineering*, Vol. 54, pp. 279-301.

Belytschko, T., W.K. Liu, J.S.J. Ong and D. Lam, [1985], "Implementation and Application of a 9-Node Lagrange Shell Element With Spurious Mode Control," *Computers and Structures*, Vol. 20, No. 1-3, pp. 121-128.

Belytschko, T., J.S.-J. Ong, W.K Liu & J.M. Kennedy [1984], "Hourglass Control in Linear and Nonlinear Problems," *Computer Methods in Applied Mechanics and Engineering*, Vol. 43, pp. 251-276.

Bicanic, N. & E. Hinton, [1979], "Spurious Modes in Two-Dimensional Isoparametric Elements," *International Journal for Numerical Methods in Engineering, Vol. 14, pp. 1545-1557.*

Cook, R. D. [1987], "A Plane Hybrid Element With Rotational d.o.f. and Adjustable Stiffness," *International Journal for Numerical Methods in Engineering*, Vol. 24, pp. 1499-1508.

Dvorkin, E.N. & K.J. Bathe, [1984], "A Continuum Mechanics Based Four-Node Shell Element for General Non-Linear Analysis," *International Journal for Computer-Aided Engineering and Software*, Vol. 1, pp. 77-88.

Flanagan, D.P., & T. Belytschko, [1981], "A Uniform Strain Hexahedron and Quadrilateral With Orthogonal Hourglass Control," *International Journal for Numerical Methods in Engineering*, Vol. 17, pp. 679-706.

Fraeijs de Veubeke, B., [1965], "Displacement and Equilibrium Models in the Finite Element Method," in *Stress Analysis*, editors O.C. Zienkiewicz & G.S. Holister. London: John Wiley.

Hinton, E. & H.C. Huang, [1986], "Shear Forces and Twisting Moments in Plates Using Mindlin Elements," *Engineering Computations*, Vol. 3, pp. 129-142.

Huang, H.C. & E. Hinton, [1984], "A Nine-Node Lagrangian Mindlin Element With Enhanced Shear Interpolation," *Engineering Computations*, Vol. 1, pp. 77-88.

Hughes, T.J.R., [1977], "Equivalence of Finite Elements for Nearly Incompressible Elasticity," *Journal of Applied Mechanics, Vol. 44, pp. 181-183.*

Hughes, T.J.R., [1980], "Generalization of Selective Integration Procedures to Anisotropic and Nonlinear Media," *International Journal for Numerical Methods in Engineering*, Vol. 15, pp. 1413-1418.

Hughes, T.J.R., [1987], *The Finite Element Method*, Prentice-Hall, Inc., Englewood Cliffs, New Jersey.

Hughes, T.J.R, M. Cohen & M. Haroun, [1978], "Reduced and Selective Integration Techniques in the Finite Element Analysis of Plates," *Nuclear Engineering and Design*, Vol. 46, pp. 203-222.

Hughes, T.J.R. & T.E. Tezduyar, [1981], "Finite Elements Based Upon Mindlin Plate Theory with Particular Reference to the Four Node Bilinear Isoparametric Element," *Journal of Applied Mechanics*, Vol. 46, pp. 587-596.

Kant, T. & E. Hinton, [1983], "Mindlin Plate Analysis by Segmentation Method," *Journal of Engineering Mechanics Division, ASCE*, Vol. 109, pp. 537-556.

Lax, P.D. & R.D. Richtmyer, [1956], "Survey of the Stability of Linear Finite Difference Equations," *Communications in Pure and Applied Mathematics, Vol. 9, pp. 267.*

Liu, W.K. & T. Belytschko, [1984], "Efficient Linear and Nonlinear Heat Conduction With a Quadrilateral Element," *International Journal for Numerical Methods in Engineering*, Vol. 20, pp. 931-948.

Liu, W.K., T. Belytschko, S.E. Law & D. Lam, [1987], "Resultant Stress Degenerated Shell Element," *Computer Methods in Applied Mechanics and Engineering*, to appear.

Lukasiewicz, S., [1979], "*Local Loads in Plates and Shells*", Sijthoff & Noordhoff, the Netherlands.

MacNeal, R.H., [1978], "A Simple Quadrilateral Shell Element," *Computers & Structures*, Vol. 8, pp. 175-183.

MacNeal, R.H., [1982], "Derivation of Element Stiffness Matrices by Assumed Strain Distributions," *Nuclear Engineering and Design*, Vol. 70, pp. 3-12.

MacNeal, R.H., [1987], "A Theorem Regarding the Locking of Tapered Four-Noded Membrane Elements," *International Journal for Numerical Methods in Engineering*, Vol. 24. pp. 1793-1799.

MacNeal, R.H. & R.L. Harder, [1985], "A Proposed Standard Set of Problems to Test Finite Element Accuracy," *Finite Elements in Analysis and Design*, Vol. 1, pp. 3-20.

Malkus, D.S. & T.J.R. Hughes, [1978], "Mixed Finite Element Methods - Reduced and Selective Integration Techniques: A Unification of Concepts," *Computer Methods in Applied Mechanics and Engineering*, Vol. 15, No. 1, pp. 63-81.

Mindlin, R.D., [1951], "Influence of Rotatory Inertia and Shear in Flexural Motions of Isotropic Elastic Plates," *Journal of Applied Mechanics*, Vol. 18, pp. 31-38.

Morley, L.S.D., [1963], "Skew Plates and Structures," *International Series of Monographs in Aeronautics and Astronautics*, New York.

Morris, G.R., [1986], "Kinematic Formulation of Finite Elements for Plate Bending," Ph.D. dissertation, University of California at Berkeley.

Pawsey, S.F. & R.W. Clough, [1971], "Improved Numerical Integration for Thick Slab Finite Elements," *International Journal for Numerical Methods in Engineering*, Vol. 3, pp. 575-586.

Pian, T.H.H. & K. Sumihara, [1984], "Rational Approach for Assumed Stress Finite Elements," *International Journal for Numerical Methods in Engineering*, Vol. 20, pp. 1685-1695.

Pian, T.H.H. & C.-C. Wu, [1988], "A Rational Approach for Choosing Stress Terms for Hybrid Finite Element Formulations", *International Journal for Numerical Methods in Engineering*, Vol. 26, pp. 2331-2343.

Reissner, E., [1945], "The Effect of Transverse Shear Deformation on the Bending of Elastic Plates," *Journal of Applied Mechanics*, Vol. 12, pp. 69-76.

Savin, G.N., [1961], Stress Concentration Around Holes," *International Series of Monographs in Aeronautics and Astronautics*, Pergamon Press.

Simo, J.C., D.D. Fox and M.S. Rifai, [1989], "On a Stress Resultant Geometrically Exact Shell Model. Part II: The Linear Theory; Computational Aspects," *Computer Methods in Applied Mechanics and Engineering*, Vol. 73, pp. 53-92.

Simo, J.C. & M.S. Rifai, [1989], "A Class of Mixed Assumed Strain Methods and the Method of Incompatible Modes," to appear.

Simo, J.C., R.L. Taylor & K.S. Pister, [1985], "Variational and Projection Methods for the Volume Constraint in Finite Deformation Elasto-Plasticity," *Computer Methods in Applied Mechanics and Engineering*, Vol. 51, pp. 177-208.

Strang, G. & G.J. Fix, [1973], *An Analysis of the Finite Element Method*, Prentice-Hall, Inc., Englewood Cliffs, New Jersey.

Taylor, R.L., P.J. Beresford, & E.L. Wilson, [1976], "A Nonconforming Element for Stress Analysis," *International Journal for Numerical Methods in Engineering*, Vol. 10, pp. 1211-1219.

Taylor R.L., O.C. Zienkiewicz, J.C. Simo & A.H.C. Chan, [1986], "The Patch Test for Mixed Formulations," *International Journal for Numerical Methods in Engineering*, Vol. 22, pp. 32-62.

Timoshenko, S. & S. Woinowsky-Krieger, [1959], *Theory of Plates and Shells*, McGraw-Hill, New York.

Weissman, S.L. & R.L. Taylor, [1988], "Four-Node Axisymmetric Element Based Upon the Hellinger-Reissner Functional," Report No. UCB/SEMM-88/18.

Wilson, E.L., R.L. Taylor, W.P. Doherty & J. Ghaboussi, [1973], "Incompatible Displacement Modes," *Numerical and Computer Models in Structural Mechanics*, Editors S.J. Fenves, N. Perrone, A.R. Robinston & W.C. Schnobrich. Academic Press, New York.

Wu, C.-C., M.-G. Huang & T.H.H. Pian, [1987], "Consistency Condition and Convergence Criteria of Incompatible Elements: General Formulation of Incompatible Functions and its Application," *Computers & Structures*, Vol. 27, No. 5, pp. 639-644.

Zienkiewicz, O.C., S. Qu, R.L. Taylor & S. Nakazawa, [1986], "The Patch Test for Mixed Formulations," *International Journal for Numerical Methods in Engineering*, Vol. 23, pp. 1873-1883.

Zienkiewicz, O.C., R.L. Taylor & J. Too, [1971], "Reduced Integration Technique in General Analysis of Plates and Shells", *International Journal for Numerical Methods in Engineering*, Vol. 3, pp. 275-290.

Zienkiewicz, O.C. & R.L. Taylor, [1989], *The Finite Element Method*, 4th edition, MacGraw-Hill Book Co., London.